Climate Dynamics of the Late Paleozoic Ice Age

by

Daniel Ethan Horton

A dissertation submitted in partial fulfillment
of the requirements for the degree of
Doctor of Philosophy
(Geology)
in The University of Michigan
2011

Doctoral Committee:

        Associate Professor Christopher J. Poulsen, Chair
        Assistant Professor Jeremy N. Bassis
        Assistant Professor David C. Lund
        Assistant Professor Nathan D. Sheldon

ACKNOWLEDGEMENTS

TABLE OF CONTENTS

LIST OF FIGURES

ABSTRACT

The late Paleozoic era ($\sim$360-250 Ma) witnessed the vegetated Earth's only known transition from an icehouse to a greenhouse climate. This transition brought Earth from the Phanerozoic's most severe glaciation, the late Paleozoic ice age (LPIA), into a greenhouse climate that would dominate the next 220 million years of Earth history. Developing an understanding of the late Paleozoic icehouse climate and the mechanisms that drove Earth into a protracted greenhouse state are fundamental to the study of climate dynamics in both the distant past and the near future. The traditional understanding of late Paleozoic climate contends that massive continental-scale ice sheets formed when the southern hemisphere land masses were located near to the austral pole and repetitively waxed and waned due to orbital insolation variations. A recent re-analysis of the temporal and geographic distribution of glacial deposits, in conjunction with a re-examination of glacioeustasy records, indicates that LPIA climate was much more dynamic. In addition to ice sheets waxing and waning on orbital time-scales, the emerging view of LPIA climate contends that icehouse conditions were episodic, divided by multiple intervals ($\sim$10 Myrs) of ice-free greenhouse conditions. This newfound variability in the LPIA climate state has been hypothesized to result from fluctuations in atmospheric pCO$_2$ concentrations. To constrain the climatic dynamics discussed in these disparate LPIA views, this dissertation employs numerical climate-modeling techniques to explore the interactions of the late Paleozoic atmosphere, biosphere, cryosphere, hydrosphere, and lithosphere.

In this dissertation, we utilize the GENESIS General Circulation Model (GCM) asynchronously coupled to a three-dimensional thermomechanical ice sheet model in a series of sensitivity experiments that seek to determine the influence of atmospheric $p\mathrm{CO}_2$ and orbitally-forced insolation variations on LPIA climate. In Chapter 2, results from the first late Paleozoic coupled GCM-ice sheet modeling experiment are presented. In this chapter we verify the model-coupling scheme by simulating ice sheets in equilibrium with a suite of $p\mathrm{CO}_2$ concentrations at multiple steady-state orbital configurations. We find that similar to simulations of ice sheets in other geologic time periods late Paleozoic ice sheet mass balance is highly dependent on summer temperatures as determined by $p\mathrm{CO}_2$ concentration and orbitally-controlled seasonal insolation distributions. In Chapter 3, we apply transient orbital insolation changes to our coupled GCM-ice sheet modeling scheme in an attempt to simulate glacial-interglacial cyclicity. Our results again indicate that summer temperatures play a large role in determining ice sheet mass balance, but also demonstrate that the cooling effects of ice albedo and ice height feedbacks render continental ice sheets insensitive to periods of increased orbital insolation, indicating that changes in orbital insolation alone are insufficient to drive cyclic ice accumulation and ablation. In Chapter 4, we apply the same transient-orbit modeling scheme to the LPIA climate, but we include a dynamic ecosystem model, BIOME4, to the GCM-ice sheet model coupling. In this chapter, we demonstrate that within a narrow $p\mathrm{CO}_2$ range ($840 > p\mathrm{CO}_2 > 420$), ecosystem changes at the ice sheet margins amplify orbitally-driven temperature changes and facilitate the advance and retreat of continental ice sheets. In Chapter 5, we expand on the results presented in Chapter 4 by discussing both high-latitude glacial-interglacial cyclicity and low-latitude climate change. We find that changes in the eccentricity of Earth's orbit about the Sun drive both high-

latitude ice accumulation and ablation cycles as well as low-latitude precipitation, wet-season length, and vegetation distribution fluctuations. Based on these results, we develop an orbitally-paced model of cyclic low-latitude sediment deposition consistent with climate dynamics and field-based observations.

CHAPTER I

Introduction

The late Paleozoic ice age (LPIA; ∼360-250) has long been regarded as the Phanerozoic's most-prolonged interval of icehouse climate. Studies of this period in Earth history have facilitated the development of fundamental geologic concepts and more recently have informed efforts to understand the consequences of anthropogenic climate change. LPIA glacial deposits from the Gondwanaland continents were instrumental in the reconstruction of the Pangaean supercontinent and were a critical line of evidence used in the development of the theory of continental drift (Wegener, 1915; Du Toit, 1937). More recently, the evolution of climate throughout the LPIA has garnered increased attention because it represents vegetated-Earth's last transition from an icehouse to a greenhouse climatic state (Gastaldo et al., 1996; Cleal and Thomas, 2005; Montañez et al., 2007). In this, the introductory chapter of my dissertation, I will briefly (i) summarize the current state of thinking on the nature of the LPIA, (ii) discuss near-field, far-field, biotic, and geochemical evidence pertaining to the LPIA, (iii) present the climate-modeling tools and techniques used throughout this study, and (iv) outline the results chapters (2-5) with an emphasis on my contributions to our understanding of LPIA climate dynamics.

Traditionally, the LPIA has been interpreted as a period of protracted super-

continental glaciation (Crowell, 1978; Frakes and Francis, 1988; Frakes et al., 1992; Veevers and Powell, 1987; Veevers et al., 1994). Massive ice sheets were hypothesized to have formed due to the amalgamation of the Gondwanaland continents (Africa, Antarctica, Australia, Arabia, India, and S. America), about the austral pole. Over long time periods (10^7 yrs), the volume of ice sequestered on land was thought to be determined by the tectonic drift of Gondwanaland relative to the South Pole (Caputo and Crowell, 1985); when Gondwanaland was located over the pole, ice sheet volumes were thought to be relatively large, whereas when Gondwanaland drifted into higher latitudes away from the pole, ice sheet volumes were thought to decrease. Evidence of long-lived continental glaciation was pieced together from both near-field (ice-proximal) and far-field (ice-distal) deposits. Near-field evidence, including tillites, diamictites, and striated pavements were found distributed throughout the Gondwanaland continents, suggesting supercontinental-scale glaciation. Evidence from far-field deposits, particularly those found in the paleo-equatorial basins of Euramerica, consist of rhythmic sedimentary sequences that were interpreted to be the result of repetitive (10^4-10^5 yrs) changes in sea-level. It was hypothesized that these sea-level fluctuations were driven by the waxing and waning of the Gondwanaland ice sheets (Wanless and Shepard, 1936). Due to the wide distribution of Gondwanaland glaciogenic deposits and the long record of low-latitude glacioeustatic change preserved in rhythmic low-latitude sedimentary deposits, the LPIA has traditionally been viewed as a period of protracted continental-scale glaciation.

More recent evidence, much of it produced over the past decade, has challenged some aspects of this traditional view of the LPIA. Near-field studies of Gondwanaland glaciogenic deposits have found evidence for multiple 10 Myr glacial hiatuses within the greater LPIA interval and have also suggested that not all regions of Gond-

wanaland were glaciated contemporaneously (Isbell et al., 2003a,b; Fielding et al., 2008a,b; Birgenheier et al., 2009). In addition, improved dating techniques indicate that some non-glacial episodes are contemporaneous with low-latitude rhythmic sedimentary sequences, suggesting that factors other than glacioeustasy likely played a role in their deposition (Isbell et al., 2003b). In conjunction with these high-latitude records of ice-free intervals, Rygel et al. (2008) synthesized published estimates of late Paleozoic low-latitude eustasy-change and found that the estimated magnitude of inferred sea-level changes were consistent with a more episodic view of continental glaciation in the LPIA.

Other studies, outside the realm of glaciogenic and glacioeustatic deposits, have also indicated that the LPIA climate was more dynamic than originally thought. Paleobotanaical analyses of LPIA flora have chronicled both short to intermediate-term cycles of species dominance and long-term floral transitions throughout the LPIA and attribute these changes to climatic variations (Cleal and Thomas, 2005; DiMichele et al., 2001, 2009, 2010; Falcon-Lang, 2004; Falcon-Lang et al., 2009, 2011). Geochemical analyses of the temporal trend of stable carbon and oxygen isotopes within marine carbonates also point to dynamic climate variability in the LPIA (Veizer et al., 1999; Mii et al., 1999, 2001; Saltzman, 2005; Montañez et al., 2007). While isotopic records in the late Paleozoic are often challenging to interpret due to dating and preservational difficulties, inferences of icehouse and greenhouse climate intervals have been made on the basis of positive excursions within the δ^{13}C and δ^{18}O trends. Higher δ^{13}C values are interpreted to correspond to increased burial of organic carbon and a reduction in atmospheric pCO$_2$ concentration, while higher δ^{18}O values are interpreted as periods of atmospheric cooling and/or ice sheet formation. A recent attempt to correlate published isotopic records with periods of

high-latitude glaciation met with mixed results, but based on the secular variations in the compiled isotopic record, a LPIA punctuated by multiple ice-free intervals was suggested (Frank et al., 2008).

In sum, the traditional view of a relatively stable LPIA climate, dominated by prolonged continental-scale glaciation, has of late, been called into question. Recent glaciogenic, glacioeustatic, geochemical, and paleofloral evidence instead suggests that the LPIA climate was dynamic, with multiple pulses of glaciation, often regional in scale, interspersed with warmer ice-free intervals.

Considering this newly proposed LPIA climatic paradigm, this dissertation sets out to develop a better understanding of the processes that influence LPIA climate dynamics using numerical climate modeling techniques. Based on the accumulated evidence, LPIA climatic changes were diverse, occurred over multiple time-scales, and likely arose due to a number of different forcing mechanisms (Tabor and Poulsen, 2008). In light of this complexity, the experimental design employed in this dissertation focuses less on a one-to-one re-creation of late Paleozoic climate and more on sensitivity tests that elucidate the roles of various factors in the LPIA climate system.

The late Paleozoic sensitivity experiments conducted in this dissertation utilize the Global Environmental and Ecological Simulation of Interactive Systems (GENESIS) general circulation model (GCM; Pollard and Thompson, 1992). GENESIS was developed at the National Center for Atmospheric Research (NCAR) and is composed of atmosphere, 50 m slab-ocean, sea-ice, and land-surface components. Since its creation at NCAR, the GENESIS GCM has been maintained and updated by David Pollard, and is currently in version 3.0 (Pollard and Thompson, 1995). GENESIS has an extensive usage history and has been successfully applied to climatic problems

relevant to the past, present, and future (i.e. Barron et al., 1993; Bonan et al., 1992; Levis et al., 1999). In the experiments presented in this dissertation, GENESIS is asynchronously coupled to a thermomechanical ice sheet model. This model uses an alternating-direction-implicit numerical scheme to solve for the vertically integrated two-dimensional mass continuity equation and has been used in glacial studies of the early Cenozoic, Plio-Pleistocene, and late Ordovician (DeConto and Pollard, 2003; Pollard and DeConto, 2009; Herrmann et al., 2003). The final component of the modeling-scheme utilized in this study is the BIOME ecosystem model. BIOME was developed by Haxeltine and Prentice (1996) to simulate the distribution of ecosystem types as a function of biogeophysical and biogeochemical constraints. BIOME4, the latest version of the BIOME-model lineage (and the version used in this study), was developed by Kaplan et al. (2003) to more accurately simulate high-latitude ecosystems found in ice-proximal environments. Throughout the studies presented in this dissertation, these modeling components are used in various configurations to gauge the sensitivity of the late Paleozoic climate to a suite of different environmental parameters (boundary conditions). Each dissertation chapter includes a detailed description of these experimental designs and explores a different aspect of the LPIA climate system.

The dissertation is comprised of four main results-based chapters (2-5) preceeded by this introductory chapter (1) and followed by a summary chapter (6). Chapters 2-5 utilize the numerical climate modeling tools discussed above to explore the dynamic interaction of the late Paleozoic's atmosphere, biosphere, cryosphere, hydrosphere, and lithosphere. Chapter 2 investigates the roles of atmospheric $p\mathrm{CO_2}$ concentration and the Earth-Sun orbital configuration on equilibrium ice sheets (Horton et al., 2007). These experiments were the first to incorporate a coupled GCM-ice sheet

model into late Paleozoic climate simulations and represent a benchmark advance in LPIA studies. Chapter 3 builds on this GCM-ice sheet modeling scheme and delves into the effect of transient orbital parameters on ice sheet mass balance. The results present a paradox; ice sheets of adequate size to account for inferred LPIA sea-level changes are insensitive to variations in orbital parameters (Horton and Poulsen, 2009). This paradox is partially resolved in Chapter 4, when a dynamic ecosystem model is incorporated into the coupled GCM-ice sheet modeling scheme. Dynamic ecosystem changes at the margin of the ice sheet are found to result from orbitally induced changes in insolation. Differences in ice-margin ecosystem properties amplify insolation-driven temperature changes and result in the successful simulation of advancing and retreating ice sheets previously immune to orbital insolation changes (Horton et al., 2010). In Chapter 5, the waxing and waning ice sheet experiments presented in Chapter 4 are analyzed with a focus on low-latitude climate change. Specifically, the role of high-latitude glaciation on low-latitude precipitation is explored, as well as the effects of orbital change and atmospheric pCO$_2$ concentrations on tropical climate. From these results, a model of eccentricity-paced low-latitude cyclostratigraphy is formulated (Horton et al., view).

1.1   Publications and abstracts resulting from this dissertation

Publications (peer-reviewed)

Horton, D. E., C. J. Poulsen, and D. Pollard (2007), Orbital and CO$_2$ forcing of late
  Paleozoic ice sheets, *Geophysical Research Letters*, v.34 L19708, doi:10.1029/2007GL031188.
  (Chapter 2)

Horton, D. E. and C. J. Poulsen (2009), Paradox of late Paleozoic glacioeustasy,

Geology, v.37, p.715-718 doi:10.1130/G30016A.1. **(Chapter 3)**

Horton, D. E., C. J. Poulsen, and D. Pollard (2010), Influence of high-latitude vegetation feedbacks on late Palaeozoic glacial cycles, *Nature Geoscience*, v.3, p.572-577, doi:10.1038/NGEO922. **(Chapter 4)**

Horton, D. E., C. J. Poulsen, I. P. Montañez, and W. A. DiMichele (in review), Eccentricity-paced late Paleozoic climate change and its role in cyclostratigraphy, *Palaeogeography, Palaeoclimatology, Palaeoecology*, **(Chapter 5)**

Conference abstracts

Horton, D. E. and C. J. Poulsen (2010), High-latitude ecosystem change enables late Paleozoic glacial-interglacial cycles, *Eos Trans. AGU*, 91, Fall Meet. Suppl., Abstract PP44B-07.

Horton, D. E., C. J. Poulsen, and D. Pollard (2007), Simulations of late Paleozoic continental ice sheets under orbital and CO_2 forcing, *Eos Trans. AGU*, 88, Fall Meet. Suppl., Abstract PP31F-07.

Poulsen, C. J., **D. E. Horton**, and D. Pollard (2007), Glacial-Interglacial climate change during the late Paleozoic: A climate modeling perspective, *Geological Society of America*, 39(6), p.354.

Bibliography

Barron, E. J., Fawcett, P. J., Pollard, D. and Thompson, S. Model Simulations of Cretaceous Climates - the Role of Geography and Carbon-Dioxide. *Philosophical Transactions of the Royal Society of London Series B-Biological Sciences*, 341(1297):307–315, 1993.

Birgenheier, L. P., Fielding, C. R., Rygel, M. C., Frank, T. D. and Roberts, J. Evidence for Dynamic Climate Change on Sub-10^6-Year Scales from the Late Paleozoic Glacial Record, Tamworth Belt, New South Wales, Australia. *Journal of Sedimentary Research*, 79(1-2):56–82, 2009.

Bonan, G. B., Pollard, D. and Thompson, S. L. Effects of boreal forest vegetation on global climate. *Nature*, 359(6397):716–718, 1992.

Caputo, M. V. and Crowell, J. C. Migration of Glacial Centers across Gondwana during Paleozoic Era. *Geological Society of America Bulletin*, 96(8):1020–1036, 1985.

Cleal, C. J. and Thomas, B. A. Palaeozoic tropical rainforests and their effect on global climates: is the past the key to the present? *Geobiology*, 3(1):13–31, 2005.

Crowell, J. C. Gondwanan Glaciation, Cyclothems, Continental Positioning, and Climate Change. *American Journal of Science*, 278(10):1345–1372, 1978.

DeConto, R. M. and Pollard, D. A coupled climate-ice sheet modeling approach to the Early Cenozoic history of the Antarctic ice sheet. *Palaeogeography Palaeoclimatology Palaeoecology*, 198(1-2):39–52, 2003.

DiMichele, W. A., Cecil, C. B., Montañez, I. P. and Falcon-Lang, H. J. Cyclic changes in Pennsylvanian paleoclimate and effects on floristic dynamics in tropical Pangaea. *International Journal of Coal Geology*, 83(2-3):329–344, 2010.

DiMichele, W. A., Montañez, I. P., Poulsen, C. J. and Tabor, N. J. Climate and vegetational regime shifts in the late Paleozoic ice age earth. *Geobiology*, 7(2):200–226, 2009.

DiMichele, W. A., Pfefferkorn, H. W. and Gastaldo, R. A. Response of Late Carboniferous and Early Permian plant communities to climate change. *Annual Review of Earth and Planetary Sciences*, 29:461–487, 2001.

Du Toit, A. L. *Our Wandering Continents: An Hypothesis of Continental Drifting.* Oliver and Boyd, Edinburgh, 1937.

Falcon-Lang, H. J. Pennsylvanian tropical rain forests responded to glacial-interglacial rhythms. *Geology*, 32(8):689–692, 2004.

Falcon-Lang, H. J., Jud, N. A., DiMichele, W. A., Chaney, D. S. and Lucas, S. G. Pennsylvanian coniferopsid forests in sabkha facies reveal the nature of seasonal tropical biome. *Geology*, 39:371–374, 2011.

Falcon-Lang, H. J., Nelson, W. J., Elrick, S., Looy, C. V., Ames, P. R. and DiMichele, W. A. Incised channel fills containing conifers indicate that seasonally dry vegetation dominated Pennsylvanian tropical lowlands. *Geology*, 37(10):923–926, 2009.

Fielding, C. R., Frank, T. D., Birgenheier, L. P., Rygel, M. C., Jones, A. T. and Roberts, J. Stratigraphic imprint of the Late Palaeozoic Ice Age in eastern Australia: a record of alternating glacial and nonglacial climate regime. *Journal of the Geological Society*, 165:129–140, 2008a.

Fielding, C. R., Frank, T. D. and Isbell, J. I. The Late Paleozoic Ice Age-a Review of Current Understanding and Synthesis of Global Climate Patterns. In Fielding, C. R., Frank, T. D. and Isbell, J. I., editors, *Resolving the Late Paleozoic Ice Age in Time and Space*, volume 441. Geol. Soc. Am. Spec. Pap., 2008b.

Frakes, L. A. and Francis, J. E. A Guide to Phanerozoic Cold Polar Climates from High-Latitude Ice-Rafting in the Cretaceous. *Nature*, 333(6173):547–549, 1988.

Frakes, L. A., Francis, J. E. and Syktus, J. I. *Climate Modes of the Phanerozoic.* Cambridge Univ. Press, Cambridge, U.K., 1992.

Frank, T. D., Birgenheier, L. P., Montanez, I. P., Fielding, C. R. and Rygel, M. C. Late Paleozoic climate dynamics revealed by comparison of ice-proximal stratigraphic and ice-distal isotopic records. In Fielding, C. R., Frank, T. D. and Isbell, J. I., editors, *Resolving the Late Paleozoic Ice Age in Time and Space*, volume 441, pages 331–342. Geol. Soc. Am. Spec. Pap., 2008.

Gastaldo, R. A., DiMichele, W. A. and Pfefferkorn, H. W. Out of the icehouse into the greenhouse: A late Paleozoic analogue for modern global vegetational change. *GSA Today*, 6(10):1–7, 1996.

Haxeltine, A. and Prentice, I. C. BIOME3: An equilibrium terrestrial biosphere model based on ecophysiological constraints, resource availability, and competition among plant functional types. *Global Biogeochemical Cycles*, 10(4):693–709, 1996.

Herrmann, A. D., Patzkowsky, M. E. and Pollard, D. Obliquity forcing with 8-12 times preindustrial levels of atmospheric pCO$_2$ during the Late Ordovician glaciation. *Geology*, 31(6):485–488, 2003.

Horton, D. E. and Poulsen, C. J. Paradox of late Paleozoic glacioeustasy. *Geology*, 37(8):715–718, 2009.

Horton, D. E., Poulsen, C. J., Montañez, I. P. and DiMichele, W. A. Eccentricity-paced late Paleozoic climate change and its role in cyclostratigraphy. *Palaeogeography, Palaeoclimatology, Palaeoecology*, in review.

Horton, D. E., Poulsen, C. J. and Pollard, D. Orbital and CO_2 forcing of late Paleozoic continental ice sheets. *Geophysical Research Letters*, 34(19):L19708, 2007.

Horton, D. E., Poulsen, C. J. and Pollard, D. Influence of high-latitude vegetation feedbacks on late Palaeozoic glacial cycles. *Nature Geoscience*, 3(8):572–577, 2010.

Isbell, J. L., Lenaker, P. A., Askin, R. A., Miller, M. F. and Babcock, L. E. Reevaluation of the timing and extent of late Paleozoic glaciation in Gondwana: Role of the Transantarctic Mountains. *Geology*, 31(11):977–980, 2003a.

Isbell, J. L., Miller, M. F., Wolfe, K. L. and Lenaker, P. A. Timing of late Paleozoic glaciation in Gondwana: Was glaciation responsible for the development of Northern Hemisphere cyclothems? In Chan, M. A. and Archer, A. W., editors, *Extreme Depositional Environments: Mega End Members in Geologic Time*, volume 370, pages 5–24. Spec. Pap. Geol. Soc. Am., 2003b.

Kaplan, J. O., Bigelow, N. H., Prentice, I. C., Harrison, S. P., Bartlein, P. J., Christensen, T. R., Cramer, W., Matveyeva, N. V., McGuire, A. D., Murray, D. F., Razzhivin, V. Y., Smith, B., Walker, D. A., Anderson, P. M., Andreev, A. A., Brubaker, L. B., Edwards, M. E. and Lozhkin, A. V. Climate change and Arctic ecosystems: 2. Modeling, paleodata-model comparisons, and future projections. *Journal of Geophysical Research-Atmospheres*, 108(D19), 2003.

Levis, S., Foley, J. A. and Pollard, D. Potential high-latitude vegetation feedbacks on CO_2-induced climate change. *Geophysical Research Letters*, 26(6):747–750, 1999.

Mii, H. S., Grossman, E. L. and Yancey, T. E. Carboniferous isotope stratigraphies of North America: Implications for Carboniferous paleoceanography and Mississippian glaciation. *Geological Society of America Bulletin*, 111(7):960–973, 1999.

Mii, H. S., Grossman, E. L., Yancey, T. E., Chuvashov, B. and Egorov, A. Isotopic records of brachiopod shells from the Russian Platform - evidence for the onset of mid-Carboniferous glaciation. *Chemical Geology*, 175(1-2):133–147, 2001.

Montañez, I. P., Tabor, N. J., Niemeier, D., DiMichele, W. A., Frank, T. D., Fielding, C. R., Isbell, J. L., Birgenheier, L. P. and Rygel, M. C. CO_2-forced climate and

vegetation instability during late paleozoic deglaciation. *Science*, 315(5808):87–91, 2007.

Pollard, D. and DeConto, R. M. Modelling West Antarctic ice sheet growth and collapse through the past five million years. *Nature*, 458(7236):329–U89, 2009.

Pollard, D. and Thompson, S. L. Users' guide to the GENESIS global climate model version 1.02. *Interdisciplinary Climate Systems Section, Climate and Global Dynamics division*, page 58, 1992.

Pollard, D. and Thompson, S. L. Users' Guide to the GENESIS Global Climate Model Version 2.0. *Interdisciplinary Climate Systems Section, Climate and Global Dynamics Division*, page 93, 1995.

Rygel, M. C., Fielding, C. R., Frank, T. D. and Birgenheier, L. P. The magnitude of late Paleozoic glacioeustatic fluctuations: a synthesis. *Journal of Sedimentary Research*, 78(7-8):500–511, 2008.

Saltzman, M. R. Phosphorus, nitrogen, and the redox evolution of the Paleozoic oceans. *Geology*, 33(7):573–576, 2005.

Tabor, N. J. and Poulsen, C. J. Palaeoclimate across the Late Pennsylvanian-Early Permian tropical palaeolatitudes: A review of climate indicators, their distribution, and relation to palaeophysiographic climate factors. *Palaeogeography Palaeoclimatology Palaeoecology*, 268(3-4):293–310, 2008.

Veevers, J. J., Conaghan, P. J., Powell, C. M., Cowan, E. J., L., M. K. and Shaw, S. E. Eastern Australia. In Veevers, J. J. and Powell, C. M., editors, *Permian-Triassic Pangean Basins and Foldbelts Along the Panthalassan Margin of Gondwanaland*, volume 184, pages 11–171. Mem. Geol. Soc. Am., 1994.

Veevers, J. J. and Powell, C. M. Late Paleozoic Glacial Episodes in Gondwanaland Reflected in Transgressive-Regressive Depositional Sequences in Euramerica. *Geological Society of America Bulletin*, 98(4):475–487, 1987.

Veizer, J., Ala, D., Azmy, K., Bruckschen, P., Buhl, D., Bruhn, F., Carden, G. A. F., Diener, A., Ebneth, S., Godderis, Y., Jasper, T., Korte, C., Pawellek, F., Podlaha, O. G. and Strauss, H. Sr-87/Sr-86, delta C-13 and delta O-18 evolution of Phanerozoic seawater. *Chemical Geology*, 161(1-3):59–88, 1999.

Wanless, H. R. and Shepard, F. P. Sea level and climatic changes related to late Paleozoic cycles. *Bulletin of the Geological Society of America*, 47(5/8):1177–1206, 1936.

Wegener, A. *Die Entstehung der Kontinente und Ozeane.* Vieweg, Braunschweig, 1915.

CHAPTER II

Orbital and CO_2 forcing of late Paleozoic ice sheets

2.1 Abstract

Contrasting views of the size, duration, and history of the Gondwanan continental ice sheets have been proposed from late Paleozoic glaciological and sedimentological evidence. To evaluate these differing views, a coupled ice sheet-climate model is used to simulate continental ice sheets under a wide range of late Paleozoic orbital and pCO_2 conditions. The model experiments indicate that orbital variations at pCO_2 concentrations below 2 × preindustrial atmospheric levels (PAL; 280 ppm) produce large changes in late Paleozoic ice volume ($\sim 1.3 \times 10^8$ km^3) and sea level (20 to 245 m). Between 2 and 8 × PAL Gondwana continental ice is simulated only under the most extreme Southern Hemisphere cold summer orbit, but still produces significant ice volumes (~ 8–12×10^7 km^3). Our results highlight the important role of atmospheric CO_2 in determining the distribution, volume, and stability of late Paleozoic ice sheets, factors that ultimately impacted sea level, cyclothem deposition, and global climate, and reconcile disparate views of the Late Paleozoic Ice Age.

2.2 Introduction

The late Paleozoic ice age (LPIA) was the most severe glaciation in the Phanerozoic, spanning 60 million years (360–250 Ma; Frakes et al. (1992)) with peak ice volumes as great or greater than that during the Last Glacial Maximum (Crowley and Baum, 1991). The LPIA has long been considered a single uninterrupted glaciation (Frakes and Francis, 1988; Crowell, 1978, 1999; Veevers and Powell, 1987; Veevers et al., 1994) during which ice volume was modulated by insolation variations arising from changes in Earth's orbit (Heckel, 1990). Cyclothems, repetitive successions of marine and non-marine sediments, are often considered to be the stratigraphic signature of orbitally- controlled ice volume fluctuations. Euramerican cyclothems, deposited between the late Namurian (326 Ma) and early Kazanian (260 Ma), are estimated to represent 100 to 230 m of sea-level change (Crowell, 1999).

Recent reevaluations of the Gondwana glacial record challenge this view of large orbitally-driven ice volume variations superimposed on a long lived continental glaciation (Isbell et al., 2003a,b; Fielding et al., 2006). Rather, Isbell et al. (2003b) propose that the LPIA consisted of three distinct glacial events (Glacial I, ~375–350 Ma; Glacial II, ~315–307 Ma; and Glacial III, ~299–276 Ma). Continental glaciation was only widespread, covering much of southern Gondwana, during the final event. The complete ablation of the Glacial III ice sheets is estimated to have raised sea-level by only 50 to 115 m, depending on whether continental ice was distributed in multiple ice sheets with small aspect ratios or a single enormous ice dome Isbell et al. (2003b), an amount that is too small to have generated the accommodation space required for cyclothem deposition.

The cause of the LPIA is not certain, but was likely related to low atmospheric

$p\mathrm{CO}_2$ levels. According to the CO_2 proxy record of the last 500 million years, only the Neogene had lower $p\mathrm{CO}_2$ levels (Royer, 2006; Berner and Kothavala, 2001). Atmospheric $p\mathrm{CO}_2$ may also have been variable; Montañez et al. (2007) report late Carboniferous–middle Permian values that oscillate between $\sim$1 and $8 \times$ PAL, with low values coincident with the deposition of glaciogenic sediments on Gondwana.

Two-dimensional energy balance models (EBMs), deriving their ice estimates from summer land temperatures, have been used to investigate the possible size, sensitivities, and location of the late Paleozoic ice age (Crowley, 1994). These models indicate that Gondwana ice sheets could have reached a size similar to that of the Pleistocene glaciation (Crowley and Baum, 1991) and predict sea-level changes of 70 to 100 m citepcrowley1992. Additionally, EBMs utilizing prescribed modern Northern Hemisphere precipitation rates (modified by the Clausius-Clapeyron relation) indicate that Permo-Carboniferous ice sheets were likely sensitive to past CO_2 levels, and suggest that past changes in CO_2 are required to explain the onset and demise of continental ice sheets (Hyde et al., 1999, 2006). Atmospheric general circulation models (AGCMs) have been used to investigate the global climate response to the glaciation of Gondwana (Poulsen et al., 2007), but to our knowledge have not been used to predict past continental ice sheets.

The goal of this study is to quantify late Paleozoic ice volumes and equivalent sea level under a broad range of likely orbital and $p\mathrm{CO}_2$ values. In contrast to previous studies, we employ an AGCM (with full hydrological cycle) coupled to a 3-D ice-sheet model. Our results provide a framework for interpreting the variability in ice sheets and sea level inferred from the geological record, and help reconcile disparate views of the late Paleozoic ice age.

2.3   Model and Methods

Late Paleozoic experiments were completed using the GENESIS AGCM version 2.3 coupled to a 3-D dynamic ice sheet model. GENESIS consists of an AGCM coupled to a land-surface model with multi-layer models of vegetation, soil or land ice, and snow. The AGCM has a spectral resolution of T31 ($3.75°\times3.75°$), and 18 vertical levels. The land-surface grid has a resolution of $2°\times2°$. Sea-surface temperatures and sea ice are computed using a 50-m slab oceanic layer with diffusive heat flux (Pollard and Thompson, 1995; Thompson and Pollard, 1997).

The 3-D ice sheet model operates on a $1°\times2°$ surface grid (DeConto and Pollard, 2003). The thermo-mechanical ice-sheet model is based on the vertically integrated continuity equation for ice mass (Huybrechts, 1993; Ritz et al., 1996). The evolution of ice geometry is determined by surface mass balance, basal melting, and ice flow. Ice temperatures are predicted to account for their effect on rheology and basal sliding. The local bedrock response to ice load is a simple relaxation toward isostasy with a time constant of 5,000 years. Lithospheric flexure is modeled by linear elastic deformation. In this version of the model, ice shelves are not simulated.

To couple the climate and ice-sheet models, we use an asynchronous technique that consists of alternating AGCM and ice sheet integrations. To begin, GENESIS is integrated for 30 yrs to produce a steady-state climate. Mean monthly meteorological fields (i.e. surface air temperature, evaporation, and precipitation) from the last ten years drive the ice-sheet model. Each ice-sheet model experiment is run for 200,000 yrs, though ice-sheet equilibria are typically reached after 50,000 yrs, and predicts ice-sheet area, thickness, and isostatically adjusted continental topography. These boundary conditions are incorporated into the AGCM, which is run for an additional

20 yrs. Meteorological fields from the last ten years of this AGCM iteration drive a final 200,000 yr iteration of the ice-sheet model. In our experience, two climate-ice sheet iterations are sufficient to bring the system into equilibrium; additional iterations have little effect on the climate and ice-sheet solutions.

In total, twenty-five Sakmarian ($\sim$290 Ma) experiments were carried out with different atmospheric pCO$_2$ and orbital parameters. Experiments were developed for five different atmospheric pCO$_2$ levels: 0.5 (140 ppm), 1 (280 ppm), 2 (560 ppm), 4 (1120 ppm) and 8 (2240 ppm) $\times$ PAL. These values span the range reported by Montañez et al. (2007) for the Permo-Carboniferous. At each pCO$_2$ level five experiments were developed with different orbital settings (Figure 1). The range of orbital settings used in these experiments is based on the solar calculations of Berger and Loutre (1991) for the last ten million years and represent seasonal insolation extremes.

All other boundary conditions are identical between experiments, and were chosen where possible to represent Sakmarian conditions. The paleogeography and paleoto-pography are based on the Paleogeographic Atlas Project's reconstruction for this time interval (Ziegler et al., 1997). Because our objective is to estimate continental ice, we modified the Sakmarian paleogeography by removing any prescribed continental ice. The ocean diffusive heat flux was set to a value that provides the best simulation for the modern climate. The late Paleozoic solar luminosity was specified as 1330.3 W m^{-2}, 3% less than modern, in accordance with solar evolution models (Gough, 1981). In the absence of proxy estimates for the late Paleozoic, trace gas concentrations of CH$_4$ (0.650 ppm) and N$_2$O (0.285 ppm) were set to pre-industrial levels.

To estimate the sea-level change represented by our ice volume simulations, we

employ the methods of Crowley and Baum (1991) and Paterson (1994). The simulated global ice volume in each experiment is converted to a water equivalent (WE) assuming an ice density of 0.917 g/mL. We then estimate an isostatically adjusted sea-level equivalent (IASLE) by:

IASLE = (1-k) × WE/ocean surface area

where k has a value of 0.284 (the ratio of seawater density to oceanic lithosphere density). The isostatic adjustment approximates the response of the oceanic lithosphere to seawater loading/unloading. The Permian ocean surface area (386.4×10^6 km^2) was calculated from the Sakmarian paleogeographic reconstruction.

2.4 Results

2.4.1 CO_2 Sensitivity

Our experiments indicate that Gondwana ice volume varies significantly with atmospheric $p\mathrm{CO}_2$ (Figures 2.1 and 2.2). Under all orbital conditions, significant ice is simulated at $p\mathrm{CO}_2$ levels below 2 × PAL. At levels of 8 × PAL or higher, no continental ice is simulated even in the most favorable orbit (Figure 2.1). In our simulations, $p\mathrm{CO}_2$ controls ice volume through its influence on high-latitude surface temperature (Figure 2.3). Significant ice volumes are simulated when high-latitude surface temperatures remain below freezing through the year. At $p\mathrm{CO}_2$ levels greater than 2 × PAL, when surface temperatures exceed the melting point of ice, continental ice disappears (for example, compare Figures 1 and 3a for NHWS case (green line)). The CO_2-ice volume relationship becomes highly non-linear as temperatures exceed the freezing point because the average annual ablation rate ($\sim$0.5 to 1.0 m $^\circ$C^{-1}) is an order of magnitude greater than variations in annual snowfall.

The distribution of continental ice on Gondwana is also sensitive to atmospheric
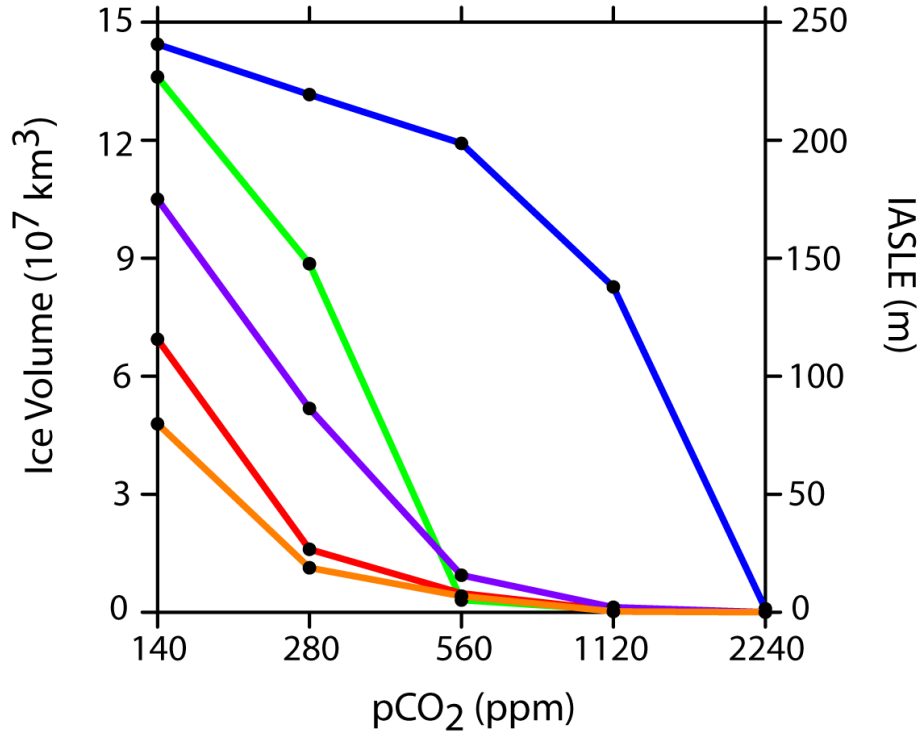
Figure 2.1: Simulated continental ice volume (10^7 km^3) and isostatically adjusted sea-level equivalent (IASLE) (m) under varying pCO$_2$ levels and orbital configurations. The filled circles represent the results from each equilibrium experiment. The various lines connect experiments with the same orbital configuration.

pCO$_2$. In all simulations, continental ice is distributed among multiple sheets on Gondwana, including south-central Africa and southern Australia, consistent with glacio-sedimentological reconstructions (Fielding et al., 2006). The location of the principal ice spreading centers coincides with those areas whose basal temperatures are sufficient to freeze the ice sheet to the surface and prohibit basal sliding. At low pCO$_2$, continental ice sheets are widespread, reaching nearly 35 °S, but are relatively thin. At higher pCO$_2$, continental ice extends to only 52 °S, but is concentrated in two ice sheets with heights over 5 km (Figure 2). This variation in icesheet thick-

ness at different CO_2 concentrations is controlled by differences in precipitation over Gondwana. The temperature increase induced by higher greenhouse gas concentrations leads to a higher saturation vapor pressure, resulting in greater atmospheric water vapor, and ultimately greater precipitation. The increase in precipitable snow accumulation (up to $\sim$20 cm yr^{-1}) at higher CO_2 levels results in greater ice sheet dome height. In these experiments, there is no direct relationship between the Sakmarian paleotopography and the spreading center locations.
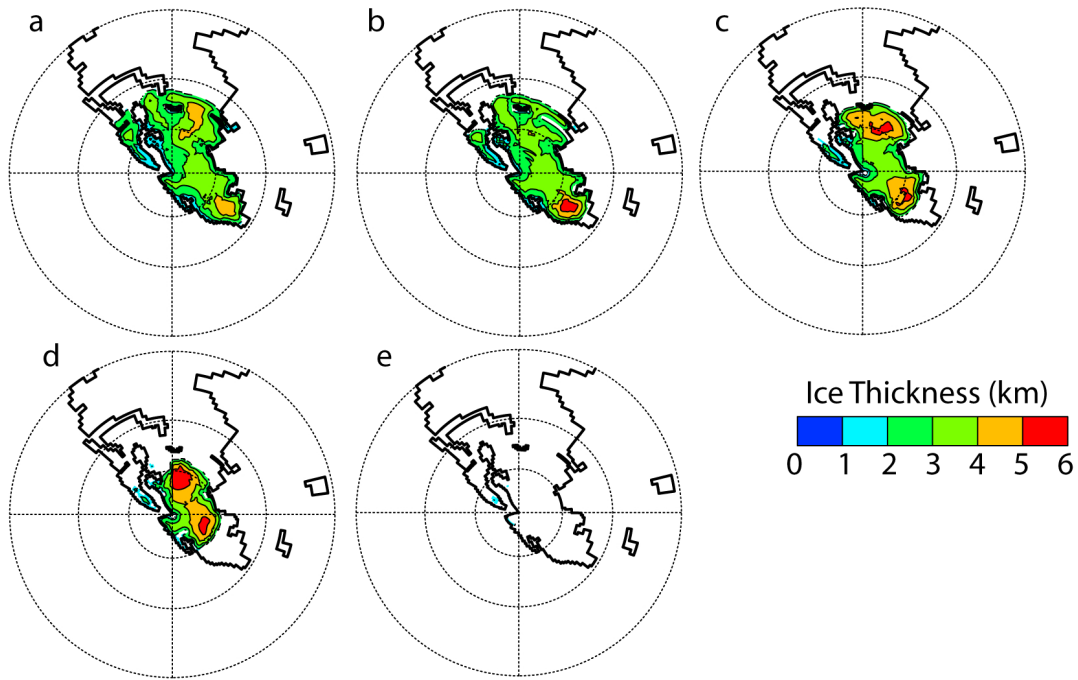
Figure 2.2: Southern Hemisphere continental ice thickness (m) response to atmospheric pCO$_2$. The orbital configuration (SHCS) is identical in all experiments. The pCO$_2$ concentration is (a) 140, (b) 280, (c) 560, (d) 1120, and (e) 2240 ppm. The dashed line in the polar projection map shows the paleolatitude with a contour interval of 30°.

2.4.2 Orbital Sensitivity

Orbital variations have a substantial impact on Pangean ice volume (Figure 2.1). In the $2 \times$ PAL CO_2 experiment, for example, global ice volume varies from 4.19×10^6 km^3 with a SHWS orbit to 1.19×10^8 km^3 with a SHCS orbit. These differences

in global ice volume mainly reflect changes in ice volume over Gondwana and are controlled by high-latitude summer insolation in the Southern Hemisphere, which varies from 520 W m^{-2} at 65 °S in the SHWS case to 375 W m^{-2} in the SHCS case. Such variations in insolation produce marked monthly average surface temperature differences (demonstrated at 65 °S in Figure 3b) and help to regulate ice-sheet growth and ablation. In orbits that minimize NH summer insolation a small continental ice sheet develops in northern Pangea, but its volume has a negligible effect on global ice volume.
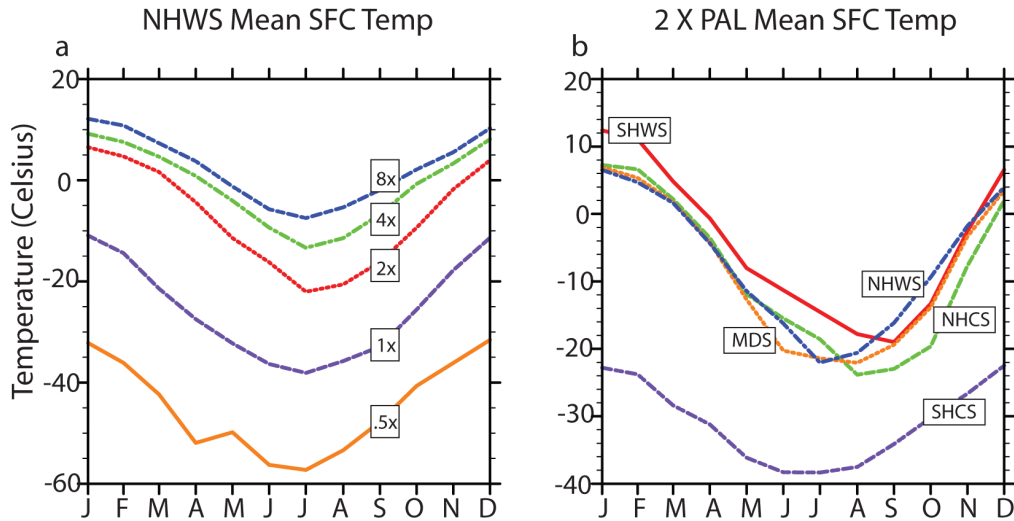
Figure 2.3: (a) Monthly average surface temperature at 65 °S for a range of pCO$_2$ concentrations during a Northern Hemisphere warm summer orbit (NHWS). (b) Monthly average surface temperature at 65 °S at $2 \times$ PAL pCO$_2$ for various orbital configurations.

2.4.3 Sea-Level Change

Atmospheric pCO$_2$ concentration and orbital variability have a significant effect on potential sea-level change in the late Paleozoic. The total ablation of simulated continental ice sheets in our experiments represents isostatically- adjusted sea-level changes of up to 245 m (Figure 2.1). Assuming that Earth's late Paleozoic orbital variability was similar to that of the last 10 million years, our results predict large

($\sim$100 m) sea-level changes on 10^4 year timescales at low pCO$_2$. However, between 2 and 4 $\times$ PAL, substantial ice develops only at the most extreme orbits. As a result, the frequency of sea-level change would have decreased, operating on 10^5 year timescales (i.e., at times of high eccentricity and low obliquity). Above 4 $\times$ PAL, large continental ice sheets are not simulated under any orbital condition, eliminating the possibility of significant glacioeustatic change.

2.5   Caveats

To our knowledge, this study is the first to estimate late Paleozoic continental ice over a large range of orbital and pCO$_2$ conditions using an AGCM. A number of simplifications and assumptions were made in the development and execution of our experiments. To predict ice volumes under a range of orbital conditions, we have simulated equilibrium ice sheets for specific orbits. In reality, equilibrium conditions were probably never attained since orbital cycles are continuous with periods that are smaller than ice-sheet equilibrium time. As such, the ice volumes attained in our low CO$_2$/CS (high CO$_2$/WS) simulations are probably too large (small) because they do not include time-marching orbital configurations. To address this issue we are developing transient simulations with complete orbital cycles.

While the paleogeography of the late Paleozoic is reasonably well understood, the paleotopography is not well constrained. Our simulations of continental ice are likely to be sensitive to continental elevations, since surface temperatures are a function of the environmental lapse rate. For this reason we used a conservative paleotopography with no elevations above 1100 m. Additionally, the model neglects marine ice (grounded below sea level) growing over continental shelves, thus preventing ice formation in embayment areas that could buttress continental ice sheets and produce

larger ice volumes.

Another potential limitation is our use of a slab ocean with modern ocean heat fluxes. The specification of a different ocean heat transports has been shown to alter the meridional surface temperature gradient in atmosphere-only GCMs of the Mesozoic (e.g., Barron et al., 1993; Poulsen et al., 1999). However this strong link between ocean heat transport and meridional temperature gradient does not exist in ocean-atmosphere GCMs (Poulsen and Huynh, 2006). Consequently, it is not clear what effect, if any, the specification of modern ocean heat fluxes has on our simulation of the late Paleozoic ice sheets. We will pursue this issue using a coupled ocean-atmosphere GCM in the future.

2.6   Discussion and Conclusion

This study provides predictions of late Paleozoic icesheet volumes under the influence of varying atmospheric $p\mathrm{CO_2}$ concentrations and orbital parameters. Below $2 \times$ PAL, significant Gondwanan ice sheets are simulated for all orbits, though large variations in ice volume exist (Figure 2.1). Above the $2 \times$ PAL threshold large-scale fluctuations in ice-sheet volume can only be expected during a SHCS orbit (Figure 2). This implies that at $p\mathrm{CO_2}$ values greater than $2 \times$ PAL glacial/inter-glacial sequences would occur only at times of maximum eccentricity and minimum obliquity. Above $4 \times$ PAL, no significant continental ice is simulated.

The results presented here are broadly consistent with previous late Paleozoic modeling studies (Crowley and Baum, 1991; Hyde et al., 1999; Herrmann et al., 2003). Although our simulations predict multiple domes of ice, our maximum ice volume ($\sim 1.44 \times 10^8$ km^3) is similar to the 1.5×10^8 km^3 reported for the Carboniferous by Hyde et al. (1999). However, our orbital sensitivity experiments indicate

that ice volumes of this extent would have endured for no more than $\sim 10^4$ yrs under maximum SHWS insolation values. Our equivalent sea-level change estimates are approximately in line with estimates of 45 to 190 m for the Carboniferous (Crowley and Baum, 1991). Importantly, our IASLE results indicate that the magnitude and frequency of sea-level change would have been very sensitive to the paleo-pCO$_2$ with maximum sea-level changes of ~ 200 m at ~ 560 ppm CO$_2$.

The variability of ice-sheet volume has profound implications for late Paleozoic sea-level change and cyclothem deposition. Cyclothems have previously been interpreted to represent at least 100 m of sea-level change (Crowell, 1999). Our results indicate that at pCO$_2$ concentrations at and below 4 × PAL, cyclothem deposition would have been possible due to the orbitally driven waxing and waning of continental ice sheets (Figure 2.1). Above 4 × PAL, cyclothem deposition would have ceased due to shrinking ice volumes (Figure 2.2); a prediction borne out by the disappearance of late Paleozoic cyclothems in the Kazanian (Crowell, 1978; Veevers and Powell, 1987) and coincident with rising atmospheric pCO$_2$ (Montañez et al., 2007). Under these pCO$_2$-cyclothem thresholds we envision a late Paleozoic with active cyclothem deposition, similar to the glaciation model of Frakes et al. (1992) while CO$_2$ remained at and below 4 × PAL. Above 4 × PAL, cyclothem deposition could not have been caused by glacioeustasy, consistent with Isbell et al. (2003b).

In summary, the results presented here indicate persistent Gondwana glaciation below 2 × PAL, and episodic Gondwanan glaciation up to 8 × PAL. These theoretical thresholds in conjunction with late Paleozoic proxy CO$_2$ data indicate that both the icehouse-greenhouse transition of the Permo-Carboniferous and the dynamic nature of orbital scale climate change were most likely the consequence of changes in greenhouse gas concentrations.

2.7 Acknowledgments

Bibliography

Barron, E. J., Peterson, W. H., Pollard, D. and Thompson, S. Past Climate and the Role of Ocean Heat-Transport - Model Simulations for the Cretaceous. *Paleoceanography*, 8(6):785–798, 1993.

Berger, A. and Loutre, M. F. Insolation Values for the Climate of the Last 10,000,000 Years. *Quaternary Science Reviews*, 10(4):297–317, 1991.

Berner, R. A. and Kothavala, Z. GEOCARB III: A revised model of atmospheric CO_2 over phanerozoic time. *American Journal of Science*, 301(2):182–204, 2001.

Crowell, J. C. Gondwanan Glaciation, Cyclothems, Continental Positioning, and Climate Change. *American Journal of Science*, 278(10):1345–1372, 1978.

Crowell, J. C. *Pre-MesoMesozoic ice ages: Their bearing on understanding the climate system*, volume 192. Mem. Geol. Soc. Am., Boulder, CO, 1999.

Crowley, T. J. Pangean climates. In Klein, G. D., editor, *Pangea: Paleoclimate, Tectonics, and Sedimentation During Accretion, Zenith, and Breakup of a Supercontinent*, volume 288, pages 25–39. Spec. Pap. Geol. Soc. Am., 1994.

Crowley, T. J. and Baum, S. K. Estimating Carboniferous Sea-Level Fluctuations from Gondwanan Ice Extent. *Geology*, 19(10):975–977, 1991.

DeConto, R. M. and Pollard, D. A coupled climate-ice sheet modeling approach to the Early Cenozoic history of the Antarctic ice sheet. *Palaeogeography Palaeoclimatology Palaeoecology*, 198(1-2):39–52, 2003.

Fielding, C. R., Bann, K. L., Maceachern, J. A., Tye, S. C. and Jones, B. G. Cyclicity in the nearshore marine to coastal, Lower Permian, Pebbley Beach Formation, southern Sydney Basin, Australia: a record of relative sea-level fluctuations at the close of the Late Palaeozoic Gondwanan ice age. *Sedimentology*, 53(2):435–463, 2006.

Frakes, L. A. and Francis, J. E. A Guide to Phanerozoic Cold Polar Climates from High-Latitude Ice-Rafting in the Cretaceous. *Nature*, 333(6173):547–549, 1988.

Frakes, L. A., Francis, J. E. and Syktus, J. I. *Climate Modes of the Phanerozoic*. Cambridge Univ. Press, Cambridge, U.K., 1992.

Gough, D. O. Solar Interior Structure and Luminosity Variations. *Solar Physics*, 74(1):21–34, 1981.

Heckel, P. Evidence for global (glacial-eustatic) control over upper Carboniferous (Pennsylvanian) cyclothems in mid-continent North America. In Hardman, R. F. P. and Brooks, J., editors, *Tectonic Events Responsible for Britains Oil and Gas Reserves*, volume 55, pages 35–47. Geol. Soc. Spec. Publ, 1990.

Herrmann, A. D., Patzkowsky, M. E. and Pollard, D. Obliquity forcing with 8-12 times preindustrial levels of atmospheric $p\mathrm{CO_2}$ during the Late Ordovician glaciation. *Geology*, 31(6):485–488, 2003.

Huybrechts, P. Glaciological modelling of the Late Cenozoic East Antarctic ice sheet: Stability or dynamism? *Geogr. Ann. Ser. A*, 75:221–238, 1993.

Hyde, W. T., Crowley, T. J., Tarasov, L. and Peltier, W. R. The Pangean ice age: studies with a coupled climate-ice sheet model. *Climate Dynamics*, 15(9):619–629, 1999.

Hyde, W. T., Grossman, E. L., Crowley, T. J., Pollard, D. and Scotese, C. R. Siberian glaciation as a constraint on Permian-Carboniferous CO_2 levels. *Geology*, 34(6):421–424, 2006.

Isbell, J. L., Lenaker, P. A., Askin, R. A., Miller, M. F. and Babcock, L. E. Reevaluation of the timing and extent of late Paleozoic glaciation in Gondwana: Role of the Transantarctic Mountains. *Geology*, 31(11):977–980, 2003a.

Isbell, J. L., Miller, M. F., Wolfe, K. L. and Lenaker, P. A. Timing of late Paleozoic glaciation in Gondwana: Was glaciation responsible for the development of Northern Hemisphere cyclothems? In Chan, M. A. and Archer, A. W., editors, *Extreme Depositional Environments: Mega End Members in Geologic Time*, volume 370, pages 5–24. Spec. Pap. Geol. Soc. Am., 2003b.

Montañez, I. P., Tabor, N. J., Niemeier, D., DiMichele, W. A., Frank, T. D., Fielding, C. R., Isbell, J. L., Birgenheier, L. P. and Rygel, M. C. CO_2-forced climate and vegetation instability during late paleozoic deglaciation. *Science*, 315(5808):87–91, 2007.

Paterson, W. S. B. *The Physics of Glaciers*. Pergamon, Oxford, U.K., 1994.

Pollard, D. and Thompson, S. L. Use of a Land-Surface-Transfer Scheme (Lsx) in a Global Climate Model - the Response to Doubling Stomatal-Resistance. *Global and Planetary Change*, 10(1-4):129–161, 1995.

Poulsen, C. J., Barron, E. J., Johnson, C. and Fawcett, P. Links between major climatic factors and regional oceanic circulation in the mid-Cretaceous. In Barrera,

E. and Johnson, C. C., editors, *Evolution of the Cretaceous Ocean-Climate System*, volume 332, pages 73–90. Spec. Pap. Geol. Soc. Am., 1999.

Poulsen, C. J. and Huynh, T. T. Paleoceanography of the Mesozoic Pacific: A perspective from climate model simulations. In Haggart, J., Enkin, R. J. and Monger, J. H., editors, *Paleogeography of the North American Cordillera: Evidence against Large-Scale Displacements*, volume 46, pages 13–27. Geol. Assoc. Can. Spec. Pap., 2006.

Poulsen, C. J., Pollard, D., Montañez, I. P. and Rowley, D. Late Paleozoic tropical climate response to Gondwanan deglaciation. *Geology*, 35(9):771–774, 2007.

Ritz, C., Fabre, A. and Letreguilly, A. Sensitivity of a Greenland ice sheet model to ice flow and ablation parameters: Consequences for the evolution through the last climatic cycle. *Climate Dynamics*, 13(1):11–24, 1996.

Royer, D. L. CO_2-forced climate thresholds during the Phanerozoic. *Geochimica Et Cosmochimica Acta*, 70(23):5665–5675, 2006.

Thompson, S. L. and Pollard, D. Greenland and Antarctic mass balances for present and doubled atmospheric CO_2 from the GENESIS version-2 global climate model. *Journal of Climate*, 10(5):871–900, 1997.

Veevers, J. J., Conaghan, P. J., Powell, C. M., Cowan, E. J., L., M. K. and Shaw, S. E. Eastern Australia. In Veevers, J. J. and Powell, C. M., editors, *Permian-Triassic Pangean Basins and Foldbelts Along the Panthalassan Margin of Gondwanaland*, volume 184, pages 11–171. Mem. Geol. Soc. Am., 1994.

Veevers, J. J. and Powell, C. M. Late Paleozoic Glacial Episodes in Gondwanaland Reflected in Transgressive-Regressive Depositional Sequences in Euramerica. *Geological Society of America Bulletin*, 98(4):475–487, 1987.

Ziegler, A. M., L., H. M. and Rowley, D. B. Permian world topography and climate. In Martini, I. P., editor, *Late Glacial and Postglacial Environmental Changes-Quaternary*, pages 111–146. Oxford Univ. Press, 1997.

CHAPTER III

Paradox of late Paleozoic glacioeustasy

3.1 Abstract

Models of Euramerican cyclothem deposition invoke orbitally driven glacioeustasy
to explain widespread cyclic marine and nonmarine late Paleozoic sedimentary se-
quences. Base-level fluctuations of $\sim$100+ m have been estimated for the deposition
of mid-continent North American subpycnoclinal black shales, subaerial exposure
relief of algal bioherms in the Sacramento Mountains, and Russian Platform carbon-
ates. Similar to the Pleistocene, these glacioeustatic fluctuations are thought to be
driven by variations in orbital parameters. To evaluate this hypothesis, a coupled
general circulation model-ice sheet model was used to simulate the effects of both
transient orbital changes and variable atmospheric pCO$_2$ concentrations on late Pa-
leozoic continental ice sheets. In our model, large continental ice sheet inception is
simulated at and below pCO$_2$ levels of 280 ppm. Model results predict that while
changing orbital parameters results in dynamic ice sheet behavior, the maximum
orbitally induced sea-level fluctuation is $\sim$25 m. The model also demonstrates that
the complete ablation of ice sheets formed at 280 ppm ($\sim$7.9$\times$10^7 km^3, sea-level

change 135 m) requires an increase in atmospheric pCO_2 to levels greater than 2240 ppm. These results present a potential paradox: while our model is able to simulate widespread Gondwanan glaciation, it is unable to reproduce significant orbitally driven glacioeustatic fluctuations without very large magnitude carbon cycle perturbations. We discuss possible solutions to this paradox.

3.2 Introduction

The late Paleozoic ice age was Earth's most extensive glaciation of the past 542 Ma. Episodic continental scale glaciation spanned a 60 Ma period (360-250 Ma ago) and, at times, ice sheets extended from the South Pole to the present-day latitude of Buenos Aires, Argentina ($\sim$35 °S; Isbell et al. (2003); Crowley and Baum (1992). The severity and persistence of this glaciation are attributed to two main factors: (1) the coalescence of Africa, Antarctica, Australia, India, and South America about the austral pole, and (2) low atmospheric pCO_2 concentrations (Kutzbach and Gallimore, 1989; Crowley et al., 1989). The cumulative effects of a high-latitude landmass, extreme continentality, and reduced greenhouse gases primed the late Paleozoic paleoenvironment for glaciation.

The ice sheets of Gondwana left not only direct geological evidence of continental glaciation, but also indirect sedimentary signatures of their waxing and waning. The presence of widespread Gondwanan glacial basins and temporally coincident Laurentian cyclic sedimentary sequences has been used to infer that late Paleozoic depositional environments were largely controlled by glacioeustasy (Crowell, 1978). Glacioeustatic amplitudes are mainly based on depositional base-level fluctuations: (1) coastal onlap fluctuations across Laurentia indicate 100-200 m of sea-level change

(Ross and Ross, 1987), (2) subaerial exposure surfaces of southwestern North American algal bioherms indicate 80-100+ m (Soreghan and Giles, 1999), and (3) mid-continent North American subpycnoclinal black core shales require 100 m of sea-level change (Heckel, 1977). In addition, stable isotopic (δ^{18}O) analyses of conodont apatite extracted from shales of mid-continent North America indicate greater than 120 m of glacioeustatic change (Joachimski et al., 2006). Heckel (1986), building on the work of Wanless and Shepard (1936), linked the glacioeustatic cyclicity of Euramerican sedimentary deposition systems to orbital insolation changes with periods corresponding to Earth's precession, obliquity, and eccentricity.

The goal of this study is to test Heckel (1986) hypothesis that late Paleozoic orbital insolation changes drove cyclic sea-level fluctuations. To that end, we use a climate-ice sheet model to (1) simulate ice sheets whose volume and extent are in agreement with available geologic evidence, (2) quantify the glacioeustatic fluctuations induced by orbital insolation changes on the ice sheets, and (3) determine the effect of a range of pCO$_2$ concentrations on the mass balance of orbitally forced ice sheets.

3.3 Methods

To determine the effects of orbital insolation changes on late Paleozoic ice sheets, we designed a series of transient experiments using an atmospheric general circulation model (GCM), GENESIS version 3.0 (Pollard and Thompson, 1995; Thompson and Pollard, 1997), coupled to a three-dimensional ice sheet model. All experiments include a Sakmarian ($\sim$290 Ma ago) paleogeography (Ziegler et al., 1997) with average topographic elevations over Gondwana of $\sim$400 m. The experiments include a

time-evolving orbital scheme (Figure 3.1) that is based on the Pliocene-Pleistocene range and variation of precession, obliquity, and eccentricity (Berger and Loutre, 1991). The period of each orbital parameter has been approximated (20, 40, and 80 ka) for computational efficiency, and each experiment has been run for the equivalent of four eccentricity cycles, or 320 ka. To encourage Southern Hemisphere ice sheet formation, the orbital regime cycles through four Southern Hemisphere cold summer orbits (SHCS; highest eccentricity, lowest obliquity, summer at aphelion). Using a procedure similar to DeConto and Pollard (2003), orbitally forced GCM meteorological conditions are asynchronously coupled to the ice sheet model every 5 ka (see Appendix 3.7.1). The resulting simulated ice sheet is fed back into the GCM and the orbital parameters are updated prior to each subsequent GCM-ice sheet iteration. Net sea-level changes are determined via a simple ice volume-mass balance-seawater isostasy calculation. To determine late Paleozoic ice sheet-$p\text{CO}_2$ initiation thresholds, simulations utilizing our orbital regime were tested on a range of atmospheric $p\text{CO}_2$ concentrations (140, 280, 560, and 1120 ppm) consistent with proxy estimates (Montañez et al., 2007).

3.4   Results

Large Gondwanan continental ice sheets are developed and sustained at $p\text{CO}_2$ levels of 280 ppm and below (Figure 3.2A). These low $p\text{CO}_2$ ice sheets gain most of their volume in a single eccentricity cycle (80 ka), but ice continues to accumulate at reduced rates throughout the simulations. In the 140 ppm simulation, permanent ice is predicted in both the Northern and Southern Hemispheres, with Southern Hemisphere (SH) ice sheets extending north from the austral pole to the present-day latitude of Buenos Aires (35 °S). Under 280 ppm $p\text{CO}_2$ concentrations, global
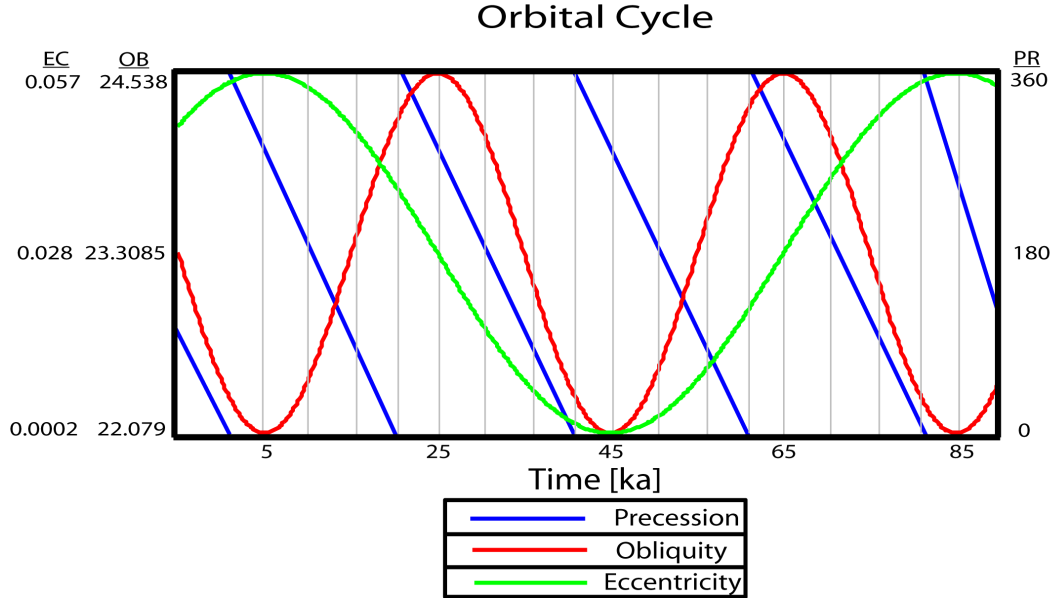
Figure 3.1: Orbital parameter regime used in coupled general circulation model-ice sheet model simulations.Precession (PR), obliquity (OB), and eccentricity (EC) have sinusoidal periods of 20, 40, and 80 ka, respectively (after DeConto and Pollard (2003), and their values are based on Plio-Pleistocene maxima and/or minima (Berger and Loutre, 1991). Ice volumes are predicted at 5 ka intervals (as indicated by vertical lines), over four orbital cycles, or 320 ka (for complete methods description, see Appendix 3.7.1).

ice sheet volume ($\sim 7.9 \times 10^7$ km^3) is similar to estimates of Last Glacial Maximum ice volume, with continental ice sheets extending northward to $\sim$55 °S (present-day latitude of Cape Horn). The continental ice sheets in both the 140 and 280 ppm $p\mathrm{CO_2}$ scenarios form from the coalescence of multiple deposition centers whose maximum heights are in excess of 4 km (Figure 3.3), similar to modern-day Antarctic ice sheet elevations.

At $p\mathrm{CO_2}$ concentrations of 560 ppm and above, only small coastal ice caps are sustained, and total ice volumes are less than 10% of the 140 and 280 ppm simulations. The ice-volume history of the 560 ppm case is notable. At this $p\mathrm{CO_2}$ level, a small ice sheet (Figure 3.3D; $\sim 2.0 \times 10^7$ km^3) forms rapidly (Figure 3.2A), but then largely disappears after it passes through the maximum-insolation Southern Hemisphere orbit at $\sim$70 and $\sim$90 ka. The ablation of this continental ice sheet is rapid,
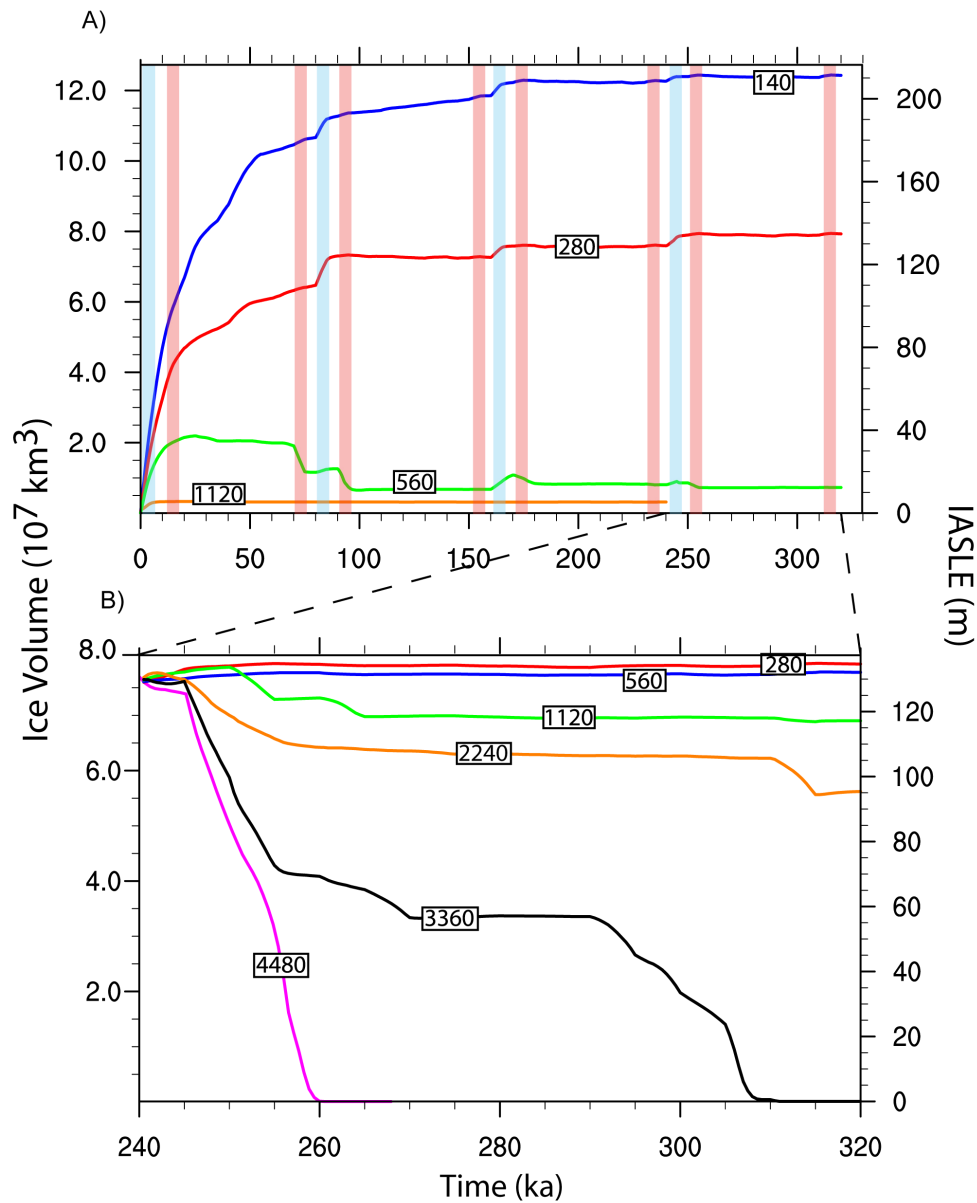
Figure 3.2: A: Time series of simulated ice volume and isostatically adjusted sea-level equivalent (IASLE) variations at $p\mathrm{CO}_2$ levels of 140, 280, 560, and 1120 ppm. Blue highlights represent time intervals of Southern Hemisphere cold summer orbits and red highlights represent time intervals of the warmest Southern Hemisphere summer orbits. After approximately one orbital cycle (80 ka), 140 and 280 ppm ice sheet volumes have achieved quasi-equilibrium. Subsequent orbitally induced ice volume and IASLE variations are minimal. B: Simulations initiated with the 280 ppm quasi-equilibrium ice sheet. Concentrations of $p\mathrm{CO}_2$ are increased to 560, 1120, 2240, 3360, and 4480 ppm. Significant ice sheet ablation does not occur until $p\mathrm{CO}_2$ levels of 2240 are attained.

but incomplete. The last vestige of 560 ppm ice is restricted to small, permanent, coastal ice caps (Figure 3.3C), whose maintenance is ensured by their proximity to moisture-laden maritime air masses and increased coastal accumulation rates. Farther inland, the effects of continentality (reduced moisture and more severe seasonal temperatures) push ablation rates beyond accumulation rates.

The dynamic response of continental ice sheet volume to our prescribed transient orbital insolation variations is modest. After approximately one orbital cycle (80 ka), ice-volume quasi-equilibrium is established and subsequent orbitally driven glacioeustatic changes are small (Figure 3.2A). At low pCO_2 levels (140 and 280 ppm), orbitally induced insolation variations produce maximum sea-level changes of ~10 m during one orbital cycle (80 ka). Greater glacioeustatic change is simulated during the 560 ppm ice sheet collapse at ~70 ka (green line in Figure 3.2A), though this event is isolated. Within ~60 ka the 560 ppm ice sheet loses 1.5×10^7 km^3 of ice, resulting in ~25 m of sea-level rise. At lower pCO_2 levels the large ice sheets are less sensitive to orbital insolation changes due to the effects of both the ice-albedo feedback and the ice-elevation feedback, which both work to produce lower average surface temperatures.

For ice initiation purposes, our orbital scheme was slightly biased toward cold Southern Hemisphere summers and did not include a true Southern Hemisphere warm summer orbit (SHWS; highest eccentricity, highest obliquity, summer at perihelion). To verify that the lack of orbitally induced ice sheet ablation was not due to the absence of this orbital configuration, we incorporated a SHWS orbit into each of our pCO_2 simulations. Each experiment was initialized with a transient, equilibrium volume ice sheet that corresponds to its pCO_2 level. The results of these experiments indicate that during a SHWS orbit, continental ice sheets simulated at 140 and 280

ppm slightly increase in size (0.4% and 0.9%), while the ice caps simulated at 560 ppm decrease in size (-13%).
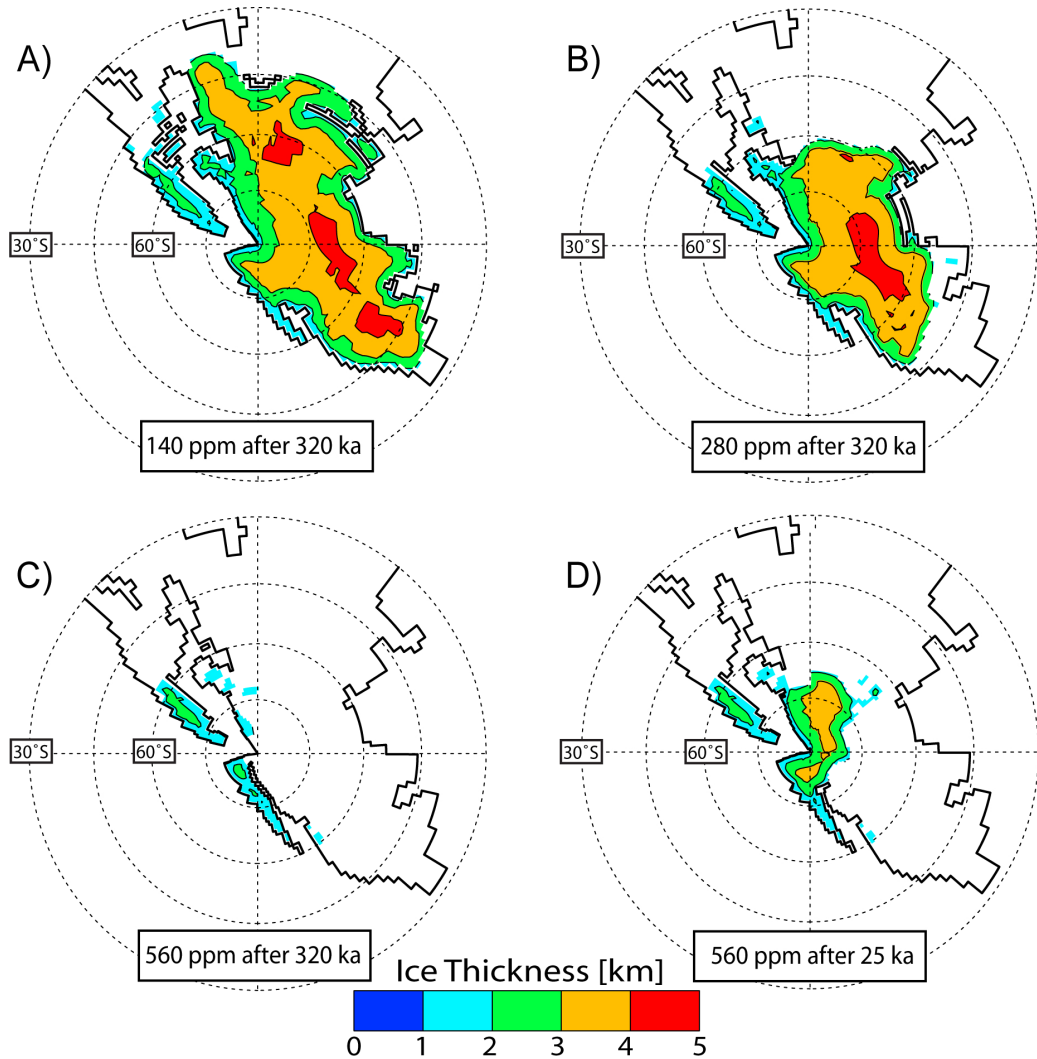
Figure 3.3: Simulated late Paleozoic Southern Hemisphere continental ice extent. Quasi-equilibrium ice thicknesses, representing state of ice sheets after 320 ka of integration, are plotted. A: 140 ppm $p\mathrm{CO}_2$. B: 280 ppm $p\mathrm{CO}_2$. C: 560 ppm $p\mathrm{CO}_2$. D: Ice sheet thickness for 560 ppm case after 25 ka, just prior to ice sheet collapse (see discussion in Results section in text for description).

The failure of orbital variations alone to induce high-amplitude glacioeustatic changes suggests that similar to the Pleistocene, orbital changes were linked to the carbon cycle through a positive feedback. In the Pleistocene, greenhouse gas concentrations have been shown to vary with glacial-interglacial cycles (Petit et al., 1999). Carbon isotopic evidence of late Paleozoic atmospheric $p\mathrm{CO}_2$ levels is sparse,

but proxy data point to variations of 1–8 × preindustrial levels throughout the late Paleozoic (Montañez et al., 2007; Grossman et al., 2008). To determine if these observed changes in $p\text{CO}_2$ concentrations, coupled with our time-marching orbital regime, could produce the glacioeustatic changes inferred from cyclothem deposits, we submitted the 280 ppm quasi-equilibrium ice sheet ($\sim$7.9×10^7 km^3) to a range of increased atmospheric $p\text{CO}_2$ concentrations (i.e., 560, 1120, 2240, 3360, and 4480 ppm). Appreciable ice-volume changes occur at $p\text{CO}_2$ concentrations in excess of 2240 ppm (Figure 3.2B). Increases in $p\text{CO}_2$ from the 280 ppm base level to 3360 and 4480 ppm led to the rapid collapse ($\sim$70 and 20 ka) of the ice sheet and $\sim$135 m of sea-level rise. A smaller $p\text{CO}_2$ increase, to 2240 ppm, reduced the ice volume by 26% and provided $\sim$40 m of sea-level change within a single orbital cycle (80 ka). Lesser increases in $p\text{CO}_2$ concentrations (less than 2240 ppm) had little effect on ice volume and eustasy (Figure 3.2B).

The CO_2 thresholds can be understood by estimating the greenhouse gas forcing required for high-latitude continental temperatures on the ice sheet to reach the melting point. Greenhouse gas forcing is a nonlinear value, which increases logarithmically as $p\text{CO}_2$ levels exceed a reference value (in our case 280 ppm). Increased radiative forcing, in turn, increases global temperatures and can have profound consequences for ice sheet longevity if the melting threshold is surmounted. In our experiments, average Southern Hemisphere summer (December, January, and February) surface temperatures at 65 °S are -10.15 °C for the 280 ppm ice sheet, indicating that at least 10 °C of warming is necessary to induce ice sheet ablation. In our experiments, 10 °C of greenhouse gas-induced warming occurs at 65 °S when $p\text{CO}_2$ concentrations rise above 2240 ppm (See Appendix, Supplementary Figure 3.7.1).

3.5 Discussion and Conclusions

Our simulation of late Paleozoic glacial conditions presents a paradox. While our simulation of large (greater than 100 m sea-level equivalent) continental ice sheets is in good agreement with sedimentological evidence of Gondwanan glaciation, our orbitally driven ice-volume changes are $\sim$10 m, much smaller than the late Paleozoic glacioeustatic variations implied by both cyclothems and isotopic analyses. The absence of significant continental-scale ice sheet ablation in the face of changing orbital insolation poses a significant challenge to our current understanding of late Paleozoic ice sheet dynamics.

The waxing and waning of Northern Hemisphere ice sheets throughout the Pleistocene is thought to have produced sea-level changes of magnitudes ($\sim$120 m; Fairbanks (1989)) similar to those of the late Paleozoic. The cause of Pleistocene glacial-interglacial cycles is still debated, but is generally thought to be due to a combination of orbitally controlled insolation forcing and greenhouse gas fluctuations. Measurements from Antarctic ice cores record $p\mathrm{CO_2}$ concentration changes of $\pm$100 ppm that are nearly coincident with the advance and retreat of Northern Hemisphere Pleistocene ice sheets (Petit et al., 1999). Glacial-interglacial variations in greenhouse gas concentrations are thought to originate from feedback mechanisms linked to orbitally forced high-latitude climate change (Sigman and Boyle, 2000). If this is the case, it is likely that the same feedback mechanisms were operating during the late Paleozoic ice age. Our modeling results, however, indicate that Pleistocene-magnitude greenhouse gas variations would have little effect on late Paleozoic glacioeustasy. Rather, $p\mathrm{CO_2}$ increases in excess of 2000 ppm were required to cause substantial melting of Gondwanan ice sheets.

Unlike the Pleistocene, late Paleozoic pCO_2 levels are not well constrained. The carbon cycling models of Berner and Kothavala (2001) predict low pCO_2 in the late Paleozoic, but the temporal resolution (10 Ma) does not approach orbital periodicities. Carbon isotopic evidence ($\delta^{13}C$), derived from fossil organic matter and pedogenic carbonates, indicates that late Paleozoic pCO_2 was highly variable (±2000 ppm) throughout the late Carboniferous and into the middle Permian; however, the temporal resolution of this record remains coarse (Montañez et al., 2007; Grossman et al., 2008). Furthermore, a mechanism by which atmospheric pCO_2 concentrations could repeatedly fluctuate by 2000 ppm over orbital time scales is not known. The only documented mechanism for producing rapid, large (750–26,000 ppm; Pagani et al. (2006)) increases in atmospheric carbon is the dissolution of methane clathrates during the Paleocene-Eocene thermal maximum. However, the long recharge rate of clathrates would prevent repeated discharges on orbital time scales (Dickens et al., 1995).

Previous climate modeling studies have suggested that changes in greenhouse gas concentrations were not necessary to provide large glacioeustatic fluctuations throughout the late Paleozoic. Simulations using an energy balance model (EBM) coupled to an ice sheet model indicate that orbital insolation variations alone can produce repeated ∼100 m sea-level fluctuations (Hyde et al., 1999). We cannot say with certainty why our results differ from those using an EBM; however, we suspect that differences in the paleoboundary conditions and/or the treatment of ablation and precipitation rates in the calculation of mass balance over the ice sheet might be responsible. For example, unlike our model where precipitation over Gondwana is explicitly calculated, EBM precipitation rates are based on prescribed modern precipitation rates (Hyde et al., 1999). Predictions of equilibrium ice sheets made

using GCM-ice sheet models with fixed (nontransient) orbital conditions have also been used to infer large late Paleozoic glacioeustatic fluctuations (of as much as 245 m; Horton et al. (2007)). However, our new results indicate that these estimates are too large. The reason is straightforward: in the fixed-orbit experiments, there is no preexisting ice sheet to influence the final mass balance. In contrast, in our transient experiments, the preexisting ice sheet (simulated during the previous orbital step) has a substantial influence on local conditions due to temperature-elevation and ice-albedo feedbacks. Orbitally driven insolation changes are not large enough to overcome these local ice sheet effects; consequently, orbital changes produce only small ice-volume fluctuations.

The lack of large orbitally induced ice-volume changes and the improbability of repeated 2000 ppm atmospheric $p\text{CO}_2$ fluctuations have potential implications for the late Paleozoic climate system and for ice sheet dynamics in general. Using the Pleistocene as an analogue, and recognizing that our model demonstrates sufficient ice sheet volume growth, but insufficient ice sheet ablation, may indicate model limitations. Outside of orbitally driven greenhouse gas feedbacks, the glacial-interglacial cyclicity observed in the Pleistocene is thought to have been aided by feedbacks that destabilized large portions of the ice sheet, leading to rapid collapse. Mechanisms theorized to have led to rapid Pleistocene ice sheet collapse include subglacial sediment destabilization (MacAyeal, 1993; Clark and Pollard, 1998), reorganization of the ocean's thermohaline circulation (Maslin et al., 2001), and the removal of coastal sea-ice buttressing (Rignot and Thomas, 2002). None of these mechanisms is explicitly accounted for in our simulations, and therefore may prove integral to the accurate representation of late Paleozoic glacial-interglacial cycles. In the future we intend to test the effects of dynamic ocean currents, sea-ice buttressing, and

basal sliding sensitivity to determine the most probable explanation for observed late Paleozoic glacioeustatic amplitudes and to explore the applicability of Pleistocene feedback mechanisms to the late Paleozoic ice age. Alternatively, our lack of large glacioeustatic change could also indicate that the Pleistocene Northern Hemisphere glacial-interglacial cycles may not be a good analogue for late Paleozoic glaciation. Gondwanan ice sheets occupied higher land-based latitudes ($\sim$40–90 °S) than the waxing and waning Northern Hemisphere ice sheets ($\sim$40–75 °N) of the Pleistocene. The Pleistocene East Antarctic Ice Sheet, which is land based at higher latitudes ($\sim$65–90 °S) and is thought to have varied very little during Northern Hemisphere glacial-interglacial phases (Denton et al., 1993), may be a more appropriate analogue, in which case nonuniformitarian processes (e.g., very large perturbations of the carbon cycle) may have driven late Paleozoic glacioeustatic fluctuations. The resolution of this late Paleozoic paradox is fundamental for understanding the processes that drive glacioeustatic cyclicity and late Paleozoic climate change (Poulsen et al., 2007; Peyser and Poulsen, 2008), and is relevant to our current understanding of the climate-cryosphere system.

3.6 Acknowledgements

3.7 Appendix

3.7.1 Model and Methods

Late Paleozoic experiments were completed using the GENESIS atmospheric general circulation model (AGCM) version 3.0 coupled to a three-dimensional dynamic ice-sheet model. GENESIS consists of an AGCM coupled to a land-surface model with multi-layer models of vegetation, soil or land ice, and snow. The AGCM has a spectral resolution of T31 ($3.75° \times 3.75°$) and 18 vertical levels. The land-surface grid has a resolution of $2 \times 2°$. Sea-surface temperatures and sea ice are computed using a 50-m slab oceanic layer with diffusive heat flux (Pollard and Thompson, 1995; Thompson and Pollard, 1997). The thermo-mechanical ice-sheet model operates on a $1 \times 2°$ surface grid (DeConto and Pollard, 2003), and is based on the vertically integrated continuity equation for ice mass (Huybrechts, 1993; Ritz et al., 1996). The evolution of ice geometry is determined by surface mass balance, basal melting, and ice flow. Ice temperatures are predicted to account for their effect on rheology and basal sliding. The time step of the ice-sheet model is one year. The local bedrock response to ice load is a simple relaxation toward isostasy with a time constant of 5,000 years. Lithospheric flexure is modeled by linear elastic deformation. In this version of the model, ice shelves are not simulated.

For the purpose of this study, we have simplified the periods of each orbital parameter such that eccentricity, obliquity, and precessional periods occur every 80, 40, and 20 ka, respectively (Figure 4.1; DeConto and Pollard (2003)). To couple the climate and ice-sheet models, we use an asynchronous technique that consists of alternating AGCM and ice-sheet integrations. To begin, GENESIS is integrated with

specified orbital conditions (Figure 3.1) for 30 yrs to produce a steady-state climatology. Mean monthly meteorological fields (i.e. surface air temperature, evaporation, and precipitation) from the last ten years of the GENESIS run are then used to drive the ice-sheet model. Each ice-sheet model experiment is run for 5,000 yrs and predicts ice-sheet area, thickness, and isostatically adjusted continental topography. These new boundary conditions and updated orbital conditions are incorporated into the subsequent AGCM iteration. After the initial iteration, the AGCM is run in 15 yr segments and the meteorological fields from the last ten years are passed to the ice-sheet model. For each experiment, this scheme is repeated 48 times representing 320 ka and 4 eccentricity cycles.

Experiments were developed for four different atmospheric pCO_2 levels: 0.5 (140 ppm), 1 (280 ppm), 2 (560 ppm), and 4 (1120 ppm) $\times$ PAL. The $4 \times$ PAL experiment was discontinued after $\sim$240 ka due to the lack of significant continental ice volume. These CO_2 values were chosen to span the range of late Paleozoic pCO_2 reported by Montañez et al. (2007).

Besides pCO_2, all other boundary conditions are identical between experiments, and were chosen where possible to represent Sakmarian conditions. The paleogeography and paleotopography are based on the Paleogeographic Atlas Project's reconstruction for this time interval (Ziegler et al., 1997). Because our objective is to estimate continental ice, we modified the Sakmarian paleogeography by removing any prescribed continental ice. The ocean diffusive heat flux was set to a value that provides the best simulation for the modern climate. The late Paleozoic solar luminosity was specified as 1330.3 W m^{-2}, 3% less than modern, in accordance with solar evolution models (Gough, 1981). The range of orbital settings used in these experiments is based on the solar calculations of Berger and Loutre (1991) for the last

ten million years. In the absence of proxy estimates for the late Paleozoic, trace gas concentrations of CH_4 (0.650 ppm) and N_2O (0.285 ppm) were set to pre-industrial levels. To estimate the sea-level change represented by our ice volume simulations, we employ the methods of Crowley and Baum (1991) and Paterson (1994). The simulated global ice volume in each experiment is converted to a water equivalent (WE) assuming an ice density of 0.917 g/mL. We then estimate an isostatically adjusted sea-level equivalent (IASLE) by:

IASLE = (1-k) × WE/ocean surface area

where k has a value of 0.284 (the ratio of seawater density to oceanic lithosphere density). The isostatic adjustment approximates the response of the oceanic lithosphere to seawater loading/unloading. The Permian ocean surface area (386.4×10^6 km^2) was calculated from the Sakmarian paleogeographic reconstruction.

CO_2 (ppm)	RF (W m^{-2})	T (°C)
280	0	0
560	3.7083	2.97
1120	7.4167	5.93
2240	11.1250	8.90
3360	13.2942	10.64
4480	14.8333	11.87

Supplementary Figure 3.7.1: First order approximation of radiative forcing and temperature change. Radiative forcing (RF) describes the net change in incoming radiation versus out going radiation and is calculated from a reference pCO$_2$ level (C_o=280 ppm) [RF = 5.35 × (ln(C/C$_o$))]. The temperature change is based on the equilibrium climate sensitivity (λ = 0.8), which refers to the equilibrium change in surface air temperature following a unit change in radiative forcing [δT = λ × RF] (Myhre et al., 1998; IPCC, 2007).

Bibliography

Berger, A. and Loutre, M. F. Insolation Values for the Climate of the Last 10,000,000 Years. *Quaternary Science Reviews*, 10(4):297–317, 1991.

Berner, R. A. and Kothavala, Z. GEOCARB III: A revised model of atmospheric CO_2 over phanerozoic time. *American Journal of Science*, 301(2):182–204, 2001.

Clark, P. U. and Pollard, D. Origin of the middle Pleistocene transition by ice sheet erosion of regolith. *Paleoceanography*, 13(1):1–9, 1998.

Crowell, J. C. Gondwanan Glaciation, Cyclothems, Continental Positioning, and Climate Change. *American Journal of Science*, 278(10):1345–1372, 1978.

Crowley, T. J. and Baum, S. K. Estimating Carboniferous Sea-Level Fluctuations from Gondwanan Ice Extent. *Geology*, 19(10):975–977, 1991.

Crowley, T. J. and Baum, S. K. Modeling Late Paleozoic Glaciation. *Geology*, 20(6):507–510, 1992.

Crowley, T. J., Hyde, W. T. and Short, D. A. Seasonal Cycle Variations on the Supercontinent of Pangaea. *Geology*, 17(5):457–460, 1989.

DeConto, R. M. and Pollard, D. A coupled climate-ice sheet modeling approach to the Early Cenozoic history of the Antarctic ice sheet. *Palaeogeography Palaeoclimatology Palaeoecology*, 198(1-2):39–52, 2003.

Denton, G., Sugden, D., Marchant, D., Hall, B. and Wilch, T. East Antarctic Ice Sheet sensitivity to Pliocene climatic change from a Dry Valleys perspective. *Geografiska Annaler*, 75A:155–204, 1993.

Dickens, G. R., Oneil, J. R., Rea, D. K. and Owen, R. M. Dissociation of Oceanic Methane Hydrate as a Cause of the Carbon-Isotope Excursion at the End of the Paleocene. *Paleoceanography*, 10(6):965–971, 1995.

Fairbanks, R. G. A 17,000-Year Glacio-Eustatic Sea-Level Record - Influence of Glacial Melting Rates on the Younger Dryas Event and Deep-Ocean Circulation. *Nature*, 342(6250):637–642, 1989.

Gough, D. O. Solar Interior Structure and Luminosity Variations. *Solar Physics*, 74(1):21–34, 1981.

Grossman, E. L., Yancey, T. E., Jones, T. E., Bruckschen, P., Chuvashov, B., Mazzullo, S. J. and Mii, H. S. Glaciation, aridification, and carbon sequestration in the Permo-Carboniferous: The isotopic record from low latitudes. *Palaeogeography Palaeoclimatology Palaeoecology*, 268(3-4):222–233, 2008.

Heckel, P. H. Origin of phosphatic black sahel facies in Pennsylvanian cyclothems of Mid-Continent North America. *American Association of Petroleum Geologists Bulletin*, 61:1045–1068, 1977.

Heckel, P. H. Sea-Level Curve for Pennsylvanian Eustatic Marine Transgressive-Regressive Depositional Cycles Along Midcontinent Outcrop Belt, North-America. *Geology*, 14(4):330–334, 1986.

Horton, D. E., Poulsen, C. J. and Pollard, D. Orbital and CO_2 forcing of late Paleozoic continental ice sheets. *Geophysical Research Letters*, 34(19):L19708, 2007.

Huybrechts, P. Glaciological modelling of the Late Cenozoic East Antarctic ice sheet: Stability or dynamism? *Geogr. Ann. Ser. A*, 75:221–238, 1993.

Hyde, W. T., Crowley, T. J., Tarasov, L. and Peltier, W. R. The Pangean ice age: studies with a coupled climate-ice sheet model. *Climate Dynamics*, 15(9):619–629, 1999.

IPCC. Climate Change 2007: The Physical Science Basis. Contribution of Working Group I to the Fourth Assessment Report of the Intergovernmental Panel on Climate Change. Technical report, Intergovernment Panel of Climate Change, 2007.

Isbell, J. L., Miller, M. F., Wolfe, K. L. and Lenaker, P. A. Timing of late Paleozoic glaciation in Gondwana: Was glaciation responsible for the development of Northern Hemisphere cyclothems? In Chan, M. A. and Archer, A. W., editors, *Extreme Depositional Environments: Mega End Members in Geologic Time*, volume 370, pages 5–24. Spec. Pap. Geol. Soc. Am., 2003.

Joachimski, M. M., von Bitter, P. H. and Buggisch, W. Constraints on Pennsylvanian glacioeustatic sea-level changes using oxygen isotopes of conodont apatite. *Geology*, 34(4):277–280, 2006.

Kutzbach, J. E. and Gallimore, R. G. Pangaean Climates - Megamonsoons of the Megacontinent. *Journal of Geophysical Research-Atmospheres*, 94(D3):3341–3357, 1989.

MacAyeal, D. R. Binge/Purge Oscillations of the Laurentide Ice-Sheet as a Cause of the North-Atlantics Heinrich Events. *Paleoceanography*, 8(6):775–784, 1993.

Maslin, M., Seidov, D. and Lowe, J. Synthesis of the nature and causes of rapid climate transitions during the Quaternary. In Seidov, D., editor, *The oceans and rapid change: Past, present, and future*, volume 126, pages 9–52. American Geophysical Union Geophysical Monograph, 2001.

Montañez, I. P., Tabor, N. J., Niemeier, D., DiMichele, W. A., Frank, T. D., Fielding, C. R., Isbell, J. L., Birgenheier, L. P. and Rygel, M. C. CO_2-forced climate and vegetation instability during late paleozoic deglaciation. *Science*, 315(5808):87–91, 2007.

Myhre, G., Highwood, E. J., Shine, K. P. and Stordal, F. New estimates of radiative forcing due to well mixed greenhouse gases. *Geophysical Research Letters*, 25(14):2715–2718, 1998.

Pagani, M., Caldeira, K., Archer, D. and Zachos, J. C. An ancient carbon mystery. *Science*, 314(5805):1556–1557, 2006.

Paterson, W. S. B. *The Physics of Glaciers*. Pergamon, Oxford, U.K., 1994.

Petit, J. R., Jouzel, J., Raynaud, D., Barkov, N. I., Barnola, J. M., Basile, I., Bender, M., Chappellaz, J., Davis, M., Delaygue, G., Delmotte, M., Kotlyakov, V. M., Legrand, M., Lipenkov, V. Y., Lorius, C., Pepin, L., Ritz, C., Saltzman, E. and Stievenard, M. Climate and atmospheric history of the past 420,000 years from the Vostok ice core, Antarctica. *Nature*, 399(6735):429–436, 1999.

Peyser, C. E. and Poulsen, C. J. Controls on Permo-Carboniferous precipitation over tropical Pangaea: A GCM sensitivity study. *Palaeogeography Palaeoclimatology Palaeoecology*, 268(3-4):181–192, 2008.

Pollard, D. and Thompson, S. L. Use of a Land-Surface-Transfer Scheme (Lsx) in a Global Climate Model - the Response to Doubling Stomatal-Resistance. *Global and Planetary Change*, 10(1-4):129–161, 1995.

Poulsen, C. J., Pollard, D., Montañez, I. P. and Rowley, D. Late Paleozoic tropical climate response to Gondwanan deglaciation. *Geology*, 35(9):771–774, 2007.

Rignot, E. and Thomas, R. H. Mass balance of polar ice sheets. *Science*, 297(5586):1502–1506, 2002.

Ritz, C., Fabre, A. and Letreguilly, A. Sensitivity of a Greenland ice sheet model to ice flow and ablation parameters: Consequences for the evolution through the last climatic cycle. *Climate Dynamics*, 13(1):11–24, 1996.

Ross, C. and Ross, J. Late Paleozoic sea levels and depositional sequences. In Ross, C. and Haman, D., editors, *Timing and depositional history of eustatic sequences: Constraints on seismic stratigraphy*, volume 24, pages 137–149. Cushman Foundation for Foraminiferal Research Special Publication, 1987.

Sigman, D. M. and Boyle, E. A. Glacial/interglacial variations in atmospheric carbon dioxide. *Nature*, 407(6806):859–869, 2000.

Soreghan, G. S. and Giles, K. A. Amplitudes of Late Pennsylvanian glacioeustasy. *Geology*, 27(3):255–258, 1999.

Thompson, S. L. and Pollard, D. Greenland and Antarctic mass balances for present and doubled atmospheric CO_2 from the GENESIS version-2 global climate model. *Journal of Climate*, 10(5):871–900, 1997.

Wanless, H. R. and Shepard, F. P. Sea level and climatic changes related to late Paleozoic cycles. *Bulletin of the Geological Society of America*, 47(5/8):1177–1206, 1936.

Ziegler, A. M., L., H. M. and Rowley, D. B. Permian world topography and climate. In Martini, I. P., editor, *Late Glacial and Postglacial Environmental Changes-Quaternary*, pages 111–146. Oxford Univ. Press, 1997.

CHAPTER IV

Influence of high-latitude vegetation feedbacks on late Palaeozoic glacial cycles

4.1 Abstract

Glaciation during the late Palaeozoic era (360–250 Myr ago) is thought to have been episodic, with multiple, often regional, ice-age intervals, each lasting less than 10 million years. Sedimentary deposits from these ice-age intervals exhibit cyclical depositional patterns, which have been attributed to orbitally driven glacial-interglacial cycles and resultant fluctuations in global sea level. Here we use a coupled general-circulation/biome/ice-sheet model to assess the conditions necessary for glacial-interglacial fluctuations. In our simulations, ice sheets appear at atmospheric pCO$_2$ concentrations between 420 and 840 ppmv. However, we are able to simulate ice-sheet fluctuations consistent with eustasy estimates and the distribution of glacial deposits only when we include vegetation feedbacks from high-latitude ecosystem changes. We find that ice-sheet advances follow the expansion of high-latitude tundra during insolation minima, whereas ice retreat is associated with the expansion of barren land close to the edge of the ice sheets during periods of high insolation.

We are unable to simulate glacial-interglacial cycles in the absence of a dynamic vegetation component.We therefore suggest that vegetation feedbacks driven by orbital insolation variations are a crucial element of glacial-interglacial cyclicity.

4.2 Introduction

The late Palaeozoic ice age (LPIA; 360–250 Myr ago) has conventionally been characterized as a time of protracted continental-scale glaciation (Crowell, 1978; Veevers and Powell, 1987; Heckel, 1986; Wanless and Shepard, 1936). This view was shaped by interpretations of Northern Hemisphere transgression-regression sequences (cyclothems) that required hundreds of metres of eustatic change (Crowell, 1978; Veevers and Powell, 1987; Heckel, 1986; Wanless and Shepard, 1936), and was supported by early efforts to model Gondwanaland ice sheets (Crowley and Baum, 1992; Hyde et al., 1999). Improved dating resolution of Gondwanan glacial deposits (Isbell et al., 2003; Fielding et al., 2008) and the development of geochemical proxy records (Ekart et al., 1999; Montañez et al., 2007) have led to the alternative view that continental-scale glaciation was the exception rather than the rule (Isbell et al., 2003; Fielding et al., 2008). This view of the LPIA suggests that multiple distinct regional-scale glacial intervals (<10 Myr) coincided with low (<1,000 ppmv) atmospheric pCO$_2$ and that intraglacial climate variability was driven by orbital insolation fluctuations that led to ice-sheet growth and retreat (Isbell et al., 2003; Fielding et al., 2008).

The conclusion that late Palaeozoic glaciation was episodic and regional is based on the observation that Gondwanaland glaciogenic basins are spatially disparate (located in Africa, Antarctica, Australia, India and South America) and temporally

diverse (Isbell et al., 2003; Fielding et al., 2008). This temporal heterogeneity indicates that the LPIA ice sheets were typically not continental in scale (Isbell et al., 2003). This evidence, supporting lower-volume regional glaciation, has led to a re-analysis of glacioeustatic interpretations. In a summary, 80% of all studies (64 total) indicate that global sea-level changes ranged from 5-to-60 m throughout the LPIA, whereas the total range from all studies is 5-to-250 m, reflecting the difficulty inherent in making palaeoeustasy calculations (Rygel et al., 2008). Uncertainties in palaeo-eustasy calculations arise from a number of complicating factors, among them, accounting for changes in local/regional tectonics, predicting the evolution of shoreline geometry and estimating the gravitational effect of the redistribution of land-based ice and the solid Earth (Kopp et al., 2009).

Modelling studies have demonstrated that late Palaeozoic palaeogeography and low pCO$_2$ produce below-freezing summer surface temperatures that favour accumulation of ice sheets that span the Gondwana supercontinent (Crowley and Baum, 1992; Hyde et al., 1999; Horton et al., 2007; Horton and Poulsen, 2009). Owing to feedbacks associated with their height and high surface albedo, large ice sheets have cold surface conditions that are not susceptible to changes in orbital insolation or reasonable increases in pCO$_2$ (Horton and Poulsen, 2009). At higher pCO$_2$, summer ablation outcompetes accumulation and only small ice sheets are simulated. This presents a paradox; ice sheets of adequate size to account for inferred LPIA eustasy fluctuations are too stable, whereas smaller, orbitally sensitive ice sheets do not represent sufficient volumes of water to account for observed eustatic changes (Horton and Poulsen, 2009). In this study, we demonstrate that the incorporation of ecosystem feedbacks in a coupled general circulation model (GCM)/ice-sheet model allows for the simulation of ice sheets that are sufficiently large and sensitive to orbital

variations.

4.3   Climate, ice-sheet, & vegetation response to orbital forcing

To evaluate the effects of changing vegetation on the LPIA, we couple the BIOME4 ecosystem model to the GENESIS GCM/icesheet model used in previous late Palaeozoic simulations (see Methods section 4.7; Horton and Poulsen (2009); Horton et al. (2007)). GENESIS includes atmosphere, land-surface, mixed-ocean and sea-ice climate components. Experiments were developed using an Early Permian (Sakmarian, about 290 Myr ago) palaeogeographic-palaeotopographic reconstruction (Ziegler et al., 1997) and reduced solar luminosity in accordance with solar evolution models (Gough, 1981). Transient changes in the orbital parameter configuration are applied at 5 kyr intervals to simulate the spectrum of orbital variation observed throughout the past 10 Myr (Berger and Loutre, 1991). Atmospheric pCO_2 concentrations of 420, 560 and 840 ppmv are prescribed consistent with proxy pCO_2 estimates during LPIA glacial intervals (Ekart et al., 1999; Montañez et al., 2007). To isolate the climatic effects of changing vegetation, two experiments were run for each pCO_2 experiment with (1) static land-surface vegetation or (2) the BIOME4 dynamic ecosystem model.

BIOME4 ecosystem types are determined yearly, using GCM averages of monthly mean temperature, sunshine and precipitation, as well as soil texture and pCO_2 concentration (Kaplan et al., 2003; Haxeltine and Prentice, 1996; Harrison and Prentice, 2003). BIOME4 predicts 27 distinct modern ecosystems and has been shown to successfully simulate ecosystem distributions in the modern (Kaplan et al., 2003) and at the Last Glacial Maximum (Harrison and Prentice, 2003). The floral compositions of late Palaeozoic ecosystems are not known in detail, but were distinct in

many respects from modern vegetation types (DiMichele et al., 2001, 2009; Falcon-Lang, 2004; Falcon-Lang et al., 2009; Retallack, 1999). To address this issue we have eliminated grasslands as a potential ecosystem type, as they had not yet evolved (Strömberg, 2005), while assuming that the remainder of late Palaeozoic ecosystems/plant types were analogous to the physiology of modern ecosystems/vegetation types that evolved in similar environmental conditions (see Appendix 4.8.1). A similar approach to palaeovegetation reconstruction was used to examine late Palaeozoic tropical climate-vegetation interactions in low-latitude Pangaea (Poulsen et al., 2007). For presentation purposes, BIOME4's 27 ecosystem types have been condensed into eight mega-biomes and land-based ice in Figure 4.1.

At 420 ppmv $p\mathrm{CO_2}$, with dynamic vegetation, multiple ice spreading centres form over southern Gondwana and coalesce into a single supercontinental ice sheet with an average height in excess of 2,900 m. In non-dynamic vegetation simulations with 560 ppmv $p\mathrm{CO_2}$, ice volume (Figure 4.1a) and extent are significantly reduced, with localized ice centres concentrated mainly along the Panthalassan coast. Simulations of both dynamic and non-dynamic vegetation at 840 ppmv $p\mathrm{CO_2}$ predict no significant terrestrial ice. In comparison with these experiments that produce too much or too little ice (Figure 4.1b), the 560-ppmv-$p\mathrm{CO_2}$ simulation with dynamic vegetation compares well to observed locations of glaciogenic deposits (Isbell et al., 2003) (Figure 4.2). A single ice-spreading centre forms in southern Africa and western Antarctica, whereas discrete spreading centres form in South America coastal Australia and northern Siberia.

At $p\mathrm{CO_2}$ of 420 ppmv, with dynamic vegetation, ice sheets rapidly grow to volumes that are sufficiently large to be insensitive to variations in orbital forcing (Figure 4.1b). In the 560-ppmv-$p\mathrm{CO_2}$ simulation without dynamic vegetation, the growth
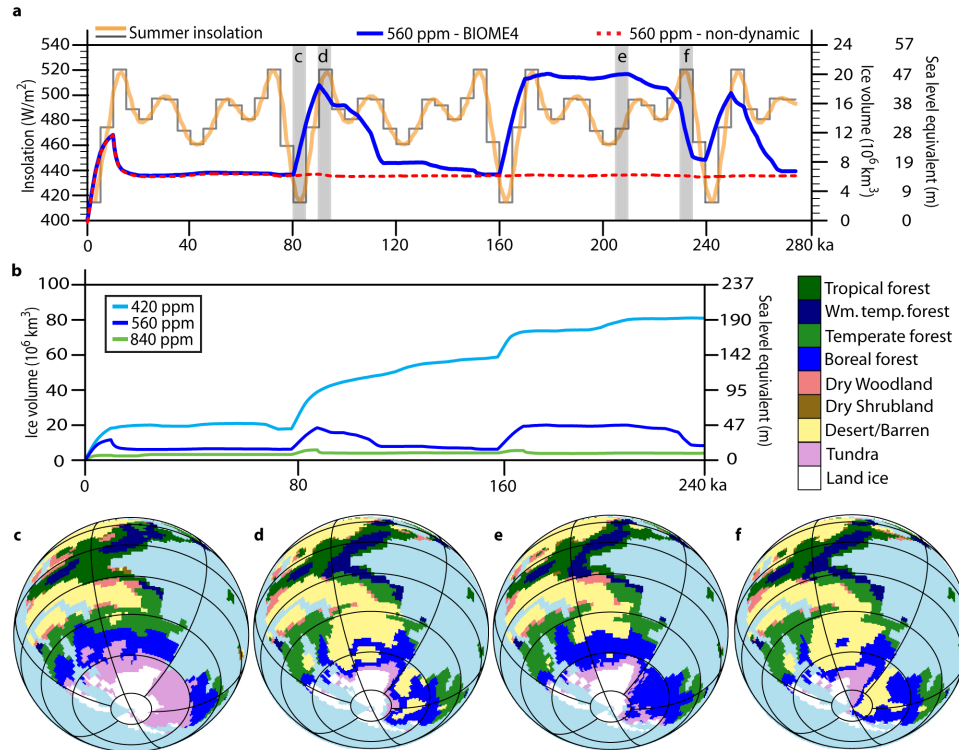
Figure 4.1: Time series of insolation, ice volume, sea level and terrestrial ecosystems. (a) Southern Hemisphere (65–70 °S) summer insolation (orange/grey lines) and ice volume for the 560-ppmv-pCO$_2$ simulations with (blue line) and without (red line) a dynamic ecosystem model. The grey line shows the actual insolation sequence used by the model, resulting from the asynchronous coupling scheme and its 5 kyr time step (see Methods section 4.7). The vertical grey bars correspond to the biome time-slices presented in c-f. Note that in the case with dynamic vegetation, ice-volume fluctuations typically correspond with maxima and minima in insolation. (b) Ice volume predicted for dynamic ecosystem experiments with 420, 540 and 840 ppmv pCO$_2$. (c–f), Early Permian (Sakmarian, about 290 Myr ago; Ziegler et al. (1997)) biome predictions for four time intervals, 85, 95, 210 and 235 kyr. At the insolation minimum (c) the tundra ecosystem expands northward to 60 °S. In medium insolation orbits (e) boreal forests dominate the high latitudes. During periods of high insolation (d,f) ice-proximal barren lands expand.

and ablation of Gondwanan ice sheets in response to orbital forcing contributes less than 2 m of glacioeustatic change (Figure 4.1a). In contrast, with the incorporation of dynamic vegetation, orbitally driven glacial- interglacial glacioeustatic fluctuations of ~33 m are simulated (Figure 4.1a), which represent both expansion/contraction and thickening/ thinning of Gondwanan ice sheets. Land-based ice volume increases when Southern Hemisphere high-latitude (65–70 °S) summer (December, January and February) insolation is at a minimum (mean insolation ~415 W m^{-2}), whereas

ice volume typically decreases when summer insolation is at a maximum (mean insolation $\sim$520 W m^{-2}; Figure 4.1a). These insolation changes drive changes in ambient temperature that are amplified by vegetation feedbacks.

4.4 Orbitally-driven vegetation feedbacks

Lower-than-average summer insolation facilitates expansion of tundra into areas previously dominated by boreal forests (Figure 4.1c). In BIOME4, tundra replaces boreal forest ecosystem when the sum of growing-degree-day temperatures above 0 °C (GDD$_0$; time-integral of temperatures above 0 °C) falls below $\sim$800 and the net primary productivity decreases below the 140 g m^{-2} threshold (Kaplan et al., 2003). The replacement of two-storey boreal forest with single-storey lower canopy tundra allows snow cover to persist through the summer unmasked by trees, which increases surface albedo and cools the periglacial environment. The net effect of tundra expansion and lengthened summer snow coverage is a 20–30% increase in summer surface albedo (Figure 4.3a), which decreases periglacial summer temperatures by 6–10 °C (Figure 4.3b). Vegetation change and persistent snow coverage magnify the insolation-induced cooling, decreasing summer snow melt (Figure 4.3c) and ultimately allowing land-based ice accumulation (Figure 4.1a).

Rapid ablation of land-based ice in the 560-ppmv-pCO$_2$ dynamic vegetation simulation occurs when Southern Hemisphere summer insolation is at a maximum (Figure 4.1a). Warm summer temperatures facilitate the expansion of barren lands along the ice margins (Figure 4.1d). BIOME4 simulates barren lands when the number of GDD$_0$ exceeds 800 and there is insufficient soil moisture to support boreal forests (Kaplan et al., 2003). The expansion of non-vegetated land cover leads to a drawdown of available soil moisture (Figure 4.3d) resulting in reduced summer latent heat flux

and increased sensible heating in the ice-proximal environment (Figure 4.3e). This anomalously high sensible heat flux increases summer temperatures at ice frontal margins by up to 4 °C (Figure 4.3f) and ultimately leads to melting. Although this vegetation/ice-ablation feedback successfully leads to deglaciation during Southern Hemisphere summer insolation maxima 95, 235 and 255 kyr ago, significant ice loss is not simulated 175 kyr ago (Figure 4.1a). This lack of ablation is attributed to a 5% decrease in barren land area, a 4.5% increase in ice volume and a 7% increase in ice area, compared with the 95 kyr iteration (Figure 4.4). Owing to an increase in local albedo and a decrease in summer sensible heat flux, these differences lead to lower high-latitude temperatures and a reduced melt susceptibility to orbitally driven insolation changes. This missed deglaciation underscores the sensitivity of nonlinear systems to stochastic elements and demonstrates that subtle variations in ice extent, local climate and ecological factors can cause glacial and deglacial cycles to diverge from orbital pacing.

4.5 Comparison with the LPIA geologic record

Our results demonstrate that the pCO$_2$ window allowing for large ice sheets that are sensitive to orbital fluctuations is relatively narrow (420–840 ppmv). This range of atmospheric pCO$_2$ is consistent with calculations based on the isotopic composition of soil carbonates during periods of late Palaeozoic glaciation (Ekart et al., 1999; Montañez et al., 2007). Although our model simulates ice in most late Palaeozoic glaciogenic basins (Isbell et al., 2003), it does not predict ice in northern South America, northern Africa, the Arabian Peninsula, India or western Australia. It is likely that the lack of ice in these regions is due to our specification of palaeogeography and

Ice height (km)
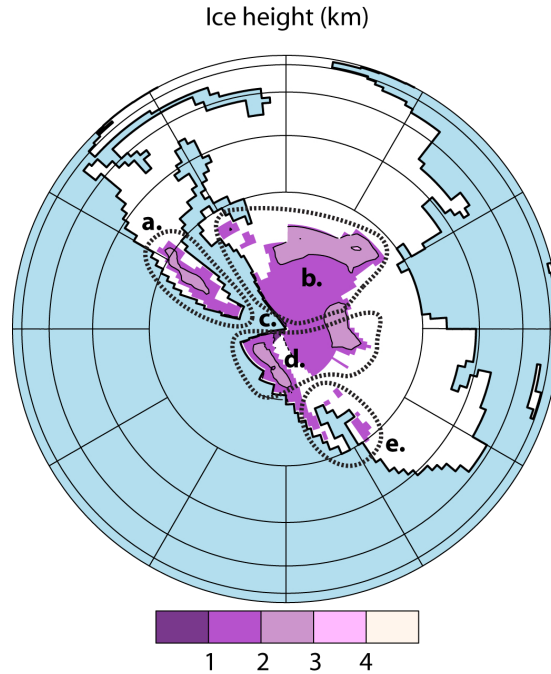
Figure 4.2: Maximum simulated Southern Hemisphere ice extent in the 560-ppmv-pCO$_2$ dynamic vegetation simulation at 175 kyr. The location of simulated ice is in agreement with glacial evidence found in (A) South America (Paraná, Chaco-Paraná, Paganzo, Calingasta-Uspallata, Sauce Grande, San Rafael, Teupel and Golondrina basins), (B) Africa (Congo, Haub, Tanzanian, Zambesi, Limpopo, Kalahari, Warmbad and Karoo basins), (C) the Falkland Islands, (D) Antarctica (Heimefrontfjella and Victorialand basins and the Ellsworth, Pensecola and central Transantarctic mountains) and (E) Australia (Murray, Oaklands, Tasmanian, Bowen-Gunnedah, Sydney and Tamworth belt basins) (Isbell et al., 2003).

palaeotopography (Ziegler et al., 1997). (1) The Sakmarian reconstruction represents one snapshot in time, and does not account for the evolution of palaeogeography (for example, drifting of continents) or palaeotopography (for example, orogenic events) throughout the late Palaeozoic. (2) Climate modelling studies have shown that uncertainties in late Palaeozoic palaeogeographic reconstructions are substantial enough to alter the climate (Fluteau et al., 2001) and therefore may influence the location of ice accumulation. (3) The location and elevation of plateaux and alpine regions in the late Palaeozoic are not well constrained. The existence of relatively low high-latitude plateaux that would not violate any geological constraints could explain the existence of ice sheets where our model failed to simulate them. To illustrate this

point, we carried out further experiments, in which plateaux of modest elevations (that is, 1,000–1,500 m) were added to areas of the Australian continent on which glaciogenic sedimentation has been observed (Eyles et al., 2002). The addition of these plateaux led to the growth of small ice sheets ($\sim 2 \times 10^6$ km^3) in areas that were previously ice free.

Glacioeustatic fluctuations of ~ 33 m represent a significant proportion of the 5–60 m range of observed LPIA eustasy change. Owing to the (static) palaeogeography and (conservative) palaeotopography employed in our simulations, the magnitude of this glacial component should be considered a lower estimate. An increase in land area near the austral pole or the addition of highlands could increase the glacial contribution to total eustasy. For example, the Australian plateau ice-growth experiments increase the potential glacioeustatic change by ~ 5 m.

Palaeovegetation studies of low-latitude depositional systems report dynamic ecosystem fluctuations throughout the LPIA (DiMichele et al., 2001, 2009; Falcon-Lang, 2004; Falcon-Lang et al., 2009). These ecological changes are interpreted to correspond to Southern Hemisphere glacial advance and retreat. Studies of high-latitude palaeovegetation demonstrate an interchange between tundra and forest ecosystems, which is interpreted to be driven by periodic climate deterioration and amelioration (Retallack, 1999). These observed palaeofloral fluctuations are consistent with the LPIA BIOME4 simulations of dynamic vegetation. Ecosystem variability in the 560-ppmv-pCO$_2$ dynamic vegetation simulation is regionally complex, but generally demonstrates aridification in low latitudes coincident with decreasing ice volume and variable dominance of boreal forest, tundra and barren lands in the periglacial environment coincident with glacial advance and retreat (Figure 4.1b–e and 4.4). High-latitude periglacial vegetation fluctuations correspond to changes in orbital forcing
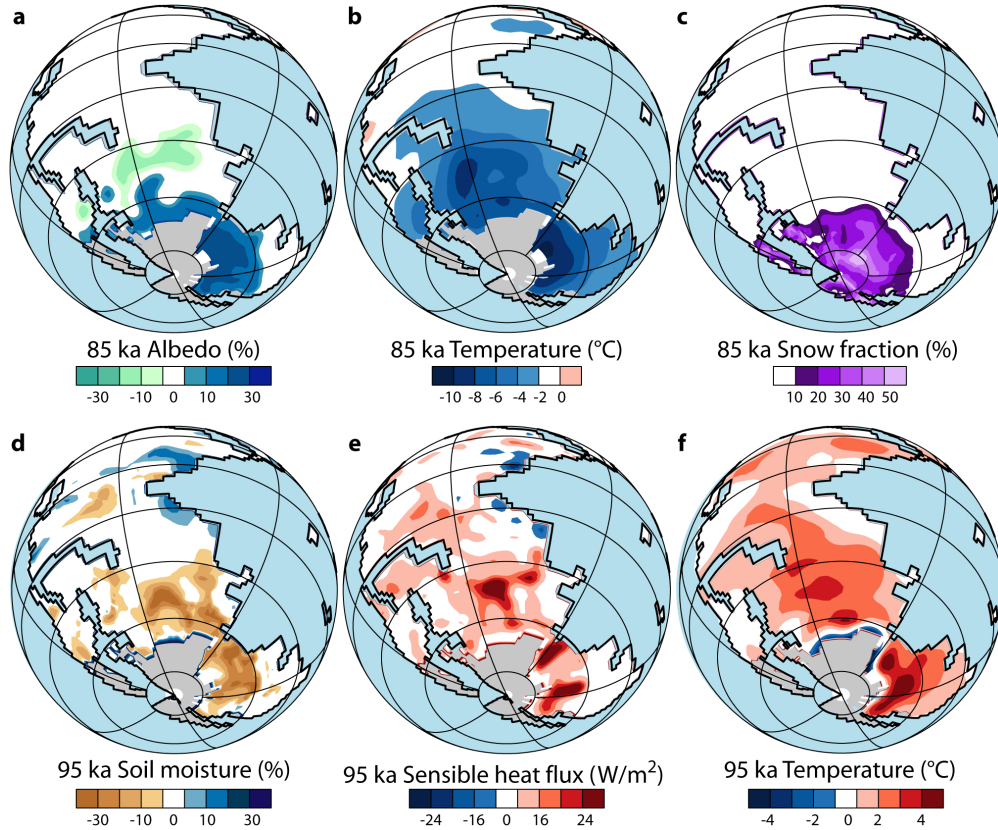
Figure 4.3: Climatic anomalies at the summer insolation minimum and maximum. The effects of ecosystem change at the insolation minimum (85 kyr; Figure 4.1c) on surface albedo (a), surface air temperature (b) and snow fraction (c) and at the insolation maximum (95 kyr; Figure 4.1d) on soil moisture (d), surface sensible heat flux (e) and surface air temperature (f). Southern Hemisphere summer anomalies are calculated as the difference from the average conditions over one complete orbital cycle (85–165 kyr).

and indicate no hysteresis behaviour.

4.6   Vegetation is king?

Although orbitally driven ecosystem feedbacks can account for a considerable portion of the estimated sea-level fluctuations, it is likely that other feedback mechanisms not considered here, involving greenhouse gases, ocean circulation and/or dust, contributed to LPIA glacial-interglacial fluctuations. Plio-Pleistocene glacial-interglacial cycles, for example, were accompanied by changes in pCO_2 concentra-

tions of up to ~100 ppmv (Stott et al., 2007). A previous study of Last Glacial Maximum climate notes that whereas pCO_2 has a larger influence on global temperature, vegetation feedbacks can dominate the temperature response on localized scales (Jahn et al., 2005). To quantify the local high-latitude surface heat response to changes in pCO_2 during the late Palaeozoic, we ran another experiment (using orbital/biome conditions from the 90 to 95 kyr time slice, Figure 4.1a) in which pCO_2 was increased from 560 to 660 ppmv, but vegetation was not allowed to change. The local surface heat response to increased pCO_2 ranged from 0 to 1.5 W m^{-2} near the ice-sheet margin. In comparison, the transition from boreal forest to barren land at the same time yielded a 6 to 12 W m^{-2} increase in surface heating near the ice margin. These results indicate that variations in greenhouse gas concentrations contributed to orbitally paced insolation amplification, but probably played a secondary role to high-latitude ecosystem change in driving LPIA glacial-interglacial cycles. This conclusion is supported by the observation that Plio-Pleistocene greenhouse gas variations mostly lagged glacial-interglacial fluctuations (Stott et al., 2007). The contributions of ocean circulation changes and dust flux to late Palaeozoic glacial-interglacial changes are unresolved. Previous ocean-atmosphere studies suggest that the ocean responds dynamically to orbital cycles, although the surface heat response to these changes is typically small (for example, Lee and Poulsen (2005)). The net radiative effect of increased dust flux during glacial periods is uncertain, with surface dust deposited on ice and snow decreasing the albedo, and airborne dust both reducing the amount of insolation reaching Earth's surface and altering the absorption/reflection properties of clouds (Bar-Or et al., 2008).

Previous studies using either GCMs without dynamic icesheet models (Gallimore and Kutzbach, 1996; Crucifix and Hewitt, 2005) or Earth models of intermediate
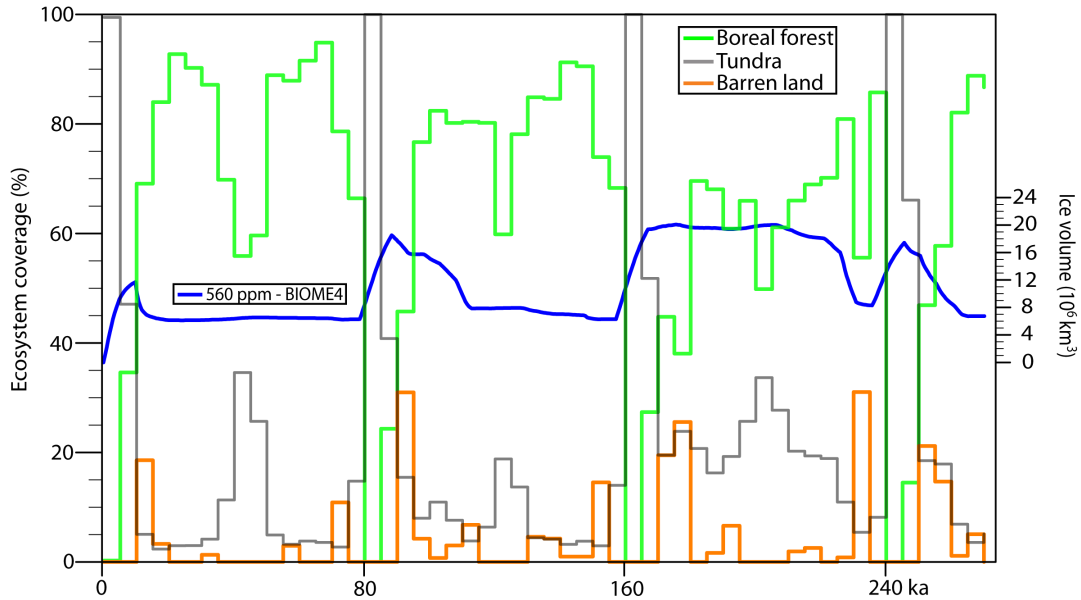
Figure 4.4: Time series of global ice volume and ecosystem coverage variability from 65-to-70 °S. Dominant ice-proximal ecosystem type varies with and amplifies insolation-driven temperature change. Ice volume increases when tundra expands and decreases when barren land expands.

complexity with (Meissner et al., 2003; Kubatzki et al., 2006) and without (Claussen et al., 2006) dynamic ice-sheet models have explored the effects of vegetation on Quaternary climates. These studies demonstrate that vegetation feedbacks are important for glacial inception (for example, Kubatzki et al. (2006)) and suggest that the advance and retreat of Northern Hemisphere boreal forests may have amplified the temperature response to orbital insolation change through vegetation-snow-albedo feedbacks. Using a coupled GCM/biome/ice-sheet model, this study demonstrates that orbitally forced vegetation feedbacks amplify the ice-sheet response to both insolation minima and maxima, and thus permit long-term glacial-interglacial fluctuations. So far, the simulation of LPIA and Plio-Pleistocene glacial-interglacial cycles has been a major challenge for dynamic climate/ice-sheet models (Charbit et al., 2007; Horton and Poulsen, 2009). The omission of high-latitude vegetation feedbacks might be an important reason.

4.7 Methods

The simulations presented in this study use the Genesis version 3.0 atmospheric GCM synchronously coupled to the BIOME4 ecosystem model and asynchronously coupled to a three-dimensional dynamic ice-sheet model. The Genesis GCM includes dynamic atmosphere, land-surface, sea-ice and slab-ocean components (Thompson and Pollard, 1997; Pollard and Thompson, 1995). The atmospheric GCM has a spectral resolution of T31 ($3.75° \times 3.75°$) and 18 vertical levels. The land surface has a $2° \times 2°$ grid spacing. BIOME4 is a coupled carbon and water flux model that predicts global steady-state vegetation distribution, structure and biogeochemistry at a $2° \times 2°$ resolution (Harrison and Prentice, 2003; Haxeltine and Prentice, 1996; Kaplan et al., 2003). The thermomechanical ice-sheet model is based on the vertically integrated continuity equation for ice mass and predicts ice-geometry evolution through surface-mass-balance, basal-melting and ice-flow calculations on a $1° \times 2°$ surface grid (DeConto and Pollard, 2003). Orbitally driven climate changes were simulated using an asynchronous transient ice-sheet/atmosphere coupling scheme (Horton and Poulsen, 2009), which consists of alternating short (15 yr) GCM-biome integrations and long (5 kyr) ice-sheet integrations. Between the integration of each component, updated boundary conditions (that is, meteorological information to the ice-sheet model or ice geometry to the GCM-biome model) are passed from one model component to the other, and orbital parameters are updated. Each transient experiment was run over multiple orbital cycles and represents 275 kyr or 55 iterations. A full discussion of individual model components and the coupling scheme can be found in the Supplementary Methods (Appendix 4.9.2).

4.8 Acknowledgments

4.9 Appendix

4.9.1 Supplementary Discussion

Knowledge of late Paleozoic ecosystems on a global scale is limited. The removal of the grassland ecosystem, including tropical and temperate-grasslands and savannah, from BIOME4 is consistent with evidence suggesting that grasslands did not become ecologically dominant until the early Oligocene (34 Ma; Strömberg (2005). In our late Paleozoic BIOME4 simulations the temperate grassland niche, which is characterized by low temperature ($GDD_0 < 800$) and arid conditions, is replaced by the barren land ecosystem. While the removal of grasses form BIOME4 is consistent with the geological record, it is possible that an ecosystem with similar physiological characteristics to modern temperate grasslands occupied the high-latitude barren lands simulated during the LPIA. To determine the climatic effects of changing from a barren land to a temperate grassland ecosystem, we simulated one complete orbital cycle (80 ka) using the GENESIS-BIOME4-ice sheet model with grassland ecosystems enabled in BIOME4. Similar to our BIOME4 simulations without grassland ecosystems, ice sheet volumes wax and wane (Supplementary Figure 4.9.1). While the magnitude of ice volume change is slightly less pronounced (4% difference in total volume change) than simulations with the barren land ecosystem, the net ef-

fect is similar. Our supplemental experiments indicate that should a late Paleozoic ecosystem akin to modern temperate grasslands have occupied the barren land niche, similar ecosystem feedbacks to those invoked for barren land ecosystems would continue to facilitate continental glaciation and deglaciation.
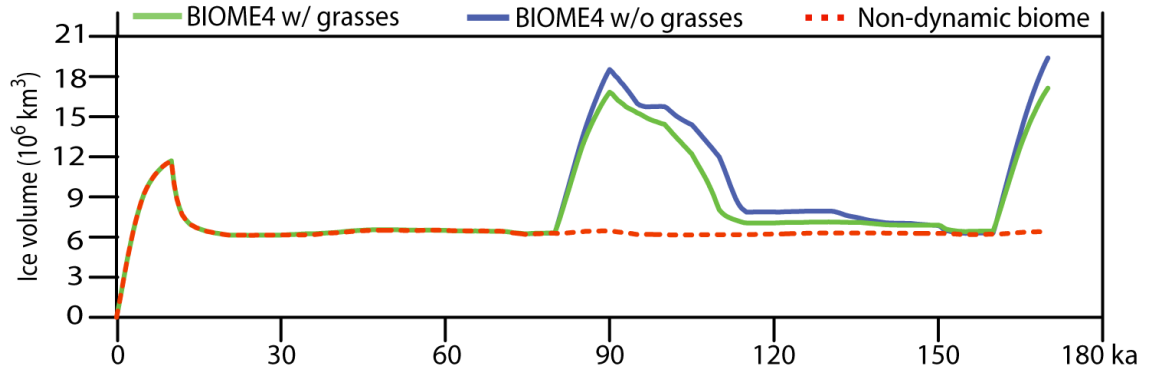
Supplementary Figure 4.9.1: Time series of ice volume with various BIOME4 modeling configurations. Note that glacial waxing and waning is maintained with the addition of grasses to BIOME4 with only a minor (4% difference) reduction in total ice volume change.

4.9.2 Supplementary Methods

GENESIS incorporates dynamic atmosphere, land-surface, sea-ice and slab-ocean components (Thompson and Pollard, 1997; Pollard and Thompson, 1995). Sea-surface temperatures and sea ice are computed using a 50-m slab ocean with diffusive heat flux. The thermo-mechanical ice sheet model (DeConto and Pollard, 2003) predicts ice temperatures to account for their effect on rheology and basal sliding. The time step of the ice-sheet model is one year. The local bedrock response to ice load is a simple relaxation toward isostasy with a time constant of 5,000 years. Lithospheric flexure is modeled by linear elastic deformation. In this version of the model, ice shelves are not simulated.

For the purpose of this study, we have simplified the periods of each orbital parameter such that eccentricity, obliquity, and precessional periods occur every 80,

40, and 20 ka, respectively (Supplementary Figure 4.9.2; Horton and Poulsen (2009); DeConto and Pollard (2003)). To couple the climate with the ice-sheet model, we use an asynchronous technique that consists of alternating GENESIS-BIOME4 iterations with ice-sheet model integrations. To begin, GENESIS-BIOME4 is integrated with specified orbital conditions for 30 years to produce a steady-state climatology. Mean monthly meteorological fields (i.e. surface air temperature, evaporation, and precipitation) from the last ten years of the GENESIS-BIOME4 run are then used to drive the ice-sheet model. Each ice-sheet model experiment is run for 5,000 yrs and predicts ice-sheet area, thickness, and isostatically adjusted continental topography. These new boundary conditions and updated orbital conditions are incorporated into the subsequent GCM iteration. After the initial iteration, GENESIS-BIOME4 is run in 15 yr segments and the meteorological fields from the last ten years are passed to the ice-sheet model. For each experiment, this scheme is repeated 48 times representing 240 ka and 4 eccentricity cycles. To investigate a fourth glacial-deglacial cycle an additional 35 ka of simulation time were completed for the 560 ppm experiments. Non-dynamic vegetation simulations were completed in the same manner as dynamic simulations, but after the 30 ka iteration (this iteration has an average insolation orbital configuration) BIOME4 is turned off and vegetation is not allowed to change. To estimate sea-level change we employ an ice-volume-ocean surface area calculation (DeConto and Pollard, 2003):

SLE = WE/ocean surface area

where the sea-level equivalent (SLE) converts the global ice volume to a water equivalent (WE) assuming a uniform ice density of 0.917 g $(mL)^{-1}$ and the surface area of the ocean (3.86×10^8 km^2) is calculated from the Sakmarian paleogeographic reconstruction (Ziegler et al., 1997). In previous studies, an isostatically adjusted sea-level

equivalent approximation has been used to estimate late Paleozoic glacioeustatic change (Horton et al., 2007; Horton and Poulsen, 2009). Here, we use the SLE since orbitally-paced glacioeustatic changes are faster than the oceanic-lithosphere isostatic response to sea-water loading and unloading.
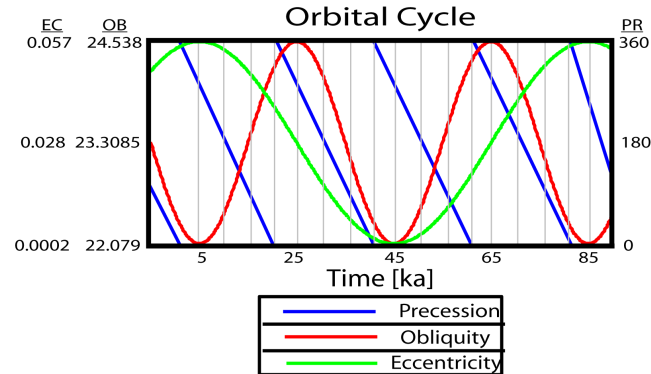
Supplementary Figure 4.9.2: Orbital parameter regime used in transient climate model simulations. Precession (PR), obliquity (OB), and eccentricity (EC) have sinusoidal periods of 20, 40, and 80 ka, respectively (Horton and Poulsen, 2009; DeConto and Pollard, 2003), and their values are based on maxima and/or minima calculated from the past 10 million years (Berger and Loutre, 1991). Ice volumes are predicted at 5 ka intervals (as indicated by vertical lines), over multiple orbital cycles [Modified from Horton and Poulsen (2009)].

Bibliography

Bar-Or, R., Erlick, C. and Gildor, H. The role of dust in glacial-interglacial cycles. *Quaternary Science Reviews*, 27(3-4):201–208, 2008.

Berger, A. and Loutre, M. F. Insolation Values for the Climate of the Last 10,000,000 Years. *Quaternary Science Reviews*, 10(4):297–317, 1991.

Charbit, S., Ritz, C., Philippon, G., Peyaud, V. and Kageyama, M. Numerical reconstructions of the Northern Hemisphere ice sheets through the last glacial-interglacial cycle. *Climate of the Past*, 3(1):15–37, 2007.

Claussen, M., Fohlmeister, J., Ganopolski, A. and Brovkin, V. Vegetation dynamics amplifies precessional forcing. *Geophysical Research Letters*, 33(9):–, 2006.

Crowell, J. C. Gondwanan Glaciation, Cyclothems, Continental Positioning, and Climate Change. *American Journal of Science*, 278(10):1345–1372, 1978.

Crowley, T. J. and Baum, S. K. Modeling Late Paleozoic Glaciation. *Geology*, 20(6):507–510, 1992.

Crucifix, M. and Hewitt, C. D. Impact of vegetation changes on the dynamics of the atmosphere at the Last Glacial Maximum. *Climate Dynamics*, 25(5):447–459, 2005.

DeConto, R. M. and Pollard, D. A coupled climate-ice sheet modeling approach to the Early Cenozoic history of the Antarctic ice sheet. *Palaeogeography Palaeoclimatology Palaeoecology*, 198(1-2):39–52, 2003.

DiMichele, W. A., Montañez, I. P., Poulsen, C. J. and Tabor, N. J. Climate and vegetational regime shifts in the late Paleozoic ice age earth. *Geobiology*, 7(2):200–226, 2009.

DiMichele, W. A., Pfefferkorn, H. W. and Gastaldo, R. A. Response of Late Carboniferous and Early Permian plant communities to climate change. *Annual Review of Earth and Planetary Sciences*, 29:461–487, 2001.

Ekart, D. D., Cerling, T. E., Montañez, I. P. and Tabor, N. J. A 400 million year carbon isotope record of pedogenic carbonate: Implications for paleoatmospheric carbon dioxide. *American Journal of Science*, 299(10):805–827, 1999.

Eyles, N., Mory, A. J. and Backhouse, J. Carboniferous-Permian palynostratigraphy of west Australian marine rift basins: resolving tectonic and eustatic controls during Gondwanan glaciations. *Palaeogeography Palaeoclimatology Palaeoecology*, 184(3-4):305–319, 2002.

Falcon-Lang, H. J. Pennsylvanian tropical rain forests responded to glacial-interglacial rhythms. *Geology*, 32(8):689–692, 2004.

Falcon-Lang, H. J., Nelson, W. J., Elrick, S., Looy, C. V., Ames, P. R. and DiMichele, W. A. Incised channel fills containing conifers indicate that seasonally dry vegetation dominated Pennsylvanian tropical lowlands. *Geology*, 37(10):923–926, 2009.

Fielding, C. R., Frank, T. D. and Isbell, J. I. The Late Paleozoic Ice Age-a Review of Current Understanding and Synthesis of Global Climate Patterns. In Fielding, C. R., Frank, T. D. and Isbell, J. I., editors, *Resolving the Late Paleozoic Ice Age in Time and Space*, volume 441. Geol. Soc. Am. Spec. Pap., 2008.

Fluteau, F., Besse, J., Broutin, J. and Ramstein, G. The Late Permian climate. What can be inferred from climate modelling concerning Pangea scenarios and Hercynian range altitude? *Palaeogeography Palaeoclimatology Palaeoecology*, 167(1-2):39–71, 2001.

Gallimore, R. G. and Kutzbach, J. E. Role of orbitally induced changes in tundra area in the onset of glaciation. *Nature*, 381(6582):503–505, 1996.

Gough, D. O. Solar Interior Structure and Luminosity Variations. *Solar Physics*, 74(1):21–34, 1981.

Harrison, S. P. and Prentice, A. I. Climate and CO_2 controls on global vegetation distribution at the last glacial maximum: analysis based on palaeovegetation data, biome modelling and palaeoclimate simulations. *Global Change Biology*, 9(7):983–1004, 2003.

Haxeltine, A. and Prentice, I. C. BIOME3: An equilibrium terrestrial biosphere model based on ecophysiological constraints, resource availability, and competition among plant functional types. *Global Biogeochemical Cycles*, 10(4):693–709, 1996.

Heckel, P. H. Sea-Level Curve for Pennsylvanian Eustatic Marine Transgressive-Regressive Depositional Cycles Along Midcontinent Outcrop Belt, North-America. *Geology*, 14(4):330–334, 1986.

Horton, D. E. and Poulsen, C. J. Paradox of late Paleozoic glacioeustasy. *Geology*, 37(8):715–718, 2009.

Horton, D. E., Poulsen, C. J. and Pollard, D. Orbital and CO_2 forcing of late Paleozoic continental ice sheets. *Geophysical Research Letters*, 34(19):L19708, 2007.

Hyde, W. T., Crowley, T. J., Tarasov, L. and Peltier, W. R. The Pangean ice age: studies with a coupled climate-ice sheet model. *Climate Dynamics*, 15(9):619–629, 1999.

Isbell, J. L., Miller, M. F., Wolfe, K. L. and Lenaker, P. A. Timing of late Paleozoic glaciation in Gondwana: Was glaciation responsible for the development of Northern Hemisphere cyclothems? In Chan, M. A. and Archer, A. W., editors, *Extreme Depositional Environments: Mega End Members in Geologic Time*, volume 370, pages 5–24. Spec. Pap. Geol. Soc. Am., 2003.

Jahn, A., Claussen, M., Ganopolski, A. and Brovkin, V. Quantifying the effect of vegetation dynamics on the climate of the last glacial maximum. *Climate of the Past*, 1(1):1–7, 2005.

Kaplan, J. O., Bigelow, N. H., Prentice, I. C., Harrison, S. P., Bartlein, P. J., Christensen, T. R., Cramer, W., Matveyeva, N. V., McGuire, A. D., Murray, D. F., Razzhivin, V. Y., Smith, B., Walker, D. A., Anderson, P. M., Andreev, A. A., Brubaker, L. B., Edwards, M. E. and Lozhkin, A. V. Climate change and Arctic ecosystems: 2. Modeling, paleodata-model comparisons, and future projections. *Journal of Geophysical Research-Atmospheres*, 108(D19), 2003.

Kopp, R. E., Simons, F. J., Mitrovica, J. X., Maloof, A. C. and Oppenheimer, M. Probabilistic assessment of sea level during the last interglacial stage. *Nature*, 462(7275):863–U51, 2009.

Kubatzki, C., Claussen, M., Calov, R. and Ganopolski, A. Sensitivity of the last glacial inception to initial and surface conditions. *Climate Dynamics*, 27(4):333–344, 2006.

Lee, S. Y. and Poulsen, C. J. Tropical Pacific climate response to obliquity forcing in the Pleistocene. *Paleoceanography*, 20(4):–, 2005.

Meissner, K. J., Weaver, A. J., Matthews, H. D. and Cox, P. M. The role of land surface dynamics in glacial inception: a study with the UVic Earth System Model. *Climate Dynamics*, 21(7-8):515–537, 2003.

Montañez, I. P., Tabor, N. J., Niemeier, D., DiMichele, W. A., Frank, T. D., Fielding, C. R., Isbell, J. L., Birgenheier, L. P. and Rygel, M. C. CO_2-forced climate and vegetation instability during late paleozoic deglaciation. *Science*, 315(5808):87–91, 2007.

Pollard, D. and Thompson, S. L. Use of a Land-Surface-Transfer Scheme (Lsx) in a Global Climate Model - the Response to Doubling Stomatal-Resistance. *Global and Planetary Change*, 10(1-4):129–161, 1995.

Poulsen, C. J., Pollard, D., Montañez, I. P. and Rowley, D. Late Paleozoic tropical climate response to Gondwanan deglaciation. *Geology*, 35(9):771–774, 2007.

Retallack, G. J. Carboniferous fossil plants and soils of an early tundra ecosystem. *Palaios*, 14(4):324–336, 1999.

Rygel, M. C., Fielding, C. R., Frank, T. D. and Birgenheier, L. P. The magnitude of late Paleozoic glacioeustatic fluctuations: a synthesis. *Journal of Sedimentary Research*, 78(7-8):500–511, 2008.

Stott, L., Timmermann, A. and Thunell, R. Southern hemisphere and deep-sea warming led deglacial atmospheric CO_2 rise and tropical warming. *Science*, 318(5849):435–438, 2007.

Strömberg, C. A. E. Decoupled taxonomic radiation and ecological expansion of open-habitat grasses in the Cenozoic of North America. *Proceedings of the National Academy of Sciences of the United States of America*, 102(34):11980–11984, 2005.

Thompson, S. L. and Pollard, D. Greenland and Antarctic mass balances for present and doubled atmospheric CO_2 from the GENESIS version-2 global climate model. *Journal of Climate*, 10(5):871–900, 1997.

Veevers, J. J. and Powell, C. M. Late Paleozoic Glacial Episodes in Gondwanaland Reflected in Transgressive-Regressive Depositional Sequences in Euramerica. *Geological Society of America Bulletin*, 98(4):475–487, 1987.

Wanless, H. R. and Shepard, F. P. Sea level and climatic changes related to late Paleozoic cycles. *Bulletin of the Geological Society of America*, 47(5/8):1177–1206, 1936.

Ziegler, A. M., L., H. M. and Rowley, D. B. Permian world topography and climate. In Martini, I. P., editor, *Late Glacial and Postglacial Environmental Changes-Quaternary*, pages 111–146. Oxford Univ. Press, 1997.

CHAPTER V

Eccentricity-paced late Paleozoic climate change and its role in cyclostratigraphy

5.1 Abstract

Cyclic sedimentary deposits characterize low-latitude late Paleozoic successions and preserve evidence of dynamic climate change on the Pangaean supercontinent. Although their orbitally-paced glacioeustatic origins are widely accepted, their climatic signatures are open to interpretation. In this study, we utilize the GENESIS general circulation model (GCM) coupled to dynamic ice sheet and ecosystem components, to explore the response of low-latitude continental climate and high-latitude ice sheets to orbital and atmospheric pCO_2 forcing. Our results suggest that atmospheric pCO_2 concentration exerts the primary control over low-latitude continental climate and high-latitude glaciation. Our experiments constrain the atmospheric pCO_2 window within which late Paleozoic climate was amenable to orbitally-driven glacial-interglacial fluctuations. The results suggest that both high-latitude ice-sheet accumulation and ablation and low-latitude climate change were paced by the eccentricity of Earth's orbit. Periods of high eccentricity amplified precession-driven changes in insolation and promoted high-latitude ice sheet volume fluctuations as

well as increased low-latitude precipitation variability. When eccentricity was low, the amplification of precessionally-driven insolation fluctuations was reduced, which promoted high-latitude continental ice sheet stability and less variable low-latitude precipitation. Based on these modeling results we develop an eccentricity-paced cyclothem deposition model in which high-latitude glaciation and low-latitude climate change are simultaneously driven by orbital insolation fluctuations.

5.2   Introduction

Climate change within the late Paleozoic Ice Age (LPIA; 360–250 Ma) was dynamic. Long-term (10^6–10^7 yrs) mean climatic states, hypothesized to be driven by fluctuations in greenhouse gas concentrations (Montañez et al., 2007) and the evolving configuration of continents about the South Pole (Caputo and Crowell, 1985; Crowell, 1978), alternated between icehouse and greenhouse conditions (Fielding et al., 2008a,b; Isbell et al., 2003, 2008). On shorter timescales (10^4–10^5 yrs) glacial-interglacial fluctuations are thought to have been driven by cyclic changes in Earth's orbit and associated feedbacks (Heckel, 1986; Horton et al., 2010). Geologic evidence of LPIA climate change is preserved within cyclic (0.1 to 0.5 Myr) sedimentary deposits, commonly called cyclothems, that span paleo-equatorial Pangaea from the carbonate-dominated Bird Spring platform that rimmed the western tropical Panthalassic margin (Bishop et al., 2010), to the Appalachian Basin coal-rich sequences of the mid-continent (e.g., Cecil (1990)), to the classic cyclothems of the Donets and Canadian Maritime basins that bordered the western Paleotethys (e.g., Eros et al. (sion); Gibling and Rygel (2008)). Cyclothem deposits throughout low-latitude Pangaea show considerable compositional variability, both regionally and temporally,

but generally consist of repetitive lithological sequences whose stratigraphic facies variations record a wide range of depositional environments.

Since Wanless and Shepard (1936) first suggested a link between Euramerican low-latitude rhythmic sedimentary deposits and high-latitude Gondwanaland glaciation, lithofacies variations within cyclothems have been interpreted to record climate change. Numerous studies have identified transgressive-regressive signatures in late Paleozoic Euramerican deposits and have attributed these sequences to glacioeustatic fluctuations (i.e., Bohacs and Suter, 1997; Heckel, 1977; Ramsbottom, 1973, 1977; Veevers and Powell, 1987). The periodic nature of transgressive-regressive sequences was hypothesized to result from orbitally-driven waxing and waning of high-latitude Gondwanaland ice sheets, analogous to Milankovitch's theory of orbital control of Northern Hemisphere ice sheets during the Pleistocene (Heckel, 1986). Subsequent studies have identified orbital frequencies in transgressive-regressive deposits across paleo-equatorial Pangaea and it is now widely accepted that cyclothems were orbitally-paced (Boardman and Heckel, 1989; Izart et al., 2003; Maynard and Leeder, 1992; Strasser et al., 2006; Rasbury et al., 1998; Weedon and Reed, 1995). While glacioeustatic changes are capable of explaining some of the observed lithofacies variations found in late Paleozoic deposits, they are unable to explain the variability observed in depositional environments not directly influenced by glacioeustasy, e.g., the terrestrial-only sequences of the Appalachian Basin (Cecil, 1990; Soreghan, 1994). It was subsequently proposed that variations in low-latitude climate, driven by high-latitude glacial-interglacial cycles, controlled both the delivery of sediment to, and the geochemical conditions within, disparate depositional environments and could, in conjunction with glacioeustatic change and regional tectonics, better explain cyclothem lithofacies variations across a wide range of depositional settings (Cecil, 1990).

Based on the hypothesis that low-latitude climate change played a significant role in cyclothem lithofacies variation, multiple orbitally-paced climate-change deposition models have been proposed (Heckel, 1995; Miller et al., 1996; Soreghan, 1994; Tandon and Gibling, 1994). In these deposition models orbital insolation variations either alter atmospheric circulation patterns (Miller et al., 1996; Soreghan, 1994) or drive glacioeustatic fluctuations that alter moisture availability within the continental interior (Heckel, 1995; Tandon and Gibling, 1994). The climatic responses detailed in these studies are similar to those inferred from the Pleistocene; periods of high-latitude continental glaciation are expected to be cool and dry in the low latitudes while interglacial intervals are predicted to be warm and wet. This Pleistocene-climate analogue has gained considerable acceptance in the late Paleozoic community and has been widely invoked to explain cyclic lithological variations throughout the Pangaean paleotropics (i.e., Falcon-Lang, 2003, 2004; Falcon-Lang et al., 2009, 2011; Joeckel, 1999; Olszewski and Patzkowsky, 2003; Soreghan et al., 2002).

The appropriateness of the Pleistocene analogue is questionable (Peyser and Poulsen, 2008). Numerous factors were fundamentally different in the late Paleozoic Ice Age: among them, (1) the amalgamation of continental land masses into the Pangaean super-continent, (2) the greater distribution of land within the tropical latitudes, and (3) the more poleward location of waxing and waning continental ice sheets. In addition to these factors, building empirical evidence from paleo-equatorial cyclic successions indicates that late Paleozoic glacial periods were wetter and less seasonal than their interglacial counterparts (Bishop et al., 2010; Cecil et al., 2003; DiMichele et al., 2009; Eros et al., sion; Feldman et al., 2005). To account for these observations, an alternative orbitally-paced cyclothem deposition model was proposed. In this de-

position model, orbitally-controlled Gondwanaland ice sheets regulate the position and migration of the inter-tropical convergence zone (ITCZ), thereby controlling low-latitude precipitation, sediment flux, and geochemistry within depositional environments (Cecil et al., 2003). This deposition model predicts that the low-latitude climatic response to a period of high-latitude continental glaciation will be an increase in precipitation, whereas a warmer interglacial interval will be accompanied by lesser, more seasonal precipitation.

In this study we utilize a coupled atmosphere-ice sheet-vegetation model to investigate the influence of atmospheric $p\text{CO}_2$ and dynamic orbital configurations on low-latitude Pangaean climate and high-latitude Gondwanaland glaciation. Our results demonstrate that atmospheric $p\text{CO}_2$ concentration exerts the primary control on high-latitude late Paleozoic continental ice sheets and low-latitude precipitation. We further demonstrate that orbital insolation variations are sufficient to drive significant variability in low-latitude continental climate without the influence of ice sheets. Finally, we identify a $p\text{CO}_2$ window within which high-latitude late Paleozoic ice sheets remain sensitive to changes in orbital insolation. Using our climate modeling results, we develop a cyclothem deposition model that links both high-latitude glacial-interglacial fluctuations and low-latitude climate change with variations in the eccentricity of Earth's orbit about the Sun.

5.3   Model and Methods

To investigate LPIA climates we utilize the GENESIS Earth system climate model coupled to dynamic ecosystem and ice sheet modeling components. The GENESIS version 3.0 general circulation model has been used extensively for paleoclimatic sim-

ulations and is comprised of atmospheric, land-surface, sea-ice, and 50 m slab-ocean components (Pollard and Thompson, 1995; Thompson and Pollard, 1995, 1997). The GENESIS atmosphere is run with a T31 spectral resolution $(3.75° \times 3.75°)$and 18 vertical levels. The land surface model resolution is $2° \times 2°$ and utilizes a Sakmarian ($\sim$290 Ma) paleogeographic/paleotopographic reconstruction (Ziegler et al., 1997). We synchronously couple GENESIS to the BIOME4 ecosystem model, an equilibrium vegetation model that predicts global biome distributions and plant physiology based on monthly average temperature, precipitation, insolation, and $p\text{CO}_2$ concentration. BIOME4 was developed from the BIOME ecosystem modeling lineage with the intent to capture more accurately the distribution of high latitude ecosystems thought to have existed during the ice house conditions of the last glacial maximum (Harrison and Prentice, 2003; Kaplan et al., 2003). Since the grassland ecosystem had not yet evolved in the late Paleozoic, we exclude it (Strömberg, 2005). The three-dimensional ice sheet model is asynchronously coupled to the GENESIS-BIOME4 modeling scheme because the response time of the atmosphere and ice sheets differs by two orders of magnitude. The thermomechanical ice sheet model utilizes GCM-derived climatic data and is based on the vertically integrated continuity equation for ice mass balance. The evolution of continental ice sheet geometry is simulated via surface mass balance, basal melting, and ice-flow calculations on a $1° \times 2°$ surface grid (DeConto and Pollard, 2003).

The results presented in this manuscript address changes brought about by differences in the mean climate state as well as short-term transient climate variations. Previous modeling studies have suggested that late Paleozoic mean climatic states, e.g., glacial, interglacial, and ice-free climates, are largely controlled by the concentration of $p\text{CO}_2$ in the atmosphere (Horton et al., 2007, 2010; Horton and Poulsen,

2009). In accord with these results, the mean climate states simulated in our experiments correspond to a range of $p\text{CO}_2$ concentrations; (a) glacial conditions at 420 ppm, (b) glacial-interglacial fluctuations at 560 ppm, and (c) largely ice-free conditions at 840 ppm. To capture the transient evolution of climate due to short-term orbital parameter variation within each mean climatic state we utilize a coupling scheme that consists of alternating short (15 yr) GCM-biome integrations and long (5 kyr) ice-sheet integrations. Between the integration of each component, updated boundary conditions (e.g., meteorological information to the ice-sheet model or ice geometry to the GCM-biome model) are passed from one model component to the other, and orbital parameters are updated. For computational efficiency, we have simplified the periods of each orbital parameter such that eccentricity, obliquity, and precessional periods occur every 80, 40, and 20 kyrs, respectively (DeConto and Pollard, 2003; Horton and Poulsen, 2009). Each transient experiment began with ice-free continents and was run through three orbital cycles (80 kyrs each), for a total of 240 kyrs (48 iterations). For analysis purposes and to aid in the discussion of mean climatic states, the transient orbital scheme has been subdivided into three 80 kyr (eccentricity cycle) segments, termed Orbit 1 (1-80 kyrs), Orbit 2 (81-160 kyrs), and Orbit 3 (161-240 kyrs; Figure 5.1a). Each 80 kyr segment was run using the same orbital forcing sequence; the mean climate of each 80 kyr segment is calculated by averaging the annual mean of each individual time slice.

5.4   Results

5.4.1   Ice sheet behavior

In our simulations, ice sheet area, volume, and equatorward extent are largely controlled by the atmospheric $p\text{CO}_2$ concentration and its effect on global mean

temperature. In the 420 ppm experiment, the global average ice sheet volume increases from 1.93×10^7 km^3 to 7.70×10^7 km^3 over three orbital cycles (black line; Figure 5.1a). In southern Gondwanaland, a single supercontinental ice sheet accumulates and expands northward to 48° S, eventually covering 2.65×10^7 km^2 of the continent's surface and attaining an average height in excess of 2900 m (Figure 1b). This ice sheet contains the water-equivalent of $\sim$179 m of sea-level change, a value approaching the maximum estimates reported for high-frequency glacioeustasy in the late Paleozoic (Rygel et al., 2008). In the 560 ppm experiment, global average ice sheet volume increases from 6.88×10^6 km^3 to 1.75×10^7 km^3 over the three orbital cycles (blue line; Figure 5.1a). In Gondwanaland, multiple ice sheets form and at their maximum reach northward to 65° S and cover 1.11×10^7 km^2 of the continent's surface (Figure 5.1c). In the 840 ppm experiment, Gondwanaland is largely ice free (red line; Figure 5.1a), though isolated low-volume (5.93×10^6 km^3 maximum) ice deposition centers form along the Panthalassan coast in the extreme high southern latitudes (Figure 5.1d).

In our experiments, ice sheets demonstrate the greatest response to orbital insolation fluctuations when the eccentricity of Earth's orbit is high. High eccentricity amplifies precessional changes in insolation and leads to summer temperature maxima and minima in the high latitudes. Significant ice sheet volume increases occur during anomalously cold southern hemisphere summer orbits (high eccentricity, low obliquity, and SH summer solstice at aphelion), whereas ice sheet volume decreases coincide with anomalously warm SH summer orbits (high eccentricity, low obliquity, and the SH summer solstice at perihelion). At pCO$_2$ concentrations of 420 ppm, an ice sheet volume reduction is simulated at the end of Orbit 1, but thereafter the ice sheet grows sufficiently large to be insensitive to orbitally-induced warming due
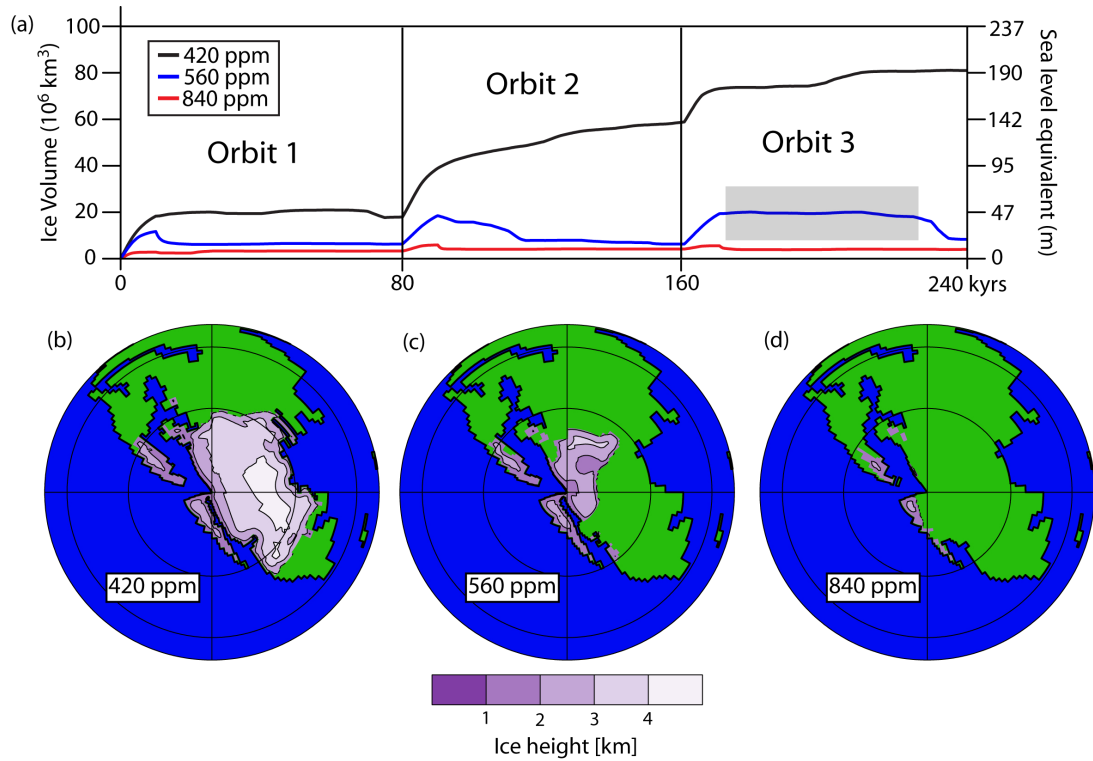
Figure 5.1: Time-series and time-slices of simulated late Paleozoic ice sheets. (a) Global ice volume and equivalent sea-level change time-series for each pCO$_2$ experiment (modified from Horton et al., 2010). Orbits 1–3 refer to periods that have been averaged to determine mean climatic states (for full description see section 2). The gray box highlights a period of low eccentricity and corresponds to a period of stable continental ice. (b-d) Late Paleozoic (∼290 Ma; Ziegler et al., 1997) southern hemisphere polar projection snapshots (170 kyr) of Gondwanaland ice sheets at each atmospheric pCO$_2$ concentration. The latitudinal contour interval is 30°.

to the cooling effects of ice height and albedo feedbacks (black line; Figure 5.1a). At pCO$_2$ concentrations of 560 ppm, the ice sheet waxes and wanes (by up to 33 m in sea-level equivalent) in response to orbital insolation fluctuations (blue line; Figure 5.1a). This response varies throughout the 240 kyr simulation due to the initialization of our experiments with ice-free boundary conditions and the interaction of ecosystems and climate at the ice sheet margin (Horton et al., 2010).

5.4.2 Effect of ice sheets on precipitation

The ice sheets simulated in our experiments have little to no influence on Pangaean mean-annual precipitation or wet-season length (Figure 5.2a-r). For each pCO_2 level the net effect of ice sheet growth on precipitation is determined by comparing the average climate early in the simulation period (Orbit 1) to the average climate late in the simulation period (Orbit 3), when substantial ice sheet volumes have accumulated. Changes in mean-annual precipitation greater than ± 1 cm per month are observed in the high latitudes of the 560 and 420 ppm experiments due to the orographic effect of ice sheets and within an isolated region of mid-continent tropical Pangaea at 420 ppm (Figure 5.2c). Changes in the length of low-latitude wet-seasons, measured here as the number of months per year with precipitation in excess of 10 cm, occur in isolated pockets at all simulated pCO_2 levels, though it should be noted that such changes rarely exceed ± 1 month per year in wet-season length (Figure 5.2j-r).

In previous late Paleozoic climate modeling studies it was found that the addition of prescribed Gondwanaland ice sheets led to significant precipitation changes in tropical Pangaea (Peyser and Poulsen, 2008; Poulsen et al., 2007). These studies attributed the change in low-latitude precipitation to ice sheet induced strengthening of the low-latitude temperature gradient which, in turn, intensified Hadley cell overturning. The prescribed ice sheet geometries, which include ice height and areal extent, used in these studies were based on mapped glacial remnant deposits (including ice-rafted debris) and in some cases represent "extreme" ice-coverage estimates (in one simulation ice extends from the pole to 20 °S). Our results in this study differ from those presented in these previous studies because we use a dynamic ice sheet model that predicts ice sheet geometries based on simulated climatology, which results in ice sheets that are taller and less extensive than those prescribed

Mean Annual Precipitation [cm mon⁻¹]

Wet Season Length
[# of months with precip > 10 cm]
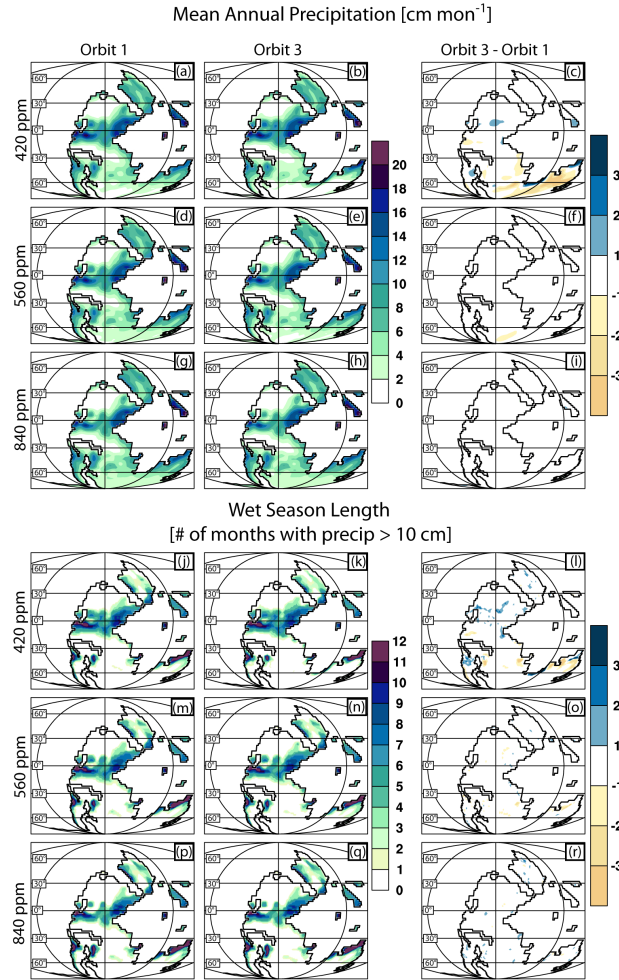
Figure 5.2: Mean annual precipitation (a–i) and wet-season length (j–r) simulated at each $p\mathrm{CO_2}$ concentration. Orbit 1 average in left column, Orbit 3 average in middle column, and Orbit 3 – Orbit 1 difference plots in right column. Wet-season length is defined as the number of months per year that precipitation exceeds 10 cm.

in the Peyser and Poulsen (2008) and Poulsen et al. (2007) studies. Because our ice sheets do not extend as far northward as those prescribed in previous studies, the low-latitude temperature gradient increase is comparatively reduced, as is the strength of the Hadley circulation (Figure 5.3b-c and Figure 6 in Peyser and Poulsen (2008)). In our present experiments, low-latitude Pangaea cools by an average of ∼1° C due to the accumulation of ice from Orbit 1 to Orbit 3 in the 420 ppm experiment (Figure 5.3a). This low-latitude cooling slightly intensifies the Hadley overturning circulation (Figure 5.3b-c) and is responsible for the small increase in mean-annual

precipitation noted above in Figure 5.2c.

Figure 5.3: Zonal temperature difference and atmospheric circulation. (a) Continental temperature differences (Orbit 3 - Orbit 1) for 420 and 560 ppm atmospheric pCO_2 concentration experiments. (b-c) The June-July-August (JJA) meridion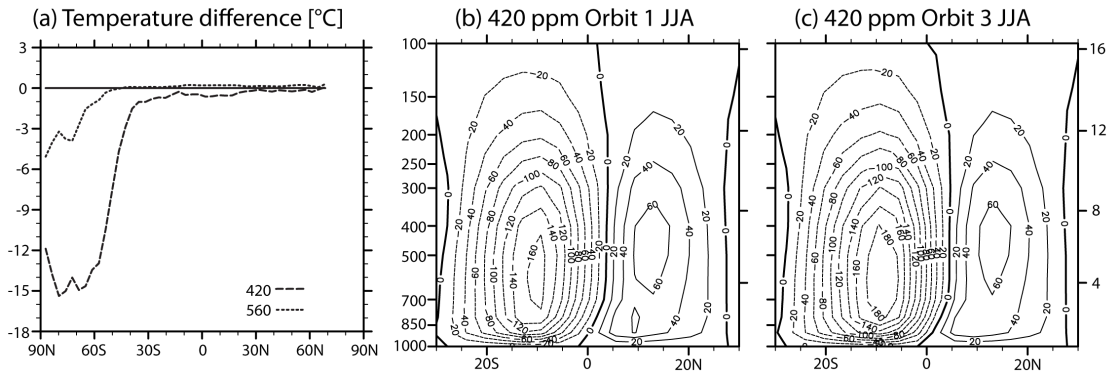al overturning streamfunction for average 420 ppm Orbit 1 (b) and Orbit 3 (c) climates [10^9 kg s^{-1}]. On each plot (b-c) the left y-axis is pressure [mb] and the right y-axis is height [km].

5.4.3 Mean climatic state effect on tropical precipitation

Our results indicate that the dominant control on tropical continental precipitation is the global mean temperature, as determined by the atmospheric pCO_2 concentration. To analyze the effect of global mean temperature on tropical continental precipitation, we compare the mean Orbit 3 climate of the 420 and 560 ppm simulations to that of the 840 ppm experiment. In all comparisons tropical mean-annual precipitation over land is greater in the lower pCO_2 simulations (Figure 5.4a and c), while over the oceans precipitation decreases with lower pCO_2 concentrations (Supplementary Figure 5.9.1). In the 420 versus 840 ppm comparison, mean-annual precipitation throughout the majority of the tropics is up to 6 cm per month higher in the lower pCO_2 experiment (Figure 5.4a). In conjunction with increased precipitation, the number of months in which precipitation exceeds 10 cm increases by an average of 1 to 5 months per year and the tropical wet-season length increases (Figure 5.4b). Mean-annual precipitation and wet-season length differences between the

560 and 840 ppm experiments show similar trends to the 420-840 ppm comparison, though the magnitude of differences is smaller (Figure 5.4c-d).
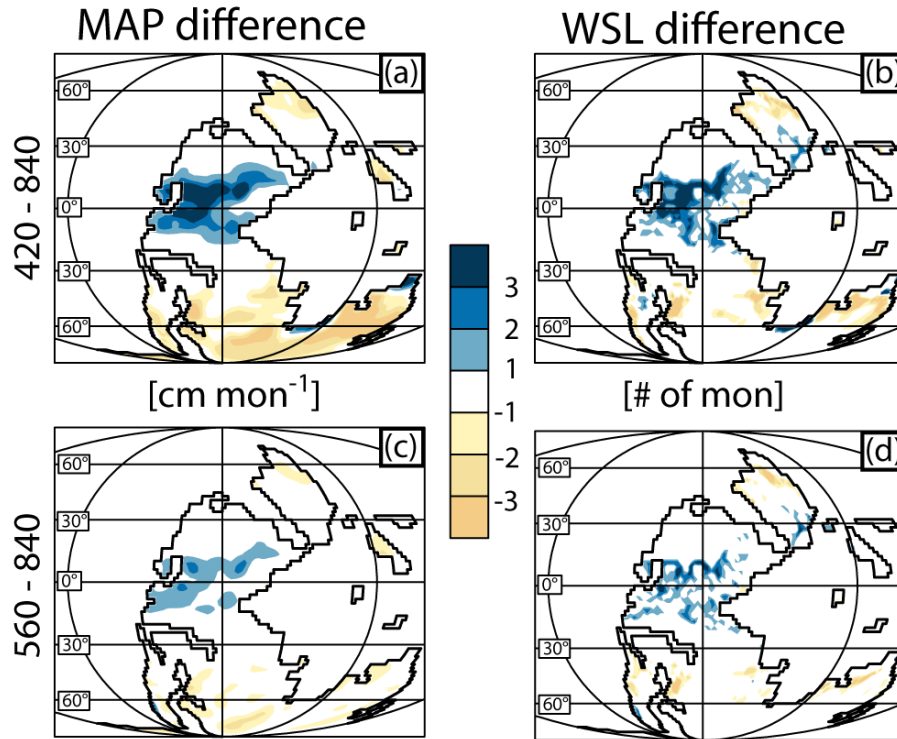
Figure 5.4: Orbit 3 difference plots of mean annual precipitation (MAP; a and c) and wet-season length (WSL; b and d). pCO$_2$ difference plots are calculated by subtracting the 840 ppm climatic conditions from those simulated at 420 and 560 ppm. Climatic conditions over the oceans have been masked (for an unmasked version, see Supplementary Figure 1).

According to the Clausius-Clapeyron (CC) relation, higher greenhouse gas concentrations increase the saturation vapor pressure of the atmosphere, leading to enhanced precipitation and evaporation. Consistent with the CC relation, precipitation over the oceans increases with increasing pCO$_2$ concentration, and is reduced with declining pCO$_2$. Over the continental tropics however, precipitation decreases with increasing atmospheric pCO$_2$ due to the expansion of desert and xerophytic ecosystems at the expense of forest, shrubland, and/or savanna ecosystems (Figure 5.5). The low vegetation density in desert and xerophytic ecosystems reduces soil moisture and precipitation rates (Poulsen et al., 2007). At lower pCO$_2$ concentra-

tions, densely vegetated ecosystems expand within the tropical latitudes, increasing soil moisture, evapotranspiration, and precipitation. Throughout the 240 kyr simulation, vegetation coverage and mean-annual precipitation are positively correlated (Figure 5.6). The role of vegetation is further established by a comparison of vegetated and desert/xerophytic low-latitude model grid cells, which indicates that areas with vegetated land cover receive ∼70% more precipitation than desert/xerophytic regions (Figure 5.7d and f).
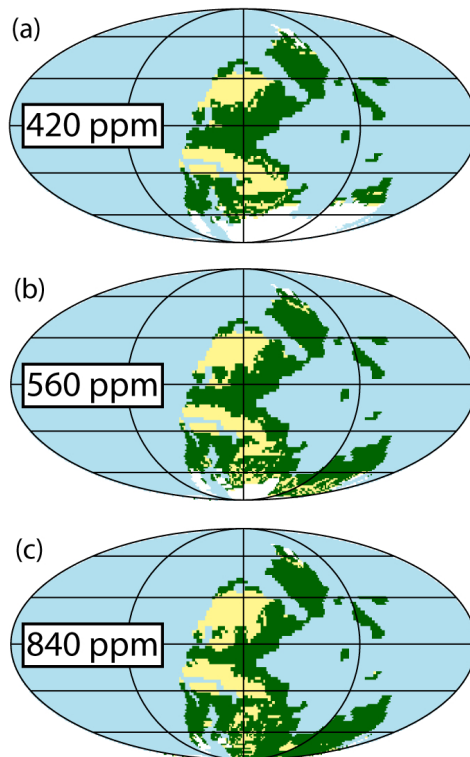
Figure 5.5: Orbit 3 mean vegetation distributions; (a) 420, (b) 560, (c) 840 ppm. Desert, barren, and xerophytic shrublands are depicted in yellow. All other ecosystems are green. Continental ice sheets are white and oceans/seas are blue. The latitudinal contour interval is 30°.

5.4.4 Orbital variability

Changes in Earth's tilt, season of perihelion, and the degree to which Earth's orbit about the Sun is eccentric influence the amount and distribution of insolation, and

alter global temperatures and precipitation patterns (Imbrie and Imbrie, 1980). In our late Paleozoic simulations, tropical continental precipitation exhibits the greatest variability during periods of high eccentricity and less variability during periods of low eccentricity (Figure 5.6c-e). When Earth's orbit about the Sun is eccentric, precession-driven temperature variations are amplified and seasonal variability increases (Figure 5.7). As the eccentricity of Earth's orbit is reduced, the amplification of precessional insolation changes weakens, and seasonality declines. Within the latitudes of cyclothem formation ($\sim$15 °S to 15 °N), mean-annual precipitation is dominated by the summer/fall wet-season. When the wet-season occurs during perihelion (aphelion) and Earth's orbit is eccentric, the insolation-driven temperature increase intensifies (weakens) the hydrological cycle, and precipitation increases (decreases). Due to the 20 kyr periodicity of the precessional cycle, when the wet-season occurs at perihelion, 10 kyrs later that hemisphere's wet-season must occur at aphelion. This leads to short-term climate extremes; when eccentricity is high, the wettest orbital configuration is followed 10 kyrs later by the driest orbital configuration. These 10 kyr climatic swings are reduced when eccentricity declines (i.e., Figure 5.6; vertical gray bars).

The wet-season precipitation that dominates cyclothem latitudes is governed by the passage of the ITCZ and its interaction with the summer monsoon circulation. The seasonal migration of the ITCZ follows the insolation maximum, with the ITCZ reaching its poleward maxima ($\sim$10 °N and S; Figure 5.8) during the summer and winter solstices and passing over the equator during the vernal and autumnal equinoxes. Changes in seasonal ITCZ precipitation intensity are amplified and dampened by eccentricity-modulated, precession-driven temperature variations (Figure 5.7). Although cyclothems are located in low, ITCZ influenced latitudes, sub-
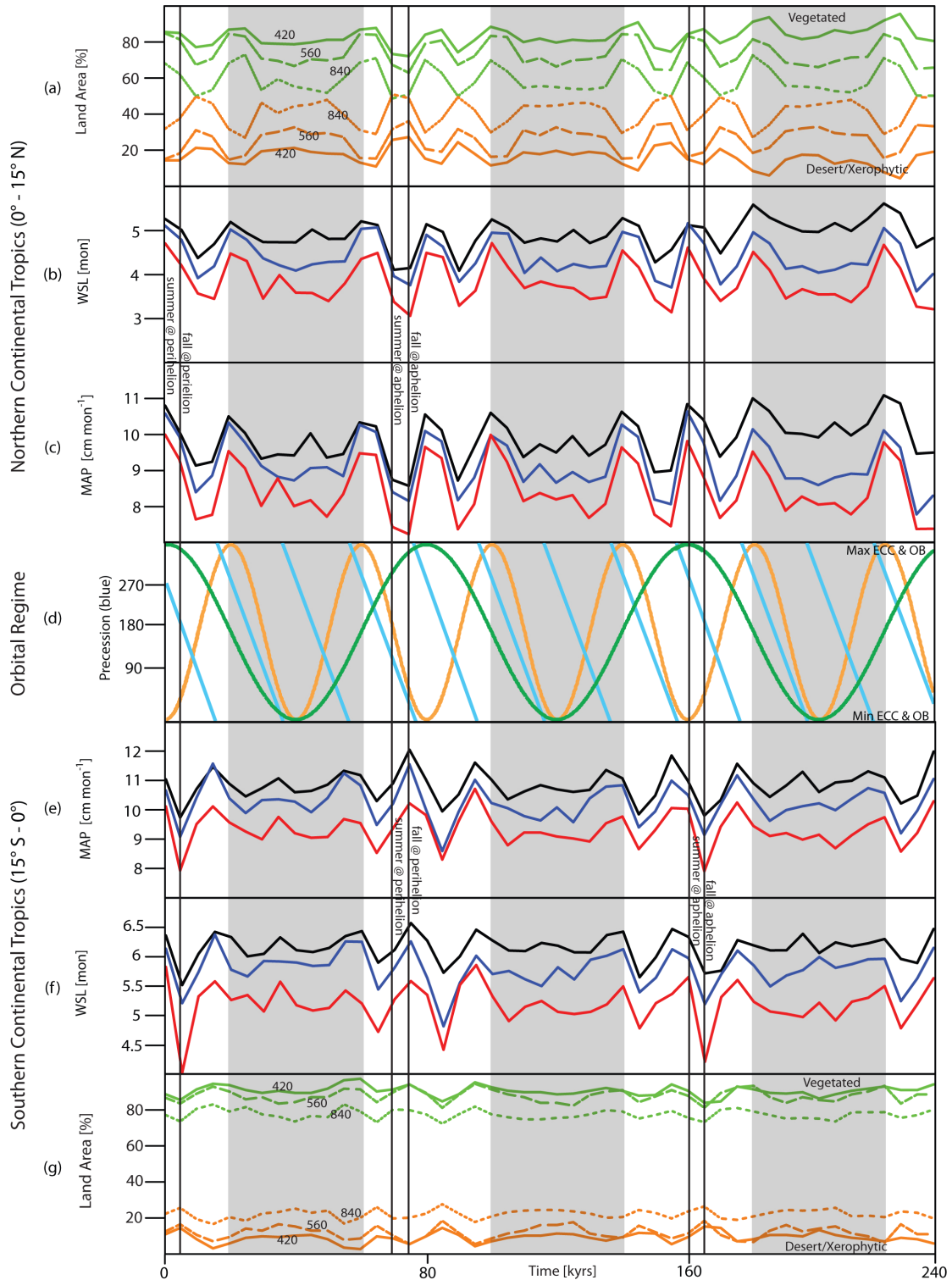
Figure 5.6: Time-series of continental low-latitude climate parameters. The percentage of Pangaea covered in desert/xerophytic or other (vegetated) ecosystems (a and g), wet-season length (b and f), and mean-annual precipitation (c and e) in both the northern and southern hemisphere tropics (0-15 °S and 0-15 °N). (d) The simulated orbital regime used in our experiments; values are based on Plio-Pleistocene maxima and/or minima (Berger and Loutre, 1991). Precession (light blue) is measured as the angle between northern hemisphere vernal equinox and perihelion. Eccentricity (ECC; green) ranges from a maximum of 0.057 to a minimum of 0.0002. Obliquity (OB; orange) ranges from 24.538° to 22.079°. Thick vertical gray bars highlight periods of low eccentricity. Thin vertical black lines indicate the season of aphelion/perihelion.
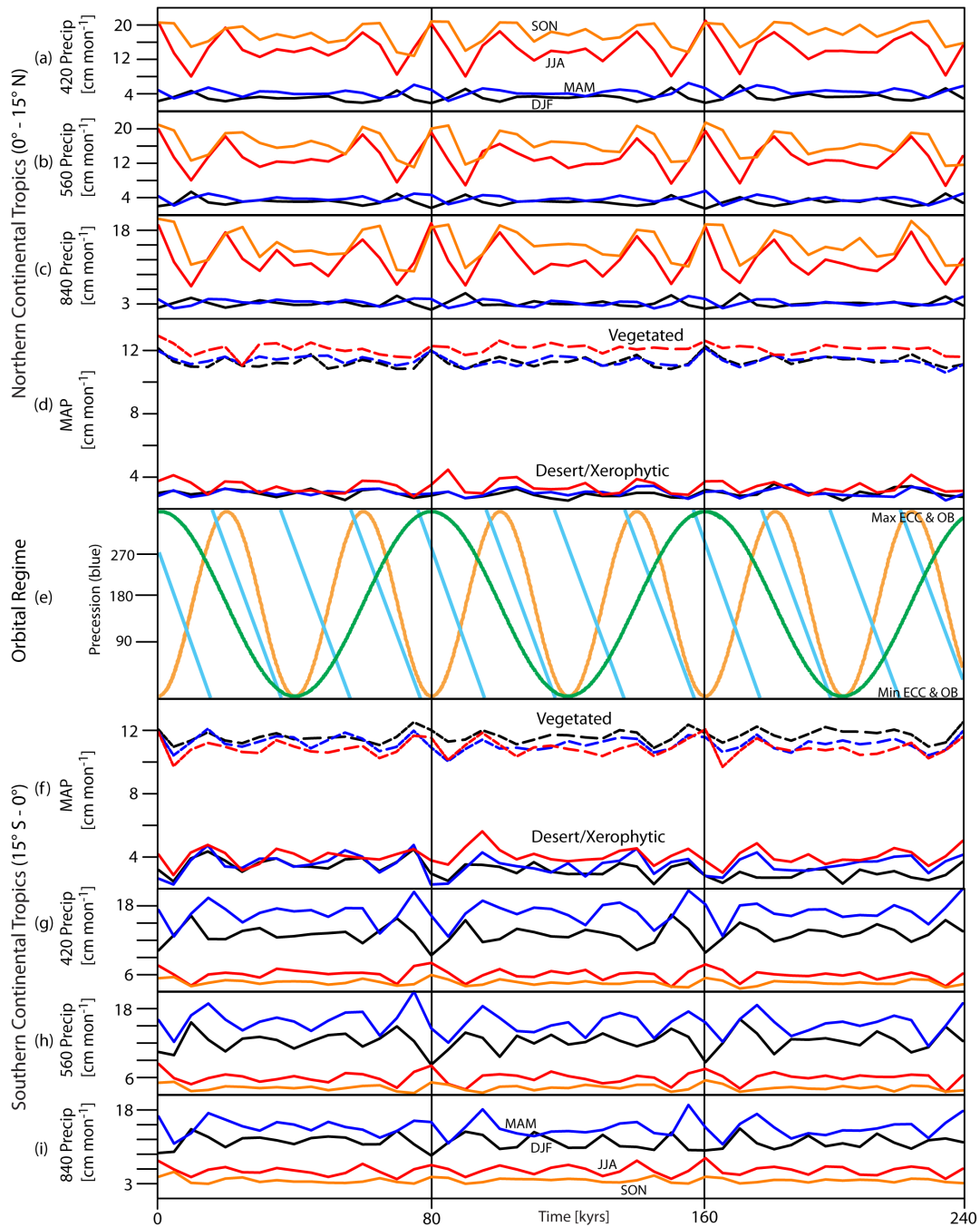
Figure 5.7: Time-series of continental precipitation. (a-c) Low-latitude northern hemisphere (NH; 0-15 °N) seasonal precipitation for each pCO$_2$ level experiment (DJF: December-January-February, MAM: March-April-May, JJA: June-July-August, SON: September-October-November). (d) NH mean-annual precipitation in vegetated versus desert/xerophytic grid cells. (e) Orbital regime used in simulations (See Figure 5.6 caption). (f) Low-latitude southern hemisphere (SH; 0-15 °S) mean-annual precipitation for vegetated versus desert/xerophytic grid cells. (g-i) SH seasonal precipitation for each pCO$_2$ level.

tropical to mid-latitude insolation changes play a large role in determining tropical precipitation distributions due to their influence on the summer monsoon strength. In the late Paleozoic northern hemisphere the summer-monsoon low forms at $\sim$20° N and tends to be relatively weak (1005-1010 mb) compared to its southern hemisphere counterpart, which forms at $\sim$40 °S and maintains sea-level pressures of 995-1000 mb (Figure 5.8a-d). The southern hemisphere monsoon is significantly stronger than that of the northern hemisphere due to the greater distribution of continental landmass located south of the equator (Kutzbach, 1994; Kutzbach and Gallimore, 1989). During the SH summer (Figure 5.8a), the monsoonal low diverts equatorial easterlies southward, which decreases low-latitude on-shore moisture-laden flow and reduces tropical precipitation. This diverted moisture increases mid-latitude precipitation, particularly along the Paleotethys coast (Figure 5.8e). On an annual basis, the result of this diversion is that the wettest period within the southern hemisphere cyclothem latitudes occurs during the fall (Figure 5.8f). On orbital timescales, the consequence of this summer monsoon influence is that the wettest cyclothem-latitude orbital configuration occurs when the autumnal equinox is at perihelion (Figure 5.7 and Figure 5.8f and h).

5.5 Discussion

5.5.1 Model results summary

The model results presented in this study demonstrate the substantial roles that both atmospheric $p\mathrm{CO}_2$ concentrations and orbital parameter fluctuations play in determining high-latitude Gondwanan glaciation and low-latitude Pangaean climate variability. Our simulations indicate that average low-latitude Pangaean vegetation coverage, mean-annual precipitation, and wet-season length are governed by atmo-
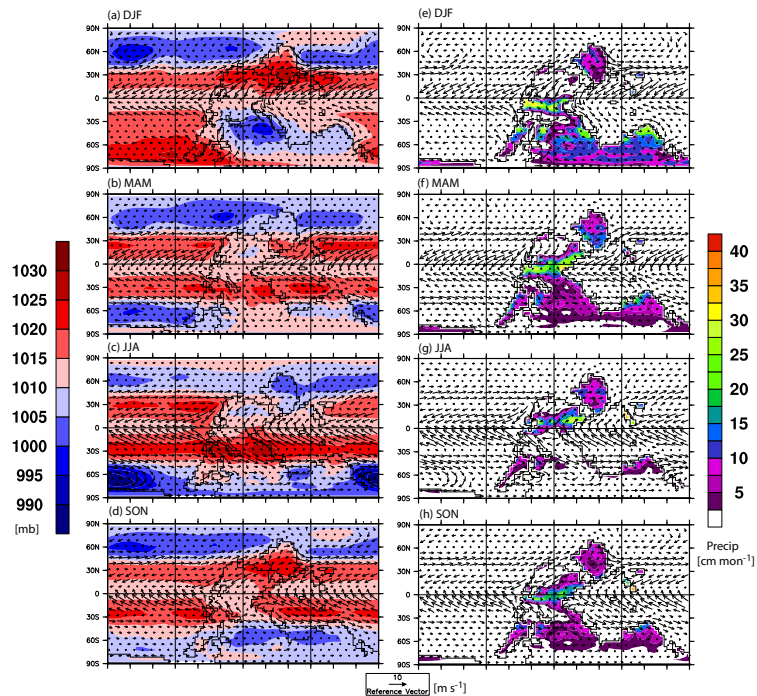
Figure 5.8: ITCZ-monsoon interactions. (a-d) Snapshots (65 kyr) of seasonal sea-level pressure and surface winds. Monsoon lows form in the summer hemispheres at 40° S (a) and 20° N (c). (e-h) Snapshots (65 kyr) of seasonal precipitation and winds (precipitation over the ocean has been masked). In the SH summer (e) the monsoon low diverts equatorial on-shore easterly flow toward high latitude Gondwanaland, increasing precipitation along the western Paleotethys coast.

spheric pCO_2 concentration, but that short-term variations in these climatic variables can be driven by orbital insolation fluctuations. We find that the low pCO_2 concentrations conducive to large-scale Gondwanaland glaciation are accompanied by higher mean-annual low-latitude continental precipitation, longer wet-season length, and increased vegetation coverage. High pCO_2 concentrations promote ice-free high latitudes, lower mean-annual low-latitude continental precipitation, shorter wet-season length, and reduced vegetation coverage. Such fluctuations ($\pm$140-420 ppm or more)

in atmospheric pCO$_2$ concentrations were unlikely to have occurred over short-to-intermediate (10^4-10^5 yrs) time intervals in the late Paleozoic, but likely played a larger role in the long-term (10^6-10^7 yrs) evolution of mean climatic states (DiMichele et al., 2009; Montañez et al., 2007).

On orbital time-scales, variations in high-latitude continental ice sheets and low-latitude continental precipitation are paced by the eccentricity of Earth's orbit; when eccentricity is high, precessionally-driven temperature changes are amplified and seasonality is increased, when eccentricity is low, precessional changes are not amplified and seasonality decreases. Our experiments indicate that low eccentricity corresponds to climates that produce high-latitude glaciation and stable low-latitude precipitation, whereas high eccentricity climates produce high-latitude interglacials and low-latitude precipitation volatility.

In our experiments these orbital-scale climatic trends are largely unaffected by Gondwanaland ice sheets, but based on both the upward trend in precipitation through time in the 420 ppm experiment (Figure 5.6c) and the results of Peyser and Poulsen (2008) and Poulsen et al. (2007), it is reasonable to assume that if ice sheets reached further northward than those simulated in our experiments larger changes to tropical precipitation would result. Beyond the direct atmospheric influence of continental ice sheets on climate, the accumulation and ablation of continental ice sheets helps to regulate global sea level. In our experiments, ice sheets of adequate volume to account for the sea-level fluctuations required of cyclothem deposition models are simulated at atmospheric pCO$_2$ concentrations of 420 and 560 ppm, but not at 840 ppm. Cyclothem-style fluctuations in ice volume, wherein ice sheets wax and wane with changing orbital insolation, occur only in the 560 ppm simulation and result in ice sheet volume fluctuations equivalent to $\sim$33 m of glacioeustatic change

(Figure 5.1a). The ice sheet simulated at 420 ppm is resistant to orbitally-driven temperature increases due to ice height and ice albedo feedbacks (Horton et al., 2010). These results suggest a relatively narrow window ($840 > p\text{CO}_2 > 420$) within which orbitally-driven glacioeustatic fluctuations are sufficient to develop cyclothems that require large-magnitude eustastic fluctuations.

5.5.2 Pangaean climatic change and deposition models

The results presented in this study suggest that the Pleistocene climate analogue is a poor fit for the late Paleozoic Ice Age. The Pleistocene analogue suggests that the low-latitude climatic response to periods of high-latitude glaciation should be a decrease in precipitation and an increase in seasonality (Heckel, 1995; Miller et al., 1996; Soreghan, 1994; Tandon and Gibling, 1994). On both orbital and carbon-cycle (10^6 yrs) time-scales our results indicate the opposite. (a) Low-latitude Pangaea receives more precipitation and has a longer wet-season when $p\text{CO}_2$ concentrations promote extensive Gondwanaland glaciation (Figure 5.4). (b) When atmospheric $p\text{CO}_2$ concentrations remain the same (420 ppm), but ice sheet volumes change, low-latitude climate is not significantly altered until ice sheet geometries are large enough to influence the Hadley circulation strength, at which point precipitation and wet-season length increase with increasing ice volume (Figure 5.2 and Figure 5.6b-f; black line). (c) Lastly, when ice sheet volumes do vary on orbital time-scales (560 ppm), precipitation is not significantly affected by the ice volume, but instead responds to changes in orbital insolation, demonstrating reduced seasonality during periods of low eccentricity, coincident with periods of high-latitude glaciation (Figure 5.7a-c and g-i). Our model does not simulate changes in sea level, although it does allow inferences of glacioeustasy. Thus the idea of a transgressive zone of increased precipitation due

to moisture proximity during glacial minima (Heckel, 1995) cannot be addressed explicitly, but a comparison of mean-annual precipitation along moisture-proximal coastal regions of western tropical Pangaea indicates that the 840 ppm minimal-ice experiment receives less precipitation than the higher ice volume experiments simulated at lower pCO$_2$ concentrations (Figure 5.4a-b).

Our modeling results are also at odds with the cyclothem deposition model presented by Cecil et al. (2003), though in this case the disagreement centers on the mechanism of low-latitude climate change and not on the lithology-based low-latitude climate inferences or the position of these lithotypes relative to glacial-interglacial/sea-level conditions. Contrary to the Cecil et al. (2003) cyclothem deposition model, the growth of Gondwanaland ice sheets and the strengthening of the SH polar high does not restrict the migration of the ITCZ (Peyser and Poulsen, 2008). Our results indicate that regardless of ice volume, pCO$_2$ concentration, or orbital parameter configuration the ITCZ follows the seasonal migration of the insolation maximum. In our simulations, it is orbital insolation variations that drive low-latitude precipitation variability, not the accumulation or ablation of ice sheets.

5.5.3 Influence of eccentricity-paced climatic change on cyclic deposition

To summarize, our results present a linkage between low-latitude climate, high-latitude glaciation, and inferred sea-level change that is nearly 180 degrees at odds with the Pleistocene analogue models and mechanistically at odd with the Cecil et al. (2003) model. Thus, we present here, a new deposition model that incorporates orbital insolation variations as the primary driving mechanism of both high and low-latitude climatic change. According to our modeling results, when pCO$_2$ concentrations are in the range of 560 ppm, changes in orbital insolation will drive

both glacioeustatic fluctuations and low-latitude variations in continental precipitation, wet-season length, and vegetation coverage. Utilizing these relationships, we apply our results to both a mixed terrestrial-marine (paralic) depositional environment typical of the shallow seaways of the Illinois and Donets Basins and a terrestrial-dominated depositional environment typical of areas distal to epeiric seaways such as those of the Appalachian Basin (Figure 5.9). The orbital configuration, low-latitude climatic conditions, relative (epeiric) sea-level curve, glacial-interglacial state, and corresponding numbered lithotypes in the following descriptions are illustrated in Figure 5.9.
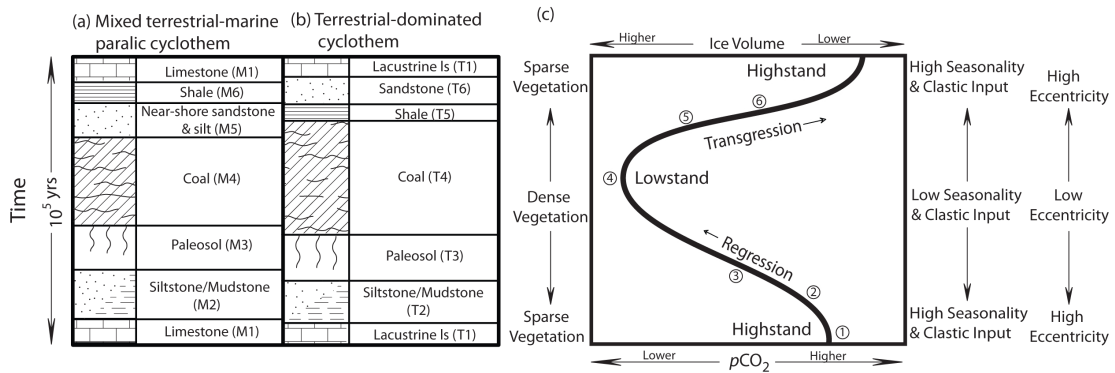
Figure 5.9: Eccentricity-paced cyclothems. (a) Generalized mixed terrestrial-marine cyclothem patterned after those found in the upper middle Pennsylvanian Carbondale Formation, Illinois Basin (Willman et al., 1975) and in Carboniferous deposits of the Donets Basin, Ukraine (Eros et al., sion). (b) Generalized terrestrial-dominated cyclothem patterned after those of the upper middle to upper Pennsylvanian Allegheny and Monogahela formations (Cecil, 1990). (c) Summary of parameters that drive cyclothem lithofacies variations. Curve depicts relative sea level in Pangaean epeiric seaways.

(i) High eccentricity, low obliquity, and the southern hemisphere summer solstice at aphelion produced an anomalously cold southern hemisphere summer. Cooler summer temperatures, in conjunction with a low atmospheric $p\mathrm{CO}_2$ concentration allowed snow cover to persist throughout the summer season, and ice sheets began to accumulate in high-latitude Gondwanaland (Figure 5.1a). In the low-latitudes, high eccentricity modulated precessional insolation changes, and led to a period

of maximum rainfall, followed shortly thereafter by a period of minimum rainfall (Figure 5.6; vertical white bars). These rapid climatic shifts had the potential to deposit thin, lithologically distinct facies in short periods of time. In terrestrial environments, short-lived anomalously dry periods were likely to deposit lacustrine limestones (T1), while short-lived anomalously wet periods may have led to the formation of thin coals (Histosols) and/or calcic soils. In some shelfal environments, the epeiric seaway had yet to regress, and water depths remained sufficient to deposit marine carbonates (M1).

(ii) As high-latitude ice sheets continued to accumulate, global sea level began to drop and regression of the epeiric seaways commenced. Continuing high eccentricity-induced low-latitude climatic variability, coupled with increasingly lower base-levels, led to fluvial incision and progradation of siliciclastics in both terrestrial (T2) and paralic depositional environments (M2).

(iii) At the transition from high-to-low eccentricity, precipitation remains seasonal, maximum high-latitude ice accumulation has been achieved, sea-level has rapidly fallen, and the epicontinental sea-floor has been left exposed. During this period vegetation began to take root and paleosols (Spodosols, Ultisols, Vertisols, and Calcic Vertisols) formed across the basins and within exposed epicontinental regions (M3 and T3).

(iv) Throughout the time that eccentricity remained low (Figure 5.6; vertical gray bars) precipitation continued to be distributed within wet and dry seasons (Figure 5.7), but orbital changes in the season of perihelion had little effect on the amount of mean-annual precipitation. A more stable distribution of precipitation, along with a net increase in accommodation due to the lowered rate of sea-level fall and background subsidence, caused the water-table to rise, vegetation to flourish, and

laterally extensive peat-forming coal-swamps formed in both paralic and terrestrial environments (M4 and T4).

(v) Peat/coal-forming conditions persisted, until the eccentricity of Earth's orbit began to increase and both low-latitude precipitation volatility returned and high-latitude ice sheets became susceptible to the anomalously warm southern hemisphere summer orbit. In shelfal environments, initial transgression ended peat/coal formation and led to the retrogradational deposition of tidalites along river channels draining peat swamps (M5) and fine-grained siliciclastics of the delta-front, including transgressive beach sands, in adjacent regions. In terrestrial environs, coal deposition likely continued until the occurrence of an anomalously dry orbit, at which point, the water-table lowered, vegetation density decreased, and siliciclastic input increased (T5-6).

(vi) As the rate of transgression increased (toward the point of maximum rate of sea-level rise), the depth of the epeiric sea over the shelfal environment increased and black shales (M6) and limestones (M1) were deposited. In terrestrial environments, the return of climate volatility is accompanied by the potential to deposit thin, lithologically distinct facies within short periods of time (T1), as is observed in the aggradational to progradational delta top deposits of the Donets cyclothems (likely reflecting the high rates of accommodation that characterize this region; Eros et al., in revision). These processes continued until orbital conditions again aligned to produce an anomalously cold southern hemisphere summer, ice sheet began to accumulate, and the cycle began anew.

Our eccentricity-paced cyclothem deposition model describes 'typical' cyclothem deposition, however, cyclothem deposits are known to display significant compositional, regional, and temporal variability. Our eccentricity-paced model cannot

explicitly account for all of this variability, but is amenable to variations caused by differences in regional climate, autocyclic depositional processes, periods of non-deposition, and/or complexities inherent to orbital parameter periodicities. For example, in the natural world, orbital parameters have multiple periodicities, each of which varies on an independent timescale. In our simulations we have minimized these complexities; we use an orbital regime that frequently aligns obliquity, eccentricity, and precession such that the parameters combine constructively to create maxima and minima in insolation (DeConto and Pollard, 2003; Horton and Poulsen, 2009). In the naturally evolving climate system, orbital parameters would not combine constructively as frequently as simulated in this study and the patterns of climate change recorded in geological units would display significant lithological and temporal variability, as is the case of cyclothems.

The climate modeling results presented in this study suggest that significant orbital-scale variability in paleo-tropical Pangaean climate may be driven by either atmospheric $p\text{CO}_2$ change or orbital insolation change, though it is probable that these parameters did not change independently. As in the Pleistocene (Petit et al., 1999), orbital insolation changes were likely accompanied by feedbacks that increased/decreased greenhouse gas concentrations and amplified climatic changes. For example, modest fluctuations in atmospheric $p\text{CO}_2$ concentrations (±100 ppm if on the scale of Pleistocene glacial-interglacial fluctuations), coincident with orbital insolation change, could facilitate the expansion and contraction of higher volume Gondwanaland ice sheets, and increase glacioeustatic change.

The long-term climatic trend of the late Paleozoic suggests that the climate transitioned from glacial-interglacial conditions that produced Carboniferous-Early Permian cyclothems to non-glacial conditions accompanied by continental aridification

in the Middle to Late Permian (Parrish, 1998; Tabor and Poulsen, 2008; Ziegler et al., 2002). Our results suggest that one factor leading to this transition could have been an increase in atmospheric greenhouse gas concentrations as has been suggested by Montañez et al. (2007). Both the near-simultaneous collapse of peat-forming coal swamps and Gondwanaland glaciation in the early Permian (Falcon-Lang and DiMichele, 2010) can be explained by an increase in atmospheric $p\text{CO}_2$ concentrations; higher $p\text{CO}_2$ levels would have prevented the accumulation of significant Gondwanaland ice sheets and promoted low-latitude aridification through a decrease in vegetated land coverage and tropical precipitation. The collapse of the peat-forming coal swamps themselves may have significantly contributed to rising $p\text{CO}_2$ levels (Cleal and Thomas, 2005). Considering the effects of increased atmospheric $p\text{CO}_2$ concentrations demonstrated in our model, rising greenhouse gas concentrations potentially could have played an important role in the massive collapse of flora and fauna recorded in the Permo-Triassic extinction event (Kidder and Worsley, 2004).

5.6   Caveats

The application of our simulated climate framework to conceptual deposition models is not without caveats. The use of Sakmarian paleogeography and paleotopography represents a single moment in the evolution of the late Paleozoic supercontinent. In reality, late Paleozoic cyclothem deposition began 30 myr prior to the Sakmarian and tropical climate dynamics were likely influenced by the evolution of continental landmass distributions (Torsvik and Cocks, 2004) and the evolution of the central Pangaean mountains (Rowley et al., 1985). For example, GCM studies of the late

Paleozoic have demonstrated that the addition of a low-latitude mountain range of moderate elevation (3 km) can decrease the seasonality of regional precipitation by creating an anomalous low-pressure center over elevated terrains during the tropical dry-season (Otto-Bliesner, 1993, 2003; Peyser and Poulsen, 2008). We predict that an increase in low-latitude topography could lead to a similar reduction in seasonality in our model, but that the cyclicity observed in cyclothem deposits must be generated by fluctuations in orbital insolation.

The use of a modern ecosystem model (BIOME4) in the simulation of late Paleozoic climate is a limitation, but given the uncertainty inherent in late Paleozoic plant physiology and the lack of a suitable late Paleozoic biome-model alternative, we think it is justified. Late Paleozoic low-latitude ecosystem change has been chronicled on glacial-interglacial time-scales, across ages, and from the start of the Carboniferous to the end of the Permian (Cleal and Thomas, 2005; DiMichele et al., 2001, 2009, 2010; Falcon-Lang, 2004; Falcon-Lang et al., 2009, 2011; Gastaldo et al., 2009). These studies attribute both short to intermediate-term cycles of species dominance and long-term floral transitions to changes in late Paleozoic climate. Whereas climate most certainly influenced late Paleozoic floral variations, the reciprocal role of these vegetation fluctuations in influencing LPIA climate is not well understood.

Of particular importance to the study of low-latitude climate is the role that tropical vegetation plays in precipitation distribution. In the modern tropics, rainforest ecosystems are largely comprised of angiosperm vegetation. Angiosperms have substantial transpiration capabilities that are thought to reduce the seasonality of precipitation (Boyce and Lee, 2010). In the late Paleozoic, angiosperms had not yet evolved, but evidence suggests that the transpiration capabilities of some coal-swamp forest vegetation types may have reached the lower range of angiosperm levels

(Wilson et al., 2008). Additionally, some types of late Palaeozoic wetland plants are thought to have had large total leaf areas (Laveine, 1986) and high growth rates, factors that in aggregate potentially offset decreased transpiration capability on a per-unit of leaf-surface-area basis (Cleal and Thomas, 2005; Phillips and DiMichele, 1992). Taken collectively, these factors suggest that some late Paleozoic vegetation types may be well represented by modern analogs, helping to justify the use of the BIOME4 ecosystem model in our simulations of late Paleozoic climate.

5.7 Conclusion

Recent efforts to constrain the timing and extent of Gondwanaland glaciation, via the mapping and dating of glaciogenic deposits, indicate that not all cyclothem deposits are contemporaneous with periods of chronostratigraphically well constrained glaciation (Fielding et al., 2008a,b; Gulbranson et al., 2010; Isbell et al., 2003, 2008). This suggests that factors other than glacioeustasy may have been responsible for the sea level fluctuations inferred from cyclothem deposits, or that factors other than sea-level change are major contributors to cyclothem deposition. In the context that the juxtaposition of marine and terrestrial facies require absolute changes in relative sea-level (accommodation space), our results suggest that regardless of the existence of ice sheets or significant ice-sheet-volume change, orbital insolation fluctuations will drive low-latitude climate variability and in turn, alter depositional environments.

In this study we utilize a climate model to investigate the processes that drove late Paleozoic climate change and address the effect of these changes on cyclic low-latitude sediment deposition. Our model results demonstrate that both atmospheric pCO_2 concentrations and orbital insolation variations are important factors in determining

the volume of high-latitude Pangaean ice sheets and the climatic conditions within low-latitude depositional environments. Our results further indicate that within a narrow atmospheric pCO$_2$ window (840<pCO$_2$<420) changes in the eccentricity of Earth's orbit paced the accumulation and ablation of Gondwanaland ice sheets, modulated glacioeustatic change, and controlled the distribution of precipitation and vegetation across low-latitude Pangaea. On the basis of these results, we propose that the rhythmic sedimentation patterns observed in Euramerican cyclothem deposits are the result of eccentricity-paced changes in both high and low-latitude late Paleozoic climate.

5.8 Acknowledgments

5.9 Appendix

(a) 420 Orbit 1 - 840 Orbit 1

(d) 560 Orbit 1 - 840 Orbit 1

(b) 420 Orbit 2 - 840 Orbit 2

(e) 560 Orbit 2 - 840 Orbit 2

(c) 420 Orbit 3 - 840 Orbit 3

(f) 420 Orbit 3 - 840 Orbit 3

-3 -2 -1 -.5 .5 1 2 3 [cm mon^{-1}]
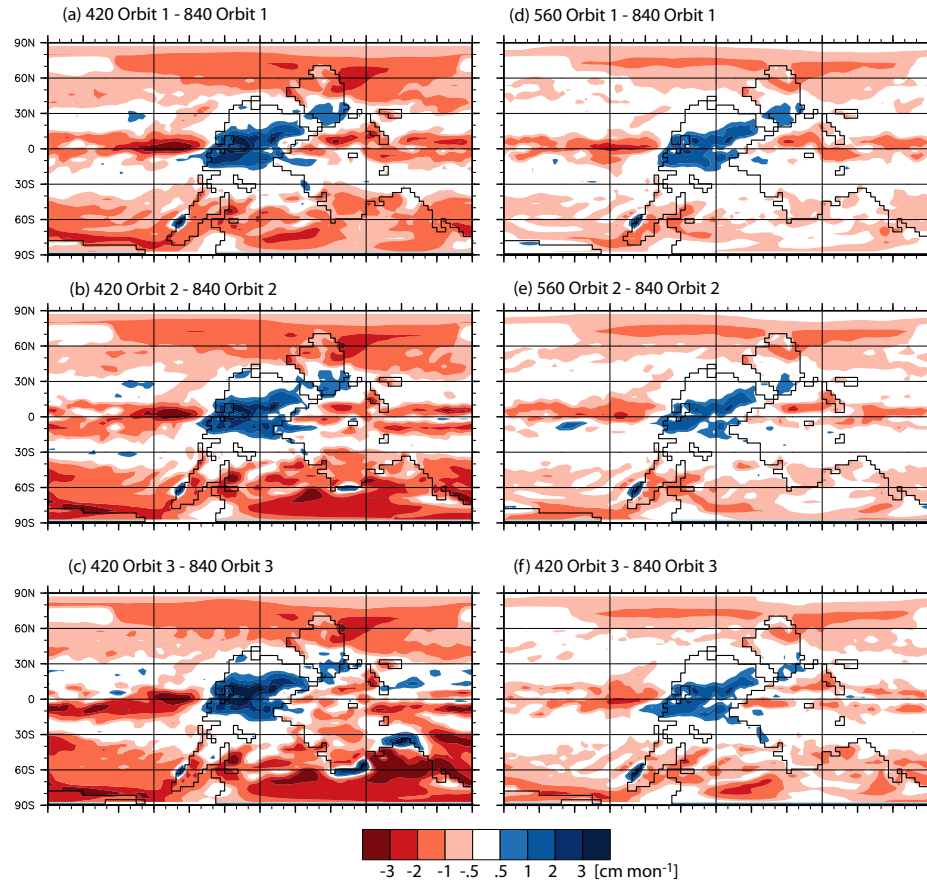
Supplementary Figure 5.9.1: Mean-annual precipitation difference plots. pCO$_2$ difference plots are calculated by subtracting the 840 ppm climatic conditions from those simulated at 420 and 560 ppm. Note that (c and f) display the same data as Figure 5.4a and c with the climatic conditions over the oceans unmasked. Precipitation over the oceans decreases with reduced atmospheric pCO$_2$, whereas precipitation over the continental tropics increases with decreasing pCO$_2$. High-latitude increases in precipitation with reduced pCO$_2$ are due to the orographic effect of accumulating ice sheets.

Bibliography

Berger, A. and Loutre, M. F. Insolation Values for the Climate of the Last 10,000,000 Years. *Quaternary Science Reviews*, 10(4):297–317, 1991.

Bishop, J. W., Montañez, I. P. and Osleger, D. A. Dynamic Carboniferous climate change, Arrow Canyon, Nevada. *Geosphere*, 6(1):1–34, 2010.

Boardman, D. R. and Heckel, P. H. Glacial-Eustatic Sea-Level Curve for Early Late Pennsylvanian Sequence in North-Central Texas and Biostratigraphic Correlation with Curve for Midcontinent North-America. *Geology*, 17(9):802–805, 1989.

Bohacs, K. and Suter, J. Sequence stratigraphic distribution of coaly rocks: Fundamental controls and paralic examples. *Aapg Bulletin-American Association of Petroleum Geologists*, 81(10):1612–1639, 1997.

Boyce, C. K. and Lee, J. E. An exceptional role for flowering plant physiology in the expansion of tropical rainforests and biodiversity. *Proceedings of the Royal Society B-Biological Sciences*, 277(1699):3437–3443, 2010.

Caputo, M. V. and Crowell, J. C. Migration of Glacial Centers across Gondwana during Paleozoic Era. *Geological Society of America Bulletin*, 96(8):1020–1036, 1985.

Cecil, C., Dulong, F., West, R., Stamm, R., Wardlaw, B. and Edgar, N. Climate controls on the stratigraphy of a middle Pennsylvanian cyclothem in North America. In Cecil, C. and Edgar, N., editors, *Climate Controls of Stratigraphy*, volume 77. SEPM Special Publication, 2003.

Cecil, C. B. Paleoclimate Controls on Stratigraphic Repetition of Chemical and Siliciclastic Rocks. *Geology*, 18(6):533–536, 1990.

Cleal, C. J. and Thomas, B. A. Palaeozoic tropical rainforests and their effect on global climates: is the past the key to the present? *Geobiology*, 3(1):13–31, 2005.

Crowell, J. C. Gondwanan Glaciation, Cyclothems, Continental Positioning, and Climate Change. *American Journal of Science*, 278(10):1345–1372, 1978.

DeConto, R. M. and Pollard, D. A coupled climate-ice sheet modeling approach to the Early Cenozoic history of the Antarctic ice sheet. *Palaeogeography Palaeoclimatology Palaeoecology*, 198(1-2):39–52, 2003.

DiMichele, W. A., Cecil, C. B., Montañez, I. P. and Falcon-Lang, H. J. Cyclic changes in Pennsylvanian paleoclimate and effects on floristic dynamics in tropical Pangaea. *International Journal of Coal Geology*, 83(2-3):329–344, 2010.

DiMichele, W. A., Montañez, I. P., Poulsen, C. J. and Tabor, N. J. Climate and vegetational regime shifts in the late Paleozoic ice age earth. *Geobiology*, 7(2):200–226, 2009.

DiMichele, W. A., Pfefferkorn, H. W. and Gastaldo, R. A. Response of Late Carboniferous and Early Permian plant communities to climate change. *Annual Review of Earth and Planetary Sciences*, 29:461–487, 2001.

Eros, J., Montañez, I., Osleger, D., Davydov, V., Nemyrovska, T., Poletaev, V. and Zhykalyak, M. Upper Carboniferous Sequence Stratigraphy and Relative Sea Level history, Donets Basin, Ukraine. *Palaeogeogr. Palaeoclimatol. Palaeoecol.*, in revision.

Falcon-Lang, H. J. Response of Late Carboniferous tropical vegetation to transgressive-regressive rhythms at Joggins, Nova Scotia. *Journal of the Geological Society*, 160:643–648, 2003.

Falcon-Lang, H. J. Pennsylvanian tropical rain forests responded to glacial-interglacial rhythms. *Geology*, 32(8):689–692, 2004.

Falcon-Lang, H. J. and DiMichele, W. A. What Happened to the Coal Forests during Pennsylvanian Glacial Phases? *Palaios*, 25(9-10):611–617, 2010.

Falcon-Lang, H. J., Jud, N. A., DiMichele, W. A., Chaney, D. S. and Lucas, S. G. Pennsylvanian coniferopsid forests in sabkha facies reveal the nature of seasonal tropical biome. *Geology*, 39:371–374, 2011.

Falcon-Lang, H. J., Nelson, W. J., Elrick, S., Looy, C. V., Ames, P. R. and DiMichele, W. A. Incised channel fills containing conifers indicate that seasonally dry vegetation dominated Pennsylvanian tropical lowlands. *Geology*, 37(10):923–926, 2009.

Feldman, H. R., Franseen, E. K., Joeckel, R. M. and Heckel, P. H. Impact of longer-term modest climate shifts on architecture of high-frequency sequences (cyclothems), Pennsylvanian of midcontinent USA. *Journal of Sedimentary Research*, 75(3):350–368, 2005.

Fielding, C. R., Frank, T. D., Birgenheier, L. P., Rygel, M. C., Jones, A. T. and Roberts, J. Stratigraphic imprint of the Late Palaeozoic Ice Age in eastern Australia: a record of alternating glacial and nonglacial climate regime. *Journal of the Geological Society*, 165:129–140, 2008a.

Fielding, C. R., Frank, T. D. and Isbell, J. I. The Late Paleozoic Ice Age-a Review of Current Understanding and Synthesis of Global Climate Patterns. In Fielding,

C. R., Frank, T. D. and Isbell, J. I., editors, *Resolving the Late Paleozoic Ice Age in Time and Space*, volume 441. Geol. Soc. Am. Spec. Pap., 2008b.

Gastaldo, R. A., Purkynova, E., Simunek, Z. and Schmitz, M. D. Ecological persistence in the late mississippian (serpukhovian, namurian a) megafloral record of the upper silesian basin, czech republic. *Palaios*, 24(5-6):336–350, 2009.

Gibling, M. R. and Rygel, M. C. Late Paleozoic cyclic strata of Euramerica: Gondwanan glacial signatures enhanced during slow-subsidence periods. In Fielding, C., Frank, T. and Isbell, J., editors, *Resolving the Late Paleozoic Ice Age in Time and Space*, pages 219–233. Geological Society of America Special Publication 441, 2008.

Gulbranson, E. L., Montanez, I. P., Schmitz, M. D., Limarino, C. O., Isbell, J. L., Marenssi, S. A. and Crowley, J. L. High-precision U-Pb calibration of Carboniferous glaciation and climate history, Paganzo Group, NW Argentina. *Geological Society of America Bulletin*, 122(9-10):1480–1498, 2010.

Harrison, S. P. and Prentice, A. I. Climate and CO_2 controls on global vegetation distribution at the last glacial maximum: analysis based on palaeovegetation data, biome modelling and palaeoclimate simulations. *Global Change Biology*, 9(7):983–1004, 2003.

Heckel, P. H. Origin of phosphatic black sahel facies in Pennsylvanian cyclothems of Mid-Continent North America. *American Association of Petroleum Geologists Bulletin*, 61:1045–1068, 1977.

Heckel, P. H. Sea-Level Curve for Pennsylvanian Eustatic Marine Transgressive-Regressive Depositional Cycles Along Midcontinent Outcrop Belt, North-America. *Geology*, 14(4):330–334, 1986.

Heckel, P. H. Glacial-eustatic base-level-Climatic model for late middle to late Pennsylvanian coal-bed formation in the Appalachian basin. *J. of Sedimentary Research*, B65(3):348–356, 1995.

Horton, D. E. and Poulsen, C. J. Paradox of late Paleozoic glacioeustasy. *Geology*, 37(8):715–718, 2009.

Horton, D. E., Poulsen, C. J. and Pollard, D. Orbital and CO_2 forcing of late Paleozoic continental ice sheets. *Geophysical Research Letters*, 34(19):L19708, 2007.

Horton, D. E., Poulsen, C. J. and Pollard, D. Influence of high-latitude vegetation feedbacks on late Palaeozoic glacial cycles. *Nature Geoscience*, 3(8):572–577, 2010.

Imbrie, J. and Imbrie, J. Z. Modeling the Climatic Response to Orbital Variations. *Science*, 207(4434):943–953, 1980.

Isbell, J. L., Kock, Z. J., Szablewski, G. M. and Lenaker, P. A. Permian glacigenic deposits in the Transantarctic Mountains, Antarctica. In Fielding, C. R., Frank, T. D. and Isbell, J. L., editors, *Resolving the Late Paleozoic Ice Age in Time and Space*, volume 441, pages 59–70. Geol. Soc. Am. Spec. Pap., 2008.

Isbell, J. L., Miller, M. F., Wolfe, K. L. and Lenaker, P. A. Timing of late Paleozoic glaciation in Gondwana: Was glaciation responsible for the development of Northern Hemisphere cyclothems? In Chan, M. A. and Archer, A. W., editors, *Extreme Depositional Environments: Mega End Members in Geologic Time*, volume 370, pages 5–24. Spec. Pap. Geol. Soc. Am., 2003.

Izart, A., Stephenson, R., Vai, G. B., Vachard, D., Le Nindre, Y., Vaslet, D., Fauvel, P. J., Suss, P., Kossovaya, O., Chen, Z. Q., Maslo, A. and Stovba, S. Sequence stratigraphy and correlation of late Carboniferous and Permian in the CIS, Europe, Tethyan area, North Africa, Arabia, China, Gondwanaland and the USA. *Palaeogeography Palaeoclimatology Palaeoecology*, 196(1-2):59–84, 2003.

Joeckel, R. M. Paleosol in Galesburg Formation (Kansas City Group, Upper Pennsylvanian), northern Midcontinent, USA: Evidence for climate change and mechanisms of marine transgression. *Journal of Sedimentary Research*, 69(3):720–737, 1999.

Kaplan, J. O., Bigelow, N. H., Prentice, I. C., Harrison, S. P., Bartlein, P. J., Christensen, T. R., Cramer, W., Matveyeva, N. V., McGuire, A. D., Murray, D. F., Razzhivin, V. Y., Smith, B., Walker, D. A., Anderson, P. M., Andreev, A. A., Brubaker, L. B., Edwards, M. E. and Lozhkin, A. V. Climate change and Arctic ecosystems: 2. Modeling, paleodata-model comparisons, and future projections. *Journal of Geophysical Research-Atmospheres*, 108(D19), 2003.

Kidder, D. L. and Worsley, T. R. Causes and consequences of extreme Permo-Triassic warming to globally equable climate and relation to the Permo-Triassic extinction and recovery. *Palaeogeography Palaeoclimatology Palaeoecology*, 203(3-4):207–237, 2004.

Kutzbach, J. Idealized Pangean climates: Sensitivity to orbital change. In Klein, G., editor, *Pangea: Paleoclimate, Tectonics, and Sedimentation during Accretion, Zenith, and Breakup of a Supercontinent*, volume Special Paper 288, pages 41–55. Geological Society of America, Boulder, CO, 1994.

Kutzbach, J. E. and Gallimore, R. G. Pangaean Climates - Megamonsoons of the Megacontinent. *Journal of Geophysical Research-Atmospheres*, 94(D3):3341–3357, 1989.

Laveine, J. The size of the frond in the genus *Alethopteris* STERNBERG (Pteridospermopsida, Carboniferous). *Geobios*, 19:49–59, 1986.

Maynard, J. R. and Leeder, M. R. On the Periodicity and Magnitude of Late Carboniferous Glacioeustatic Sea-Level Changes. *Journal of the Geological Society*, 149:303–311, 1992.

Miller, K. B., McCahon, T. J. and West, R. R. Lower Permian (Wolfcampian) paleosol-bearing cycles of the US midcontinent: Evidence of climatic cyclicity. *Journal of Sedimentary Research*, 66(1):71–84, 1996.

Montañez, I. P., Tabor, N. J., Niemeier, D., DiMichele, W. A., Frank, T. D., Fielding, C. R., Isbell, J. L., Birgenheier, L. P. and Rygel, M. C. CO_2-forced climate and vegetation instability during late paleozoic deglaciation. *Science*, 315(5808):87–91, 2007.

Olszewski, T. D. and Patzkowsky, M. E. From cyclothems to sequences: The record of eustasy and climate on an icehouse epeiric platform (Pennsylvanian-Permian, North American Midcontinent). *Journal of Sedimentary Research*, 73(1):15–30, 2003.

Otto-Bliesner, B. Tropical mountains and coal formation: A climate model study of the Westphalian (306 Ma). *Geophycical Research Letters*, 20:1947–1950, 1993.

Otto-Bliesner, B. The role of mountains, polar ice, and vegetation in determining the tropical climate during the middle Pennsylvanian: climate model simulations. In Cecil, C. and Edgar, N., editors, *Climate Controls of Stratigraphy*, pages 227–237. SEPM Special Publication No. 77, 2003.

Parrish, J. T. *Interpreting Pre Quaternary Climate from the Geologic Record.* Columbia University Press, New York, 1998.

Petit, J. R., Jouzel, J., Raynaud, D., Barkov, N. I., Barnola, J. M., Basile, I., Bender, M., Chappellaz, J., Davis, M., Delaygue, G., Delmotte, M., Kotlyakov, V. M., Legrand, M., Lipenkov, V. Y., Lorius, C., Pepin, L., Ritz, C., Saltzman, E. and Stievenard, M. Climate and atmospheric history of the past 420,000 years from the Vostok ice core, Antarctica. *Nature*, 399(6735):429–436, 1999.

Peyser, C. E. and Poulsen, C. J. Controls on Permo-Carboniferous precipitation over tropical Pangaea: A GCM sensitivity study. *Palaeogeography Palaeoclimatology Palaeoecology*, 268(3-4):181–192, 2008.

Phillips, T. and DiMichele, W. Comparative ecology and life history biology of arborescent lycopods in Late Carboniferous swamps of Euramerica. *Annals of the Missouri Botanical Garden*, 79:560–588, 1992.

Pollard, D. and Thompson, S. L. Use of a Land-Surface-Transfer Scheme (Lsx) in a Global Climate Model - the Response to Doubling Stomatal-Resistance. *Global and Planetary Change*, 10(1-4):129–161, 1995.

Poulsen, C. J., Pollard, D., Montañez, I. P. and Rowley, D. Late Paleozoic tropical climate response to Gondwanan deglaciation. *Geology*, 35(9):771–774, 2007.

Ramsbottom, W. Transgressions and regressions in the Dinantian: a new synthesis of British Dinantian stratigraphy. *Proc. Yorks. Geol. Soc.*, 39:567–607, 1973.

Ramsbottom, W. Major cycles of transgression and regression (mesothems) in the Namurian. *Proc. Yorks. Geol. Soc.*, 41:261–291, 1977.

Rasbury, E. T., Hanson, G. N., Meyers, W. J., Holt, W. E., Goldstein, R. H. and Saller, A. H. U-Pb dates of paleosols: Constraints on late Paleozoic cycle durations and boundary ages. *Geology*, 26(5):403–406, 1998.

Rowley, D. B., Raymond, A., Parrish, J. T., Lottes, A. L., Scotese, C. R. and Ziegler, A. M. Carboniferous Paleogeographic, Phytogeographic, and Paleoclimatic Reconstructions. *International Journal of Coal Geology*, 5(1-2):7–42, 1985.

Rygel, M. C., Fielding, C. R., Frank, T. D. and Birgenheier, L. P. The magnitude of late Paleozoic glacioeustatic fluctuations: a synthesis. *Journal of Sedimentary Research*, 78(7-8):500–511, 2008.

Soreghan, G. S. The impact of glacioclimatic change on Pennsylvanian cyclostratigraphy. In Embry, A., Beauchamp, B. and Glass, D., editors, *Pangea–Global environments and resources*, volume 17, pages 523–543. Canadian Society of Petroleum Geologists Memoir, 1994.

Soreghan, G. S., Elmore, R. and Lewchuk, M. T. Sedimentologicmagnetic record of western Pangean climate in upper Paleozoic loessite (lower Cutler beds, Utah). *Geological Society of America Bulletin*, 114(8):1019–1035, 2002.

Strasser, A., Hilgren, F. and Heckel, P. H. Cyclostratigraphy-Concepts, definitions, and applications. *Newsletters in Stratigraphy*, 42:75–114, 2006.

Strömberg, C. A. E. Decoupled taxonomic radiation and ecological expansion of open-habitat grasses in the Cenozoic of North America. *Proceedings of the National Academy of Sciences of the United States of America*, 102(34):11980–11984, 2005.

Tabor, N. J. and Poulsen, C. J. Palaeoclimate across the Late Pennsylvanian-Early Permian tropical palaeolatitudes: A review of climate indicators, their distribution, and relation to palaeophysiographic climate factors. *Palaeogeography Palaeoclimatology Palaeoecology*, 268(3-4):293–310, 2008.

Tandon, S. K. and Gibling, M. R. Calcrete and Coal in Late Carboniferous Cyclotherms of Nova-Scotia, Canada - Climate and Sea-Level Changes Linked. *Geology*, 22(8):755–758, 1994.

Thompson, S. L. and Pollard, D. A Global Climate Model (Genesis) with a Land-Surface Transfer Scheme (Lsx) .1. Present Climate Simulation. *Journal of Climate*, 8(4):732–761, 1995.

Thompson, S. L. and Pollard, D. Greenland and Antarctic mass balances for present and doubled atmospheric CO_2 from the GENESIS version-2 global climate model. *Journal of Climate*, 10(5):871–900, 1997.

Torsvik, T. H. and Cocks, L. R. M. Earth geography from 400 to 250 Ma: a palaeomagnetic, faunal and facies review. *Journal of the Geological Society*, 161:555–572, 2004.

Veevers, J. J. and Powell, C. M. Late Paleozoic Glacial Episodes in Gondwanaland Reflected in Transgressive-Regressive Depositional Sequences in Euramerica. *Geological Society of America Bulletin*, 98(4):475–487, 1987.

Wanless, H. R. and Shepard, F. P. Sea level and climatic changes related to late Paleozoic cycles. *Bulletin of the Geological Society of America*, 47(5/8):1177–1206, 1936.

Weedon, G. and Reed, W. Orbital-climatic forcing of Namurian cyclic sedimentation from spectral analysis of the Limestone Coal Formation, Central Scotland. *Geological Society, London, Special Publications*, 85:51–66, 1995.

Willman, H. B., Atherton, E., Buschbach, T., Collinson, C., Frye, J. C., Hopkins, M. E., Lineback, J. A. and Siman, J. A. Handbook of Illinois Stratigraphy. *Illinois State Geological Suvery Bulletin*, 95:1–261, 1975.

Wilson, J. P., Knoll, A. H., Holbrook, N. M. and Marshall, C. R. Modeling fluid flow in Medullosa, an anatomically unusual Carboniferous seed plant. *Paleobiology*, 34(4):472–493, 2008.

Ziegler, A., Rees, P. and Naugolnykh, S. The Early Permian floras of Prince Edward Island, Canada: differentiating global from local effects of climate change. *Can. J. Earth Sci.*, 39:223–238, 2002.

Ziegler, A. M., L., H. M. and Rowley, D. B. Permian world topography and climate. In Martini, I. P., editor, *Late Glacial and Postglacial Environmental Changes-Quaternary*, pages 111–146. Oxford Univ. Press, 1997.

CHAPTER VI

Summary and conclusions

This section summarizes the major results of each dissertation chapter, provides a brief synthesis of the major contributions of this thesis to our understanding of LPIA climate dynamics, and proposes new research directions motivated by these results.

6.1   Results summary

Chapter 2:   This chapter presents the first coupled GCM-ice sheet model simulations of the late Paleozoic ice age. As an initial step in LPIA climate-ice sheet modeling, these experiments use the GENESIS GCM to simulate climates in equilibrium with various orbital parameter configurations at several different atmospheric $p\mathrm{CO_2}$ concentrations. Utilizing the climatic conditions produced in these GCM experiments, the ice sheet model is compiled until an equilibrium ice sheet volume is attained. Our results demonstrate that regardless of orbital configuration, continental-scale equilibrium ice sheets are simulated when atmospheric $p\mathrm{CO_2}$ concentrations are below 560 ppmv, and that during a southern hemisphere cold summer-orbit, continental-scale equilibrium ice sheets are simulated until the $p\mathrm{CO_2}$ concentration exceeds 2240 ppmv. To the first-order, these results agree with proxy-derived esti-

mates of LPIA $p\mathrm{CO_2}$ concentrations taken from sediments contemporaneous with periods of Gondwanaland glaciation. In sum, these results suggest that the coupled GCM-ice sheet modeling scheme developed herein is an appropriate means for further studies of the LPIA.

Chapter 3: In this chapter, the modeling scheme of Chapter 2 is modified to incorporate the effects of changing orbital parameters on continental ice sheets. In this scheme, the climate is simulated with the GENESIS GCM at a constant $p\mathrm{CO_2}$ level but with transient orbital conditions. The meteorological conditions simulated at a chosen orbital configuration are passed to the ice sheet model, which is then compiled for a short interval (5 kyrs). The resulting ice sheet geometry is then used as a boundary condition in a subsequent GCM-simulation whose orbital parameter configuration has been updated. This process is repeated for multiple orbital cycles. Using this modeling-scheme, this chapter tests the hypothesis that variations in orbital insolation drove cyclic glacioeustatic fluctuations. The results of these experiments produce a paradox; when $p\mathrm{CO_2}$ concentrations are low enough to produce an ice sheet of sufficient volume to account for inferred glacioeustatic changes, the ice sheets are insensitive to changes in orbital parameters. In an effort to solve this paradox and in line with some theories of orbitally-controlled ice sheets, we increase the atmospheric $p\mathrm{CO_2}$ concentration of our experiments until significant ice sheet ablation occurs. We find that the atmospheric $p\mathrm{CO_2}$ concentration exceeds 2240 ppmv before ice sheet collapse is simulated. Based on these results, we conclude that either important components of the climate system have not been accounted for in our model, or estimates of glacioeustatic change based on low-latitude sediment deposits are incorrect.

Chapter 4: In this chapter, we add a dynamic ecosystem modeling component, BIOME4, to our GCM-ice sheet modeling scheme. We again simulate transient orbital conditions at multiple pCO_2 levels with the intention of addressing the hypothesis that orbital change drove late Paleozoic glacioeustatic cycles. The results of these experiments indicate that orbitally-driven changes in ice-margin ecosystems amplify insolation-driven temperature variations, and facilitate the expansion and contraction of continental ice sheets. Based on these results, we constrain the atmospheric pCO_2 window within which LPIA ice sheets were amenable to orbital insolation variations.

Chapter 5: In this chapter, we expand on the results presented in Chapter 4, focusing on the roles of atmospheric pCO_2 and orbital insolation variations in driving both high-latitude glacial-interglacial cycles and low-latitude continental precipitation distribution. In this chapter we test the hypothesis that high-latitude ice sheets altered low-latitude climate. Our results demonstrate that the ice sheets simulated in our experiments have a limited role in influencing low-latitude climate. Instead, we find that the atmospheric pCO_2 concentration has the largest influence on low-latitude climate. We note that orbital parameter variations, and in particular the eccentricity of Earth's orbit about the Sun, play a significant role in determining the short-to-intermediate-term variability in low-latitude climate. Using these climatic factors, we formulate a model of low-latitude late Paleozoic cyclic sedimentation that incorporates eccentricity-paced ice volume changes and low-latitude precipitation variability. Our results account for changes in sea-level, continental ice sheets, vegetation, precipitation, and sediment availability.

6.2 Conclusions and future work

The work presented in this dissertation represents a significant advancement in the methodologies used to study LPIA climate, which in turn have facilitated a greater understanding of LPIA climate dynamics. In this concluding section, I will detail the benefits of a GCM-based modeling approach to the study of the LPIA, summarize the advancements made in our understanding of LPIA climate dynamics, and suggest future LPIA research directions.

GCM-based studies of Earth's climate system are a powerful tool by which researchers have sought to find answers to questions that are fundamental to our past, present, and future. The processes that govern Earth's climate system are complex, and simple conceptual models often fail to accurately capture these complicated phenomena. In the late Paleozoic, the formation of the Pangaean supercontinent, the waxing and waning of high-latitude ice sheets, and the hypothesized fluctuations in atmospheric pCO$_2$ concentration, add complicating factors to the climate system that lend themselves to GCM-based studies. GCM studies are limited by many factors, among them their chosen resolution, their representation of sub-grid scale processes, and the quality/accuracy of their initial conditions, but the results of GCM studies often suggest complexities in the climate system not considered in conceptual climate models. For instance, in chapters four and five of this dissertation we demonstrate vegetation feedbacks that to our knowledge have not previously been suggested, yet significantly alter the LPIA climate system. Beyond suggesting new climatic complexities, GCM-based studies can also examine conceptual hypotheses within the confines of theoretical climate dynamics. For example, in chapter five of

this dissertation, we compare our GCM-based results to conceptual climate models formulated from inferences made on cyclic low-latitude sedimentary sequences and find that the conceptual models lack theoretical justification. These anecdotal examples are presented to suggest that much can be learned about past, present, and future climates within the theoretically-rigorous confines of a GCM.

The major accomplishments of this dissertation are: (1) the design and implementation of a GCM-based late Paleozoic climate-modeling technique that couples atmospheric, biospheric, cryospheric, hydrospheric, and lithospheric components, (2) the determination that under varying orbital conditions the late Paleozoic icehouse/greenhouse $p\mathrm{CO}_2$-threshold occurs below 840 ppmv, (3) the realization that ice sheets are insensitive to orbital insolation increases when $p\mathrm{CO}_2$ concentrations are low enough to support ice sheet volumes of adequate size to explain observed glacioeustatic fluctuations, (4) the discovery that the inclusion of dynamic orbitally-driven ecosystem changes at the ice sheet margin amplifies orbital temperature changes and facilitates ice sheet advance and retreat, and (5) the formulation of an eccentricity-paced low-latitude cyclostratigraphy model based on the theoretically-determined response of late Paleozoic climate to orbital, ice-sheet, and $p\mathrm{CO}_2$ forcing.

The work completed in this dissertation has motivated new research questions, some of which are in the process of being answered and some that will be left to the future. Below, I outline some of these questions and suggest possible approaches.

(i) **What effect does paleogeography have on ice sheet formation?** [underway in-collaboration with C. Poulsen and T. Torsvik] The LPIA lasted for ∼100 Myrs, during which time the continents joined, broke apart, and drifted through different latitudes. Can the icehouse/greenhouse conditions of the LPIA be explained by changes in paleogeography alone? Are there large differences in climate when a

time period's high-stand versus low-stand paleogeographic reconstruction is simulated?

(ii) **What is the climatic influence of a dynamic ocean circulation?** [underway in-collaboration with C. Poulsen] In this dissertation, the ocean has been represented as a 50 m slab that diffuses heat from the equator to the poles. What effect do dynamic ocean circulations have on high-latitude ice sheet volumes and low-latitude climate?

(iii) **How does LPIA climate influence the long-term carbon cycle?** [underway in-collaboration with C. Poulsen, Y. Godderis, and Y. Donnadieu] The carbon cycle is highly-dependent on the rate of chemical weathering of silicic continental crust. The location of the Pangaean supercontinent the paleoequator, hypothetically brought a massive volume of silicic crust to the perhumid latitudinal belt. What were the effects on the global carbon budget?

(iv) **Does late Paleozoic flora change the story?** In this dissertation, vegetation feedbacks play a significant role in determining the climate's response to various forcing mechanisms. The vegetation model we employ (BIOME4) is based on the characteristics of modern ecosystem types. What effect would Paleozoic vegetation have on the climate system?

In short, in the future, more of the past. Thanks for reading! -Dan